

Finding Close Encounters: Toward a consensus on the influence of the stellar flybys on the Solar System over 10 million years

Author:

Tabassum Shahriar Tanvir

Supervised by:

Dr Fabo Feng

Dr James L Collett

Professor Hugh Jones

Centre for Astrophysics Research
School of Physics, Astronomy and Mathematics
University of Hertfordshire

Submitted to the University of Hertfordshire in partial fulfilment of the requirements of the degree of Master of Science by Research.

October 2018

Abstract

This thesis is a study of possible stellar encounters of the Sun, both in the past and in the future within ± 10 Myr of the current epoch. This study is based on data gleaned from the first Gaia data release (Gaia DR1). One of the components of the Gaia DR1 is the TGAS catalogue. TGAS contained five astrometric parameters for more than two million stars. Four separate catalogues were used to provide radial velocities for these stars. A linear motion approximation was used to make a cut within an initial catalogue keeping only the stars that would have perihelia within 10 pc. 1003 stars were found to have a perihelion distance less than 10 pc. Each of these stars was then cloned 1000 times from their covariance matrix from Gaia DR1. The stars' orbits were numerically integrated through a model galactic potential. After the integration, a particularly interesting set of candidates was selected for deeper study. In particular stars with a mean perihelion distance less than 2 pc were chosen for a deeper study since they will have significant influence on the Oort cloud. 46 stars were found to have a mean perihelion distance less than 2 pc. Among them HIP 89825 (GL 710) still remains the closest encounter with a Solar System with a perihelion of 0.4-0.8 pc, 1.35 Myr in the future. A principal component analysis was performed in order to show the distribution of the clones around the Oort cloud. The thesis also looks into the influence of the solar apex motion on the distribution of encounter perihelia directions. Some new close encounters have been identified and refinements have been made on encounters reported in previous studies.

Declaration

I declare that no part of this work is being submitted concurrently for another award of the University or any other awarding body or institution. This thesis contains a substantial body of work that has not previously been submitted successfully for an award of the University or any other awarding body or institution.

Except where indicated otherwise in the submission, the submission is my own work and has not previously been submitted successfully for any award.

Acknowledgements

Changing disciplines is always a challenge. I must thank Boris Nedelchev and Dr. James Collett for encouraging me to transfer to astronomy.

I would also like to thank Professor Jones for giving me that opportunity and a new challenge to be successful at. I would also like to thank Dr. Fabo Feng and Dr. James Collett for helping understand the problem, giving me time to transition into astronomy. Without bothering my tutors with a million questions, especially Dr. Collett, I do not think I could have finished this project in due time.

I would also like to express my gratitude to my friends Tasiful Islam and Lord Dover for their continued encouragement and support throughout the past year and helping me learn the different aspects of latex as well. I would like to extend this gratitude to my parents for bringing me up and pushing me towards new and exciting opportunity to learn and discover new aspects of life. Finally I would like to thank the Almighty.

This work has made use of data from the European Space Agency (ESA) mission *Gaia* (<https://www.cosmos.esa.int/gaia>), processed by the *Gaia* Data Processing and Analysis Consortium (DPAC, <https://www.cosmos.esa.int/web/gaia/dpac/consortium>). Funding for the DPAC has been provided by national institutions, in particular the institutions participating in the *Gaia* Multilateral Agreement.

*To
my beloved sister*

Contents

Abstract	i
Acknowledgements	iii
Contents	v
List of Figures	vii
List of Tables	ix
List of Abbreviations	xi
1 Introduction	1
1.1 Influence of a stellar encounter on the Oort Cloud	2
1.2 Anisotropic stellar encounters caused by the Sun’s motion	10
1.3 Search for close stellar encounters	12
1.4 Thesis aim and objective	16
1.5 The structure of the thesis	16
2 Data	17
2.1 Limitations of Gaia DR1	18
2.1.1 Survey Completeness	18
2.1.2 Astrometry	18
2.2 Obtaining the Radial Velocity	18
2.2.1 RAVE DR5	19
2.3 Completion of the Catalogue	19
3 Initial Selection of candidates	20
3.1 Linear Motion Approximation	20
4 Finding encounters through simulations of stellar motions	22
4.1 Sampling the initial conditions of the candidate stars	22
4.2 The galactic potential	23
4.3 Co-ordinate transformation	26
4.4 Numerical integration of the candidate stars	28
4.5 Principal component analysis	30

5	Results	35
5.1	A new catalogue and the analysis of the new catalogue	35
5.2	Individual encounters	53
6	Discussions	70
6.1	Completeness of the catalogue	70
6.2	Data Issues	70
6.3	Difference in encounter parameters estimation	71
6.4	Dependence on the Galactic Potential Model	72
6.5	Comparing Results with another Close Encounter Study	74
7	Conclusion	76
7.1	Future Work	78

List of Figures

1.1	The results of DQT and DLDW simulation of a perihelion distance at 60000 AU	4
1.2	The results of DLDW simulation for a stellar passage at a distance of 30000 AU	5
1.3	The results of DQT and DLDW the simulation for the distant stellar passage (perihelion distance at 90000 AU)	6
1.4	Results of the numerical simulation that produce observable comets with stellar impulse and galactic disk tide acting simultaneously at a perihelion distance of 30000 AU	8
3.1	distribution of encounter parameters in linear motion approximation	21
4.1	histogram of astrometric parameters of HIP 23714	24
4.2	histogram of encounter parameters	29
4.3	distribution of astrometric parameters ($\pi, \mu_\alpha, \mu_\delta$ and rv) of the candidate stars	30
4.4	distribution of the nominal encounter parameter of the candidate stars	31
4.5	distribution of 1000 clones of star TYC 5009-137-1	33
4.6	distribution of 1000 clones of star TYC 5009-137-1 with principal component analysis	34
5.1	Nominal orbit of HIP 89825	40
5.2	d_{ph} vs t_{ph}	41
5.3	Mean perihelion distance vs mean perihelion time with their 5% and 95% quantiles	42
5.4	d_{ph}^{mean} vs v_{ph}^{mean}	43
5.5	Histogram of perihelion distance	44
5.6	Histogram of perihelion distance	45
5.7	Histogram of perihelion distance	46
5.8	$d_{ph}^{nom} - d_{ph}^{mean}$ vs parallax	47
5.9	$d_{ph}^{lin} - d_{ph}^{mean}$ vs parallax	48
5.10	Distribution of the direction of encounter velocities in galactic co ordinates as $\sin(b_{enc}$ and l_{enc}	49
5.11	Distribution of the direction of encounter perihelion in galactic co ordinates as $\sin(b_p$ and l_p	50
5.12	Distribution of encounters perihelion on the plane of the sky as a function of galactic latitude and longitude	51
5.13	Distribution of $\cos\theta$	52
5.14	Distribution of $\cos\theta$ for stars with encounter speed less than $50kms^{-1}$	53
5.15	Distribution of $\cos\theta$ for stars with perihelion speed greater than $50kms^{-1}$	54
5.16	distribution of $\cos\theta$ for stars with radial velocity smaller than $50kms^{-1}$	55
5.17	Distribution of $\cos\theta$ for stars with radial velocity greater than $50kms^{-1}$	56
5.18	Sun's orbit around the galactic centre	57

5.19	Distribution of encounters perihelion on the plane of the sky as a function of galactic latitude and longitude for encounter stars with a radial velocity greater than 50 kms^{-1}	58
5.20	Distribution of encounters perihelion on the plane of the sky as a function of galactic latitude and longitude for encounter stars with a radial velocity less than 50 kms^{-1}	58
5.21	Distribution of encounters perihelion on the plane of the sky as a function of galactic latitude and longitude for encounter stars with a perihelion speed less than 50 kms^{-1}	58
5.22	Distribution of encounters perihelion on the plane of the sky as a function of galactic latitude and longitude for encounter stars with a perihelion speed greater than 50 kms^{-1}	59
5.23	Distribution of θ	60
5.24	Distribution of clones of HIP 89825	61
5.25	Distribution of clones of TYC 6403-151-1	62
5.26	Distribution of clones of HIP 94512	63
5.27	Distribution of clones of TYC 8088-631-1	64
5.28	Distribution of clones of TYC 6622-652-1	65
5.29	Distribution of clones of TYC 8822-592-1	66
5.30	Distribution of clones of TYC 9524-1668-1	67
5.31	Distribution of clones of TYC 7068-802-1	68
5.32	Distribution of clones of TYC 7567-304-1	69

List of Tables

4.1	Galactic model parameters adopted from García-Sánchez et al. (2001)	26
4.2	Solar parameters adopted	26
5.1	the number of stars with different perihelion distances after orbital integration. .	35
5.2	Encounter parameters for all the stars with a mean perihelion distance less than 2 pc. The column named cat indicates the name of the input catalogue where the radial velocity were obtained from g= GCS catalogue, P= pulkuvo Catalogue, r= RAVE DR5 catalogue, x= XHIP catalogue.The encounter parameters are set as d_{ph}, t_{ph} respectively, nom represents the nominal values, mean represents the mean values, 5% and 95% represents the 5% and 95% quantiles of each encounter parameter.	36
5.3	Encounter parameters for all the stars with a mean perihelion distance less than 2 pc. The column named cat indicates the name of the input catalogue where the radial velocity were obtained from g=GCS catalogue, P=Pulkuvo Catalogue, R= RAVE DR5 catalogue, X= XHIP catalogue.The encounter parameters are set as v_{ph} respectively, nom represents the nominal values, mean represents the mean values, 5% and 95% represents the 5% and 95% quantiles of each encounter parameter.	37
5.4	Astrometric parameters for all the stars with a mean perihelion distance less than 2 pc. The column named cat indicates the name of the input catalogue where the radial velocity were obtained from g=GCS catalogue, P=Pulkuvo Catalogue, R= RAVE DR5 catalogue, X= XHIP catalogue.The encounter parameters are set as $\alpha \delta \pi \mu_\alpha \mu_\delta rv$ respectively.	38
5.5	Error for the astrometric parameters for all the stars with a mean perihelion distance less than 2 pc. The column named cat indicates the name of the input catalogue where the radial velocity were obtained from g=GCS catalogue, P=Pulkuvo Catalogue, r= RAVE DR5 catalogue, x= XHIP catalogue.The encounter parameters are set as $\alpha \delta \pi \mu_\alpha \mu_\delta rv$ respectively.	39
7.1	Encounter parameters for all the stars with a mean perihelion distance less than 2 pc. Stars with perihelion speed greater than $600km s^{-1}$ were omitted. The column named cat indicates the name of the input catalogue where the radial velocity were obtained from g=GCS catalogue, P=Pulkuvo Catalogue, r= RAVE DR5 catalogue, x= XHIP catalogue.The encounter parameters are set as d_{ph}, t_{ph} respectively, nom represents the nominal values, mean represents the mean values, 5% and 95% represents the 5% and 95% quantiles of each encounter parameter.	77

- 7.2 Encounter parameters for all the stars with a mean perihelion distance less than 2 pc. Stars with perihelion speed greater than 600km s^{-1} were omitted. The column named cat indicates the name of the input catalogue where the radial velocity were obtained from g=GCS catalogue, p=Pulkuvo Catalogue, r=RAVE DR5 catalogue, x= XHIP catalogue. The encounter parameters are set as v_{ph} respectively, nom represents the nominal values, mean represents the mean values, 5% and 95% represents the 5% and 95% quantiles of each encounter parameter. 78

List of Abbreviations

LPC = Long Period Comet

GMC = Giant Molecular Cloud

α = Right Ascension

δ = Declination

π = Parallax

μ_α = Proper Motion in the Right Ascension

μ_δ = Proper Motion in the Declination

rv = Radial Velocity

HIP= Hipparcos star identifier

TYC = Tycho 2 star identifier

TGAS = Tycho Gaia Astrometric Solution

RAVE = Radio Velocity experiment

LSR = Local Standard of Rest

GCS = Geneva copenhagen Survey

PCA = Principal component analysis

K-T = Cretaceous Tertiary

DR1 = Data Release 1

DR2= Data Release 2

GL = Gliese

d_{ph} = encounter perihelion distance

v_{ph} = perihelion speed of an encounter star

t_{ph} = time at the perihelion in Myr.

Myr = Millions of years

R_\odot = Distance of the Sun from the galactic centre

z_\odot = Sun's vertical height from the galactic mid-plane

b_b = scale length of the bulge

b_h = scale length of the halo

a_d = scale length of the disk

b_d = scale length of the disk

M_b = mass of the bulge

M_h = mass of the halo

M_d = mass of the disk

$(U_\odot, V_\odot$ and $W_\odot)$ = Sun's velocity components with respect to the LSR

b_p = galactic latitude of the perihelion of a stellar encounter

l_p = galactic longitude of the perihelion of a stellar encounter

b_{enc} = galactic latitude of the perihelion speed direction of a stellar encounter

l_{enc} = galactic longitude of the perihelion speed direction of a stellar encounter

Chapter 1

Introduction

The Sun is on a near-circular orbit around the Milky Way and in the course of its journey has close encounters with stars on neighbouring orbits. The orbital period of the Sun around the Milky Way is around 225 million years and the solar system has been in existence for 4.6 billion years. As a result, the Sun has made around 20 circuits during its lifetime. Stars in the solar neighbourhood e.g. travelling on nearby epicycles in the epicyclical approximation can be on orbits that bring them close to the solar system. Historically, Chamberlin and Moulton (1905) suggested that such a close approach could cause the planets to form by distortion of the stellar bodies themselves. This idea is now discredited but the idea that a tidal disturbance could lead to changes in the solar system is still sound. The smaller the relative velocity of the stellar encounters relative to the Sun and the greater its mass, the stronger will be the perturbation imposed on the Oort cloud from a star. This can lead to disturbed orbits of some of the Oort Cloud objects. These objects may ingress into the inner Solar System and are observed as Long Period Comets. In particular, stars that pass close to the solar system can influence the Earth; not directly but by influencing the weakly bound comets within the Oort cloud. Passing stars can perturb the Oort cloud which can result in an influx of long period comets (LPCs) towards the inner Solar System. The only source of LPCs that gets injected into the inner Solar System is from the Oort cloud. This Oort cloud can be tidally perturbed by close passing stars which may result in an increase in frequency with which comets are injected into the inner Solar System where some of these comets may pose a significant threat to the terrestrial biosphere. Earth's geological record shows evidence of minor body impact from objects within the Solar System. The K-T mass extinction of species that occurred 65 Myr ago may also have been caused (at least in part) by a large impact of a LPC. The example of these stellar close encounters does not mean

that they are the only way that comets get injected into the inner Solar System. There are other ways the Oort cloud can be perturbed and LPCs then get injected into the inner Solar System. Examples of potential perturbations are, for instance, irregularities in the galactic potential field or Giant Molecular clouds.

1.1 Influence of a stellar encounter on the Oort Cloud

Comets are known to be near-pristine objects within the Solar System, most probably the left-overs from the the formation of Jovian planets. In his paper, Oort (1950) analysed the distribution of the inverse semi-major axes of long period comets and concluded that the near parabolic spike of this distribution revealed that a huge reservoir of icy bodies was swarming around the Sun in a spherical structure at distances several times larger than 10^4 AU (a notional radius for the "Oort Cloud"). Oort's favoured mechanism of injecting comets into the observable orbits was the passage of star in the vicinity of this cloud of cometesimals. The long term reshuffling of angular momenta of the cometary orbits would ensure a continuous infeed into the innermost region of the Solar System. Until the 1980s, close stellar encounters were thought to be the only way to deliver long period comets into the observable orbits. By that time it became clearer that the galactic tide also plays a major role in delivering comets into the solar system. This was verified by the galactic latitudes of perihelia of new Oort cloud comets that have a double peaked distribution that is characteristic of the disk tide. Many authors (Duncan et al. (1987), Heisler and Tremaine (1986), Bailey et al. (1990)) have stated that the galactic tidal effect produces more observable long period comets than are produced by close stellar encounters. The Galactic tide is a more long-lived perturbation of the Oort cloud that causes periodic, long-term variations of the cometary orbital elements and their perihelion distances. It may be shown that only a part of the Oort cloud becomes observable due to the galactic tide effect in the absences of the other perturbing forces. Comets are not capable of migrating from the observable part to the unobservable part. without other types of perturbation (mainly stellar). These stellar perturbations are potentially capable of randomising the whole population. Many potential observable comets would have been all completely removed by planetary perturbation from the inner Solar System. Another reason for the importance of the stellar perturbation is the problem of so called "cometary showers". Cometary showers are a significant temporal increase of the observable comet influx after a close or penetrating passage of a star. This concept was first proposed by

Hills (1981) and was discussed in many other papers. In a series of papers, P.A. Dybczynski discussed the effect of a single stellar passage through or near the Oort cloud (Dybczyński (2002)), the effect of the simultaneous stellar and galactic action on the Oort cloud (Dybczyński (2005)) and the real perturbers of the Oort cloud and their output (Dybczyński (2006)). In the first paper of this series Dybczyński discussed a single stellar passage through, or near, the Oort cloud by the means of Monte Carlo simulations. This simulation was performed in two separate steady-state models for the Oort cloud, and for different parameters of the stellar passage. The first model of the Oort cloud was based on simulation of the Oort cloud (Duncan et al. (1987)-the paper refers this model to the DQT model). This distribution of the comets was first used by Weissman (1996). The second model is based on simulations by Dones et al. (2000) (the paper refers to the model as DLDW model). These models for the Oort cloud can be treated as the two most extreme cases from the point of comet densities from its inner radius to outer radius. In the DQT model the inner part of the Oort cloud dominates, while in the DLDW model the outer part is more populous and the inner part is almost absent. According to Dones, the difference between these two models is that the DQT model starts with highly eccentric orbits that prevent comet perihelia from evolving due to planetary perturbations. Thus Neptune and Uranus can directly inject bodies into the Oort cloud. On the other hand the DLDW model of the Oort cloud starts with comets on a nearly circular orbits. Also, the DLDW model of the Oort cloud is significantly different from the DQT model because the majority of comets are populated in the outer region of the cloud while the inner most part of the cloud is spherically symmetric but flattened. The paper concentrates on the results of a single stellar passage taking into account its geometry, analysing spatial distributions and time dependence of the resulting observable sample of comets. The paper also considers two interesting end states of the cometary orbit evolution under the stellar perturbation:

- a comet is called an observable comet when its perihelion distance is reduced below the observability threshold (in this paper it is 5 AU).
- a comet is considered lost when its eccentricity becomes greater or equal to unity or its aphelion distance becomes greater than the "stellar lost limit"(assumed to be 2.5×10^5 AU).

Fig 1.1 shows the distribution of perihelion points of the observable comets resulting from a stellar passage at 60000 AU from the Sun. These perihelion points are represented in a equal area projection in the celestial sphere. In the left upper corner, all the parameters of the perturbing star are presented. Below the equal area projection of the celestial sphere, a histogram displays

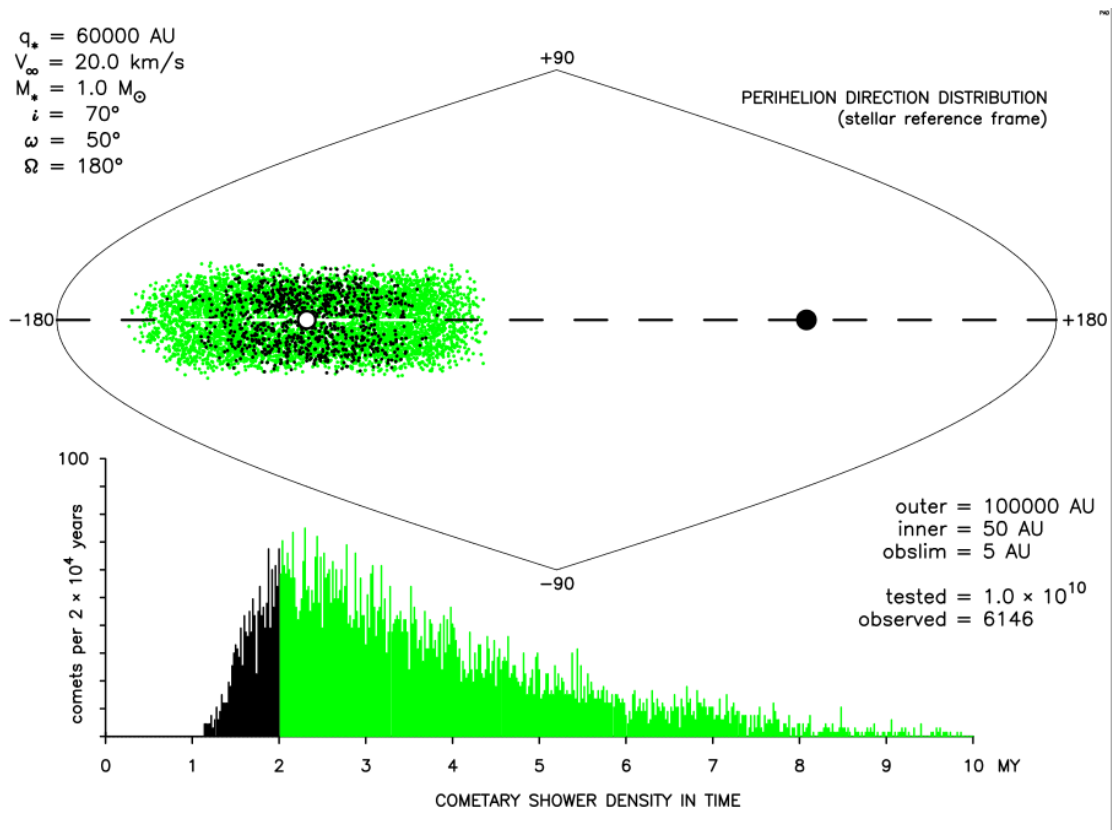


FIGURE 1.1: The results of simulation for the perihelion distance of 60000 AU. The stellar reference frame is used here so the star heliocentric orbit plane projection is represented by the dashed straight line. The star's perihelion is marked by a full circle while the anti perihelion direction is marked by an empty circle on the celestial sphere. Comets arriving in the solar vicinity during the first 2 Myr after the stellar passage are marked in black while the rest are plotted in green. In the lower part of the picture, the parameters for the cloud are presented where the obslim represents the observability threshold (a comet is observable when its perihelion distance is roughly equal to 5 AU). This figure has been taken from Dybczyński (2002)

the time dependence of the observable flux showing the number of comets per 20000 years time interval. Perihelion direction points for comets arriving in the vicinity of Sun during the first two million years after the star's passage are marked in black, while the rest are in green. The dashed line is the star's heliocentric orbit projection onto the celestial sphere with its perihelion marked by the filled circle and its anti-perihelion at the position of the open circle. Some parameters of the Monte Carlo simulation are also presented: from the cloud of 10^{10} bodies, the obtained number of observable comets is 6146. The probability of being observed is estimated to be $(6.46 \pm 0.61) \times 10^{-7}$. This was calculated for the DQT model of the cloud and for a rather weak stellar perturbation. The maximum cometary flux is obtained two million years after the star's passage. If the population of the cloud is 10^{12} it will give one comet per 3 years during the peak. The same simulation performed for DLDW model gives the similar distribution of

perihelion point directions. The probability of comets being observed for the DLDW model is significantly higher than the DQT model which is estimated at $(2.71 \pm 0.26) \times 10^{-6}$. The observable cometary flux is also higher for the DLDW model at approximately one comet a year when the population is scaled down to 10^{12} . Figure 1.2 represents a Monte Carlo simulation for

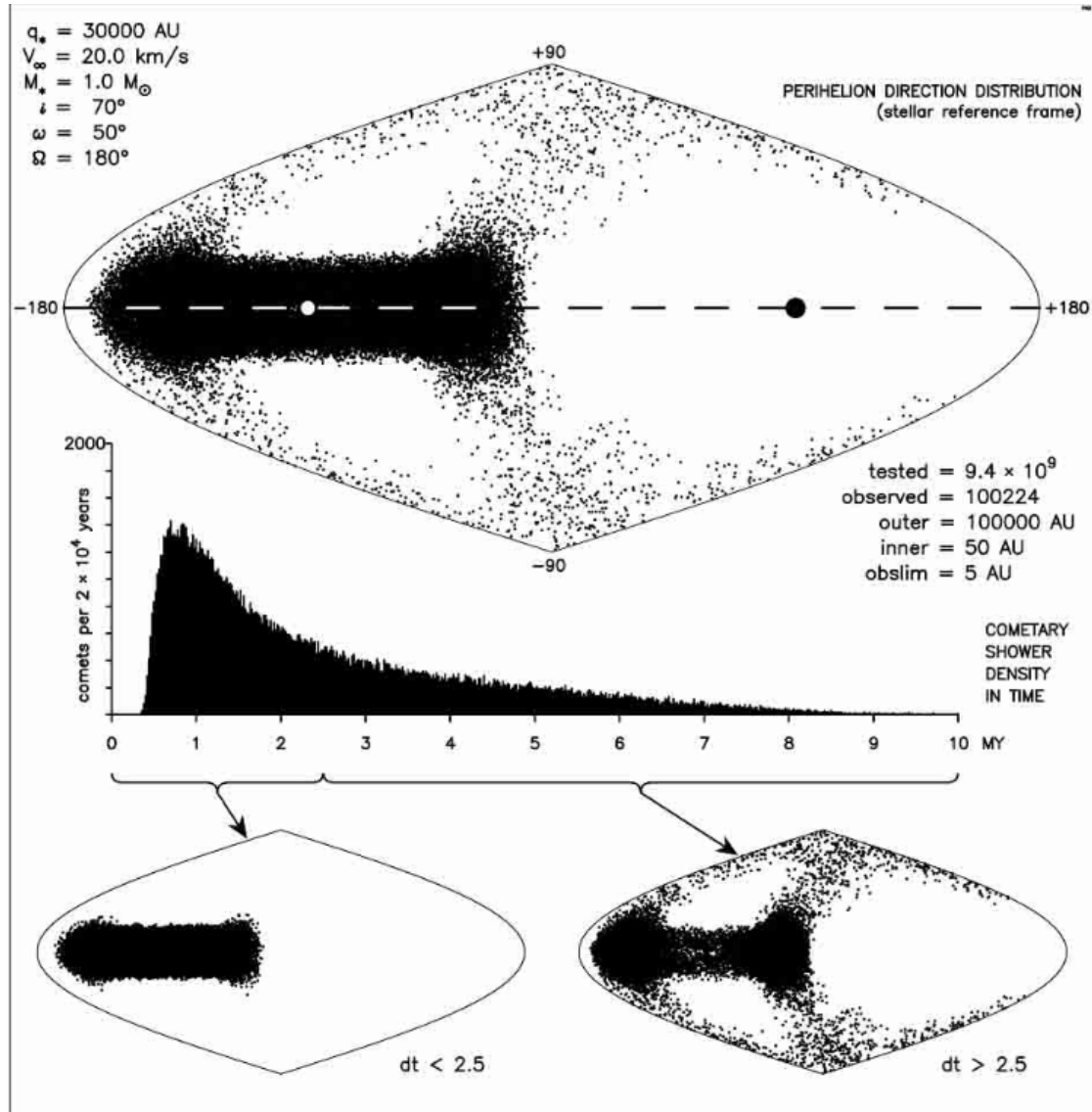


FIGURE 1.2: The results of DLDW simulation for the perihelion distance of 30000 AU. The star's heliocentric orbit plane projection is marked here with the dashed line, its perihelion with the full circle and its anti-perihelion with the open one. The cometary shower starts approximately 0.5 Myr after the star's passage and appears as a steep increase of the observable flux. Below the arrival time distribution plot two separate distribution for the first 2.5 Myr after the passage and rest of the simulated observable sample. The left plot represents more than 62% of all points presented in the upper plot. This figure has been taken from Dybczyński (2002)

the DLDW model of the Oort cloud. The perturbations from a such a passage were applied to a population of 9.4×10^9 comets: 100224 comets were found in the observable region from the

simulation. The probability of a comet being observed in this case was $(1.08 \pm 0.03) \times 10^{-5}$. Since the directional distribution is more complex here, two more plots were added in order to demonstrate the two separated time intervals in order to emphasise that during the first 2.5 Myrs the concentration of the perihelion directions around the star's anti-perihelion direction is very high and is similar to fig 1.1.

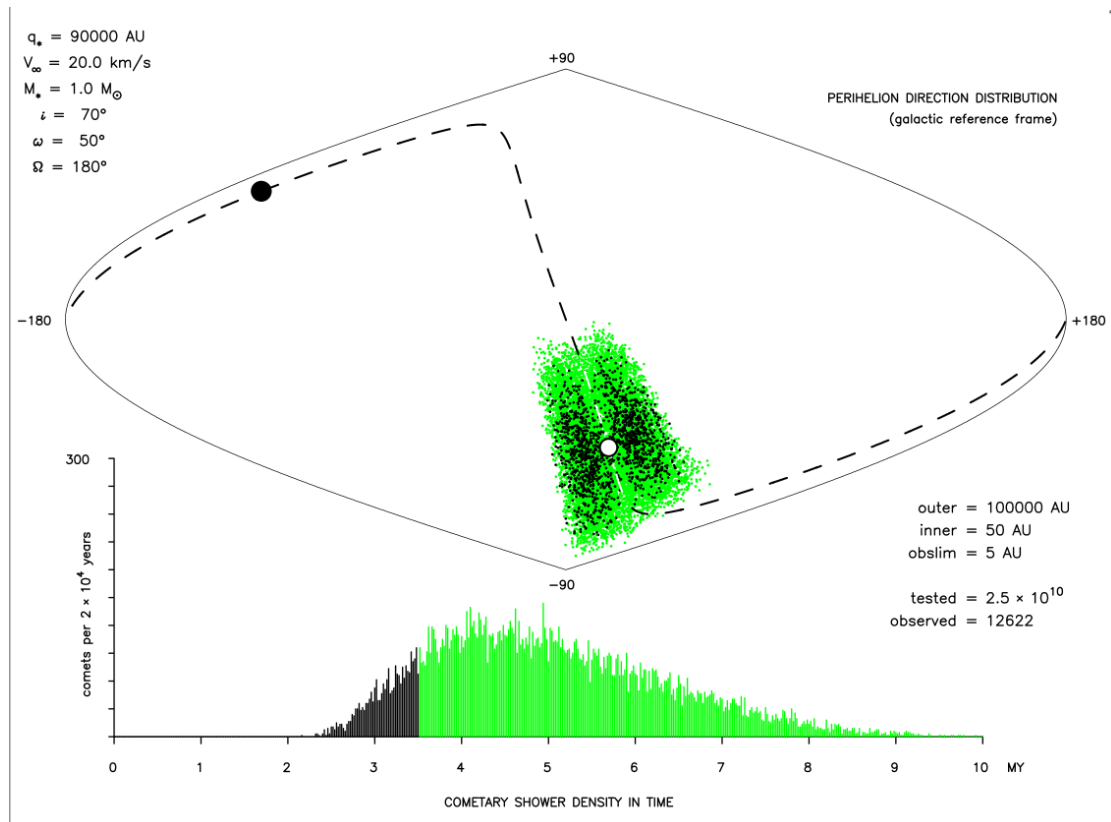


FIGURE 1.3: The results of the simulation for the distant stellar passage (perihelion distance at 90000 AU) and the DLDW model of the cloud. All perihelion directions are highly concentrated on the celestial sphere, here it is presented in the galactic reference frame. The dashed line represents the projection of the star heliocentric orbit plane with perihelion and anti-perihelion directions marked with full and open circles respectively. Comets that begin to arrive within the solar vicinity after 3.54 Myr of the stellar passage are marked in black and the rest is marked in green. Figure taken from Dybczyński (2002)

In the second paper (Dybczyński (2005)), the same author discussed the results of a single stellar passage through or near the Oort cloud under the simultaneous influence of the galactic tide. In order to find out the effect of a single stellar passage through or near the Oort cloud under the simultaneous influence of the galactic tide, a steady state model of the Oort cloud was modelled. The author used a 'dynamical filtering' to get rid of the comets which are only under the influence of the galactic tide from this model. The stellar impulse was applied and it made

some comets observable without the need for any other type of perturbation. It also stirred the whole cloud and transferred some comets to the region of phase space from where other comets might become visible because of the galactic tidal perturbation. This model was rather artificial since it considered that the stellar passages are well separated in time and did not overlap (which is not true in reality) and all observable comets were removed by planetary perturbations.

In the first paper, three scenarios were chosen to demonstrate the perihelion direction distribution of observable comets induced by stellar passages at distances 90000 AU, 60000 AU, 30000 AU. This paper follows the same scenarios for simultaneous stellar and galactic perturbations. The corresponding perihelion direction distribution along with cometary influx time dependence are shown in figure 1.4. The format of this plots are similar to the format of the plots of the first paper.

In the third paper Dybczyński used a Monte Carlo simulation to determine the current or future closest stellar encounters of the Oort cloud under the simultaneous influence of the galactic tide. The study used the Hipparcos catalogue (Perryman et al. (1997)) in order to search for these close stellar encounters and found 21 possible candidates from the catalogue. The study also identified a particular star Gliese 710 (HIP 89825) as a possible perturber of the Oort cloud in the future. I will be taking a close look at this star in chapter 5 where I present updated encounter parameters for close passage. In this earlier paper it was found that this particular star will come as close as 0.29 pc in 1.39 Myr. These values were further updated by the same author and it is interesting to compare those updated values to the ones presented in this thesis. This will be done in chapter 5. In a more recent study of the closest approach of the star by the same author (the data for the recent study of Gliese 710 was based on the first Gaia data release) it was found that the star will approach the solar system at a much closer distance than previously anticipated. The study estimates that the star will come as close as 13366 AU from the Sun and will have a significant effect on the Oort cloud comets. During its closest approach, GL 710 (HIP 89825) will be one of the brightest objects in the sky and it will become the fastest observable naked eye object of the night sky outside the Solar System. The total proper motion of the star will be five times greater than the proper motion of Bernard's star (Berski and Dybczyński, 2016).

Rickman et al. (2008) presented a detailed analysis of the injection mechanism of Oort cloud comets into observable orbits by examining the effects on the model of the Oort cloud with separate models of tidal and stellar perturbation. The study also used a million test comets without cloning them.

They describe a Monte Carlo simulation on the dynamical evolution of the Oort cloud over

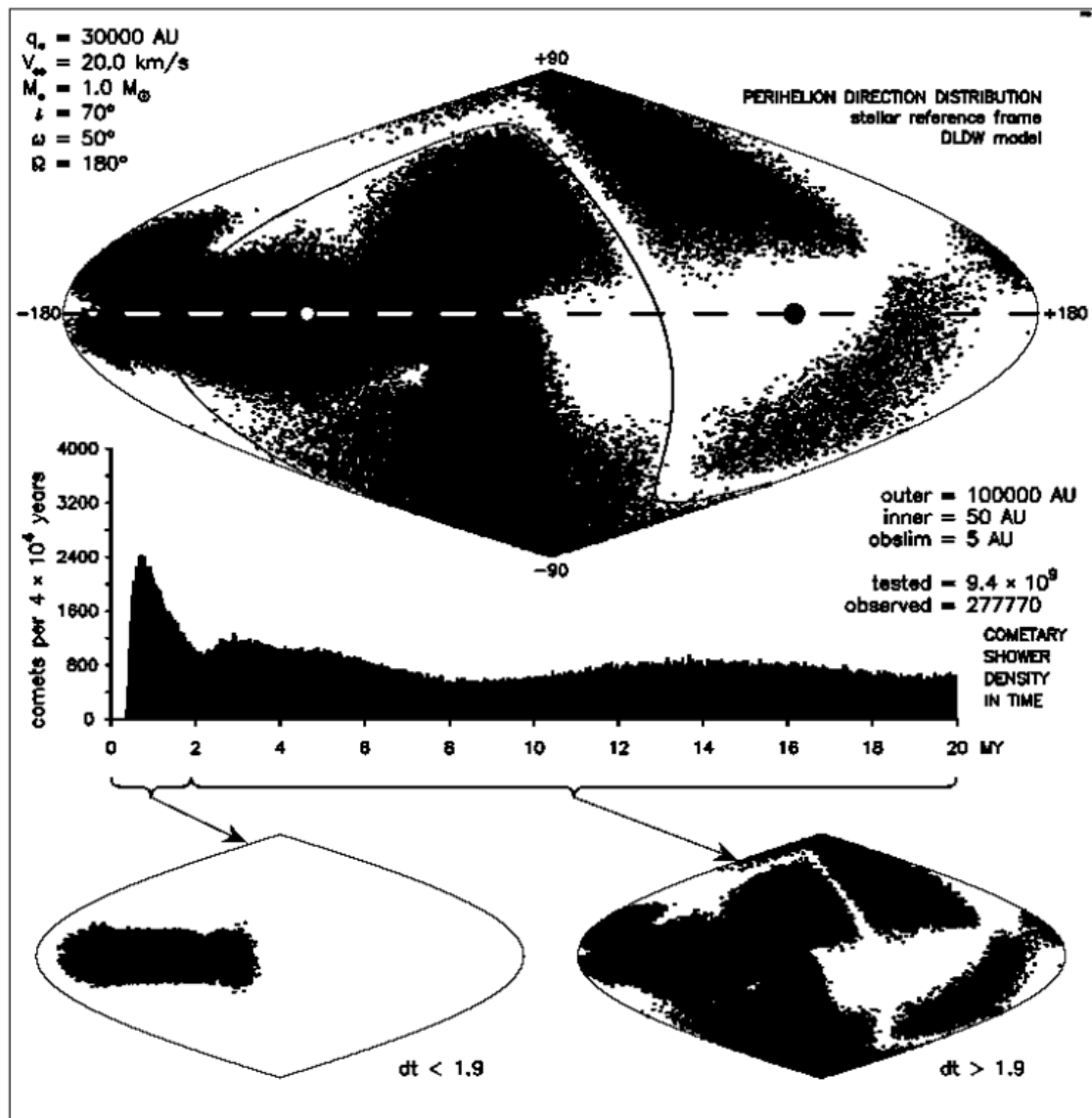


FIGURE 1.4: Results of the numerical simulation that produce observable comets with stellar impulse and galactic disk tide acting simultaneously at a perihelion distance of 30000 AU. This is an example of a strong stellar perturbation. Because of the high efficiency of such an event, two additional copies of the directional distributions of perihelion points for two separate time intervals are added at the bottom of this figure. The high concentration of perihelion points in the first 2 Myr is clearly noticeable. Figure taken from Dybczyński (2005)

5 Gyr, using for an initial condition, a relaxed cloud model with a distribution of semi-major axis $f(a) \propto a^{-1.5}$ within the interval 3000-100000 AU. The model involves perturbation due to galactic tide (with both radial and vertical components) and stellar perturbations. This model was based on the results and simulations of the Oort cloud by Duncan et al. (1987). The problem with this model was that it did not give a steady distribution as more comets are lost from the outer parts of the cloud than can be replaced from the inside. The model cloud in this study therefore used a distribution closer to $f(a) \propto a^{-2}$.

The dynamical model had some limitations as well since it does not take Giant Molecular Clouds (GMC) or star clusters into account. The justification behind this omission is that any encounters with GMC or star clusters with the Solar System are unlikely to happen and unsystematic. They also argued that, even if the Solar System had any encounter with these kinds of celestial objects and it modified the structure of the Oort cloud, the interest was not to study the dynamical history of the Oort cloud but rather how stars and galactic tides act on the cloud while injecting observable comets. The study also did not take planetary perturbations into account in any manner. They used a loss cone defined by a limiting perihelion distance (15 AU in this study) outside of which no planetary effects were included and inside which all comets were considered lost from the cloud due to the perturbations by Jupiter and Saturn. The study limited its attention to one subset of the observed population of the "new" comets. During the later parts of the simulation, the study also showed that there was a synergy effect on the Galactic tide and stellar perturbation such that the combined injection rate was on the average 70% larger than that of stars alone. This synergy was strongest among the semi-major axes of size 20000-50000 AU and it continued all the way to the inner core of the cloud. I will discuss the outer part of the cloud and inner part of the cloud separately. We begin with the outer part of the cloud. Two mechanisms of synergy were identified during the quiescent periods in the outer parts of the cloud were identified:

- the stellar perturbation provides a supply of new comets which replenishes the depleted phase space represented by the tidal in feed trajectories.
- the stellar perturbations can decrease the perihelion distance of comets and a gain in comet injection occurs when this effect overpowers the opposing perturbations. The paper further suggests that, in the inner cloud, the galactic tide provides material for the stellar injection by slowly repopulating the region of phase space in the vicinity of loss cone.

The study also states that for smaller semi major axes the galactic tide is not the dominant force for perturbing the comets contrary to Heisler et al. (1987) and Heisler (1990). [The Heisler

papers considered the injections into the loss cone primarily by slight perturbation of perihelion distance across the limiting value of 10 AU. This study considers a large jump from 15 AU into the observable region of 5 AU.]

1.2 Anisotropic stellar encounters caused by the Sun's motion

The Sun shows a quasi-periodic motion perpendicular to the galactic disc and a small motion with respect to the LSR in the plane. This solar apex motion may result in the concentration of stellar encounter perihelia close to the plane that is perpendicular to the apex direction. This concentration with low speeds relative to the Sun as explained in chapter 5. This was first outlined by García-Sánchez et al. (2001). I will have a look at this diagnostic at chapter 5. In their paper a plot was created containing the stars that they found which had encounters with perihelia less than 5 pc. The plot showed the distribution of the angle between the solar apex at the time of the closest approach and the star's position on the plane of the sky. The angular bins in this study were taken to be 20 degrees in width. This allowed a reasonable description of the distribution induced by the Solar apex motion. They found 77 stellar candidates within 90 degrees of the solar apex and 79 candidates within 90 degrees of the solar antapex direction. García-Sánchez et al. (2001) used Hipparcos data to detect the randomness on the distribution of the encounter perihelia points. Due to the incompleteness, the data is biased. I have a small sample in this thesis and it will be interesting to compare my work with theirs as I do in chapter 5.

Feng and Bailer-Jones (2014) further explored the role of the Sun's motion in terrestrial comet impacts. The paper investigated the relation between the solar motion and the large impact craters by constructing a dynamical model of the Sun's orbit, the gravitational potential and the resulting perturbation of cometary orbits. The distribution of the dynamically new LPCs is found to be anisotropic. Under this scenario, they showed that the galactic tide can deplete the cloud from its pole and equatorial regions. The study used 102 dynamically new comets found by Marsden and Williams (2008). The peaks in the longitude distribution suggests a great circle on the sky passing through $l=135$ degrees and $l=315$ degrees. The asymmetry in the distribution in the galactic latitude is caused by the Sun's location and its motion in the last 10 Myr. Since the true initial nature of the Oort cloud is still not known, two different Oort cloud models were used in this study in order to generate Oort cloud comets. Models used were the DQT model and

the DLDW model. As mentioned in the previous section, the DQT model produces more inner Oort cloud comets and the DLDW model creates more outer Oort cloud comets. Because of the difference in the initial condition of the semi-major axis boundaries in this study, the initial eccentricities and inclinations were slightly different from those of Dybczyński (2002). Feng and Bailer-Jones generated stellar encounters by following the methods of Rickman et al. (2008) where cometary orbits were simulated with an isotropic distribution of stellar encounters. The geometry of the stellar encounters is complicated due to the Sun's motion relative to the local standard of rest. This solar apex motion can by itself produce an anisotropic distribution in the direction of the stellar encounters in the heliocentric rest frame. They also initialise the stellar encounters self-consistently in order for it to have a non-uniform angular distribution.

A Monte Carlo simulation was used to generate the parameters of the stellar encounters. The encounters are divided into different stellar categories according to their frequency as it is listed in table 8 of García-Sánchez et al. (2001). The mass of the star, maxweillan velocity dispersion and peculiar solar velocity are provided in that table. The perihelion direction of the encounter is, by its very nature, perpendicular to the vector encounter velocity. The angle β (the angle in the impact plane measured from the reference axis to encounter perihelion) is uniformly distributed in the interval of $[0, 2\pi]$. The trajectory of a stellar encounter in the heliocentric reference frame is determined by the encounter velocity, encounter perihelion distance and encounter time. The study uses a non normalised probability density function of encounters for each stellar category as a function of encounter velocity, time and perihelion distance. A revised version of Rickman et al.(2008) was used in order to find their galactic latitude and longitude. In order to complete the sampling process a 5 variable probability function is required. The Monte Carlo simulation from Rickman et al.(2008) was used in this study in order to generate encounter time, velocity and perihelion distance. Some changes were made in order to determine the direction of the encounter velocity. The changes were:

- (I) to randomly generate galactic latitude and longitude of each star such that the galactic latitude and longitude distributions are uniform in the interval of $[-1, 1]$ and $[0, 2\pi]$ respectively;
- (II) to adopt a galactic latitude of 58.87 degrees and a galactic longitude of 17.72 degrees for the solar apex direction and generate the velocity of star with respect to the local standard of rest.

The encounter velocity can be calculated from this vector equation:

$$\mathbf{V}_{\text{enc}} = \mathbf{V}_{\text{starintheLSR}} - \mathbf{V}_{\text{solarpeculiarvelocity}} \cdot \quad (1.1)$$

In order to clarify the effect of solar apex motion, Feng and Bailer-Jones defined an angle κ as the angle between the encounter perihelion and the solar apex. The relevant variable is $\cos\kappa$ as this would be uniform if the effects of the solar apex motion are not present. The solar apex motion would result in the concentration of encounter perihelia close to the plane perpendicular to the apex direction. A non uniform $\cos\kappa$ represents an anisotropy in the perihelia of the long period comets.

1.3 Search for close stellar encounters

An investigation to find possible stellar perturbers of the Oort cloud with a significant number of stars was made possible after the publication of the Hipparcos astrometric catalogue (Perryman et al. (1997), Perryman ESA 1997). This contained around 118000 stars; several studies were conducted to find the close stellar encounters based on the Hipparcos catalogue most notably by García-Sánchez et al. (2001), Dybczyński (2006), Bailer-Jones (2015).

García-Sánchez et al. (2001) conducted an investigation in order to find the close stellar encounters based on the Hipparcos data. These were combined with ground-based radial velocity measurements in order to calculate the trajectory of stars relative to the Sun.

In order to construct a sample of candidate stars which had a close encounter with the Sun in the past or will pass close to the Sun in the future, stars were selected from the Hipparcos catalogue whose proper motion, combined with an artificial radial velocity of 100 km/s, implied a closest distance approach of 3 pc or less. This radial velocity is somewhat larger than most of the stars' radial velocities in the Solar neighbourhood. At that velocity the best candidate stars which have passed the Sun or will approach the Sun within 3 pc have a proper motion (in mas/yr) which is less than 0.06 times the square of parallax (in mas), where the parallax values for those candidate stars have to be greater than 4.5 mas. This is due to the fact that with smaller values of parallax the implied proper motion limit would be close to or below the Hipparcos measurement accuracy. A total number of 1189 stars was found that met these criteria. A total of 595 candidate radial velocities was found from literature and observations.

The trajectory of these candidate stars were then integrated through three different models of galactic potentials: a local potential model, a global potential model and a perturbative potential model. García-Sánchez et al. (2001) adopted Sun's velocity with respect to the local standard of rest at $9.3 \pm 0.8 \text{ km s}^{-1}$ in the direction of the galactic center, $11.2 \pm 0.7 \text{ km s}^{-1}$ in the direction

of the galactic rotation, $7.6 \pm 0.6 \text{ km s}^{-1}$ towards the north galactic pole as reported by Feast and Whitelock(1997). They assumed a rounded value for Sun's vertical height (z_{\odot}) at 10 pc. The study adopted the range of 7.5-8.5 kpc for the galactocentric distance for the Sun. They also adopted a range of $0.076\text{-}0.15 M_{\odot} \text{ pc}^{-3}$ for the local mass density and $2.19 \text{ km s}^{-1} \text{ kpc}^{-1}$ as the local angular velocity.

Among these three models of the galaxy, the global potential model is preferred because this model provides a description of the potential throughout the galaxy and its validity is not restricted to a particular region of the galaxy or to a certain fraction of the candidate stars. The global potential parameters are adjusted to optimise the agreement between the kinematical predictions and the observational constraints of galactic features. However, these large scale adjustments provided a smooth potential but it would not fit the local irregularities. In this case, additional contributions from the other components might be required but the axial symmetry of the global potential model will be broken. The strongest perturbation on the smoothed potential model comes from the potential generated by the spiral arms of the galaxy. The perturbative model of the galaxy together with the global potential model thus provides an improvement over this matter, but since the description of the spiral arm is neither (qualitatively or quantitatively) present, the determination of the effects of the global spiral structure is problematic. For that the global potential model was adopted in the study as the most reliable potential model of the galaxy to determine the stellar orbit around the galaxy of the candidate stars.

The study integrates the motion of the Sun and the candidate stars using the global galactic potential model. The integrations were performed for a time period of ± 100 Myr using a fourth order Runge-Kutta integrator. 156 candidate stars were found within a distance of 5 pc from the list of 595 candidates. Most of the candidate stars were predicted to encounter the Solar System within ± 10 Myr. Among these, 87 candidates are predicted to have an encounter with the Solar System in the future and 69 candidates had a close encounter with the Solar System in the past. The study found HIP 89825 (GL 710) a KV star as one of the closest stars to have an encounter with the Solar System in the future. The predicted minimum distance for the star is $0.337 \pm 0.177 \text{ pc}$ in 1.36 ± 0.04 Myr. The study predicted that HIP 89825(GL 710) will pass through the outer Oort cloud although this passage will not be strong enough to disrupt the Oort cloud.

The second closest stellar encounter detected by the study was HIP 85661 an F0 star. The predicted minimum distance was 0.938 pc in 1.85 Myr. The third closest encounter detected by

the study was Proxima Centauri where the predicted minimum distance was 0.954 pc in 26700 years.

The closest passage in the past was made by a G8III star HIP 103738 with a minimum distance of 1.254 pc in 3.8 Myr ago. None of these stars were found in my study.

This study of García Sanchez used the Hipparcos catalogue to find close stellar encounters. The Hipparcos catalogue is complete to a visual magnitude of 7.3 mag, which is equivalent to a completeness to absolute magnitude (M_v) 4 mag at a radius of 50 pc. Thus the Hipparcos catalogue is incomplete if the absolute magnitude (M_v) is fainter than 4. The incompleteness of the Hipparcos data increase quickly if stars fainter than $M_v \simeq 4$ are considered. This paper also anticipated that then future missions such as Gaia would increase the accuracy of the data and for a large number of stars the study can be performed to find new candidate stars. This of course is the aim of this thesis.

Bailer-Jones (2015) did a new search to identify close stellar encounters of the past and future based on Van Leeuwen's re-reduction of the Hipparcos data van Leeuwen (2007a). He used the Hipparcos-2 catalogue (CDS catalogue: I/311/hip2) complemented by original Hipparcos and Tycho 2 catalogues along with several radial velocity survey that will also be used in the thesis. He computed 50000 stellar orbits through the Galaxy searching for close encounters. The search is then refined using a Monte Carlo simulation over the covariance of the data in order to characterise the uncertainties in times, distance and speeds of the encounters properly. This study also showed that modelling stellar encounters based on the linear motion model for most of the encounters leads to inaccurate and biased results.

This new search offered improvements over previous work. This new re- reduction of the Hipparcos data provides improvements over the accuracy of the astrometry, which has led to a reduction in the formal errors compared to the original Hipparcos reduction(which was initially used by (García-Sánchez et al. (2001))).This study also included then recent radial velocity surveys which increased the number of stars available for analysis. The study adopted a broad selection criteria to select candidate stars based on the linear motion approximation. This was applied to all the stars rather than a selection of stars based on some arbitrary distance or a fixed maximum radial velocity. Then a probabilistic approach was adopted to sample over the uncertainties in the astrometry and radial velocity to construct a complete distribution of the encounter distance, time and velocity for each star. With a well sampled distribution, the probability of

a star approaching at a certain distance can also be calculated. The study used four cross-matched input catalogues in order to obtain a full six phase space co-ordinates of a star in an equatorial co-ordinate system. The four catalogues used apart from Hipparcos-2 were: a reanalysis of the Geneva-Copenhagen Survey data(GCS) by Casagrande et al.(2011) (CDS catalogue: (J/A+A/530/A138); the Pulkovo catalogue (Gontcharov 2006, CDS III/252/table8), RAVE-DR4 (Kordopatis et al.2013, CDS catalogue III/272/rave4 Kordopatis et al. (2013)), xhip(Anderson and Francis (2012), CDS catalogue: V/137D/XHIP). Only stars with the full phase space parameters were retained. Some of these entries had negative or zero parallaxes which accounts for 3 percent of the Hipparcos 2 population. Those stars were also removed from the catalogue. Under the assumption of unaccelerated relative motion of the star with respect to the Sun, perihelion for all the stars were calculated. Only stars that had a perihelion of less than 10 pc were retained. Since the linear motion approximation does not provide more accurate perihelion parameters, the motion of the stars and the Sun was integrated through a 3D galactic potential. The study adopted three component time independent and axisymmetric model for the galactic potential from Miyamoto and Nagai (1975). The values of the model parameters were taken from Dauphole and Colin (1995). The orbits of the Sun and the stars were computed by numerically integrating the equation of motion through the potential using a seventh order Runge-Kutta-Fehlberg (rk78f) algorithm.

The study found 42, 14 and 4 stars within distances of within 2pc, 1pc and 0.5pc respectively. Of the 14 stars which have a distance of less than 1 pc, 5 of them have been found by previous studies. The closest star found in this study was HIP 85605 which has a 90 percent probability of passing the Sun at a distance of 0.04 and 0.20 pc between 240 and 470 Kyr from now. However the study claims the astrometric data for this star might be incorrect. If the astrometric data is incorrect for HIP 85605 then the closest encounter found by the study was HIP 89825 (GL 710) which has a 90 percent probability of coming within 0.10-0.44 pc in about 1.3 Myr.

This search for the close encounters is naturally biased by the available data towards the nearby bright stars. The Hipparcos survey is completed to $V=7.3$ mag. But 82 percent stars are fainter than this and also radial velocity are not available for all the stars. This study suggests a larger and more statistically meaningful analysis can be possible with the new GAIA data. GAIA is expected to improve the Hipparcos astrometric solution by a factor of 50 and extend to $G=20$ mag. The greater depth and better understood completeness of the GAIA data will result in a more accurate determination of the probability of encounters as a function of perihelion time, distance than was possible from Hipparcos.

1.4 Thesis aim and objective

In the previous section I have outlined previous work in identifying future and historic encounters with the Sun. I have also suggested a knowledge of the encounters is important to understand the history of the Oort cloud. The purpose of the study is to find all stars which have passed or will pass the Sun within 2pc over the past/future 10 Myr. I plan to improve the calculation of the perihelia (closest distance from an encounter to the Sun) of currently known encounters based on the precise astrometric parameters provided by the first Gaia data release (DR1). I also intend to find new close encounters in the DR1 and compare my results with the previous studies.

1.5 The structure of the thesis

In chapter 2, I introduce the data sources from which I have gathered data in order to create a complete catalogue of stars with the full five astrometric parameters and radial velocity. At this stage I have a catalogue of 216833 stars. This very large sample will be reduced in size by the subsequent chapter by limiting criteria of the closeness of the encounter. In chapter 3, I introduce a linear motion approximation method in order to filter out the stars that do not meet a certain encounter criterion. In this thesis, a distance of less than 10 pc from the Sun is chosen. This value is somewhat arbitrary but it creates a manageable data set for orbital integration. In chapter 4, I describe the construction of a clone cloud for each star. The parameters of a clone come from randomly sampling the initial conditions of each of the candidate stars in the new catalogue. I also describe the galaxy model adopted in this thesis which will be used to numerically integrate the orbits of the stars and their clone and as well as the Sun. This chapter will also contain the Monte Carlo simulation method which was chosen in order to simulate the Sun's and candidate star's orbit around the Galaxy. In chapter 5, I present my results. This will include a table of close encounters with a mean perihelion distance less than 2 pc. The distribution is also analysed and some comparisons made with previous work described in this introduction. I discuss the completeness of my survey in chapter 6. Finally, I make summary conclusions and give some suggestions for future projects on a longer timescale. This is a one year project, so a lot of the decisions on what work could be attempted were made due to the time constraints.

Chapter 2

Data

On September 14 2016 Gaia released its first catalogue also known as Gaia DR1 Gaia Collaboration et al. (2016). This catalogue was based on observations made between 25 July 2014 and 16 September 2015. The first catalogue contains:

- I. Positions on the celestial sphere (α, δ) and G magnitudes for all stars with acceptable formal errors on positions;
- II. The five parameters for astrometric solution (RA, DEC, PMRA (proper motion in the right ascension), PMDEC (proper motion in the declination), Parallax) for stars which are common to both the Tycho 2 catalogue and Gaia DR1 will be provided. This catalogue is based on TGAS (Michalik et al. (2015));
- III. Cross-matches will be provided between Gaia sources and Hipparcos-2, Tycho-2, 2MASS PSC, GSC2.3, PPM-XL, UCAC-4, SDSS DR10 / DR12, AllWISE, and URAT-1 data.

The basis of the study is one of the components of the first data release namely the Tycho Gaia Astrometric Solution (TGAS) (Michalik et al. (2015)). The number of TGAS sources is 2057050; within this number 93635 are from the Hipparcos 2 catalogue (van Leeuwen (2007b)) and 1963415 are from the Tycho 2 catalogue (Michalik et al. (2015)). This TGAS catalogue contains the five astrometric parameters (RA, DEC, PMRA, PMDEC, Parallax) and their uncertainties. The primary astrometric solution for Gaia DR1 contains five parameters of astrometry for 2057050 stars. This primary solution is based on the 118000 stars from the Hipparcos catalogue (Perryman et al. (1997), van Leeuwen (2007a)) and 2.36 million stars from the Tycho 2 catalogue (Høg et al. (2000)) as prior information.

For Hipparcos stars only the positions at J1991.25 or at an effective Tycho 2 observation epoch were used where the observation of Tycho 2 epoch were based on the mean of their α, δ epochs. The parallaxes and the proper motion values from these previous catalogues were not used as prior. This ensured the parallax and proper motions gathered are independent of the values stated in the previous catalogues.

2.1 Limitations of Gaia DR1

2.1.1 Survey Completeness

Gaia DR1 is not a complete survey. The source list is incomplete at the celestial position. Many bright stars at $G \leq 7$ mag are missing from DR1 as well. High proper motion stars are also absent in this initial data release. In dense areas the effective magnitude of Gaia stars maybe brighter up to several magnitudes. There is also a notable decrease on completeness of the detection of the secondaries.

2.1.2 Astrometry

All sources were treated as a single star without taking their radial velocity into account. Any astrometric effect due to the orbital motion of the binaries or due to the perspective acceleration were ignored. A global parallax zero point offset of ± 0.1 mas could be present. During the validation of DR1 it was found to ± 0.3 mas.

2.2 Obtaining the Radial Velocity

The first Gaia Data Release only contains the five astrometric parameters of a star (RA, DEC, Parallax, PMRA, PMDEC). Radial velocity were obtained by cross matching with four other input catalogues:

- I. A re-analysis of the Geneva-Copenhagen Survey (GCS, Casagrande et al. (2011))
- II. Pulkovo Catalogue (Gontcharov (2006))
- III. RAVE DR5 (Kunder et al. (2017))
- IV. Xhip Catalogue (Anderson and Francis (2012))

2.2.1 RAVE DR5

The Radial Velocity Experiment (RAVE) is a multi-fibre spectroscopic astrometric survey of stars in the Milky Way which uses the 1-2 metre UK Schmidt Telescope of the Australian Astronomical Observatory(AAO). One of the aims of the project is to determine radial velocities of many faint stars in the Milky Way. So far this project has produced five data releases. The latest data release RAVE DR5 (Kunder et al. 2017) contains spectral analysis of 457588 stars. Cross matching between RAVE DR5 and TGAS gives more than 216000 stars.

2.3 Completion of the Catalogue

The five astrometry values and the radial velocity together define the six phase space co-ordinates $(\alpha, \delta, \pi, \mu_\alpha, \mu_\delta, rv)$ of a star in an equatorial co-ordinate system. The units of these six astrometric parameters are respectively (deg, deg, mas, $masyr^{-1}$, $masyr^{-1}$, kms^{-1}). Astrometric parameters will allow me to derive initial conditions for each star's orbit. Together with the galactic potential these can determine a star's orbit both in past and future. To summarise, the thesis makes use of four cross matched input catalogues in order to obtain radial velocities for TGAS stars. Only the stars that have all the six astrometric parameters were retained. At this stage I have 216833 stars with a full set of astrometric parameters with various degrees of confidence in the radial velocity.

Chapter 3

Initial Selection of candidates

3.1 Linear Motion Approximation

I first estimate the distance of the closest approach of the star to the Sun under the assumption of unaccelerated relative motion of the star with respect to the Sun.

I neglect the gravity and assume that a star moves with constant velocity v with respect to the Sun. The closest distance (q) can be written as

$$d_{ph} = 1000 \frac{1}{\pi} \frac{v_t}{v} \quad (3.1)$$

where π is the parallax in mas, d_{ph} is the perihelion distance, v_t is the transverse velocity and v is the total velocity.

$$v_t = m \frac{\sqrt{\mu_\alpha^2 + \mu_\delta^2}}{\pi} \cos \delta \quad (3.2)$$

where μ_α is the proper motion in the right ascension in mas/yr and μ_δ is the proper motion in the declination in mas/yr and m is a numerical conversion value equal to 4.74372.

The total velocity then is

$$v = \sqrt{v_t^2 + v_r^2} \quad (3.3)$$

where v_r is the radial velocity. Aside from the proper motion, all other velocities are in km/s.

This linear motion approximation to determine the closest approach of a star is not very accurate particularly for stars which are far away from the Sun or are moving slowly relative to the Sun. So only those stars that have a perihelion distance less than 10 pc were retained for further analysis. The limit is chosen to be much larger than the distances of interest (for encounter that are significant for the Solar System). 1003 stars have been found with a perihelion distance less than 10 pc relative to the Sun.

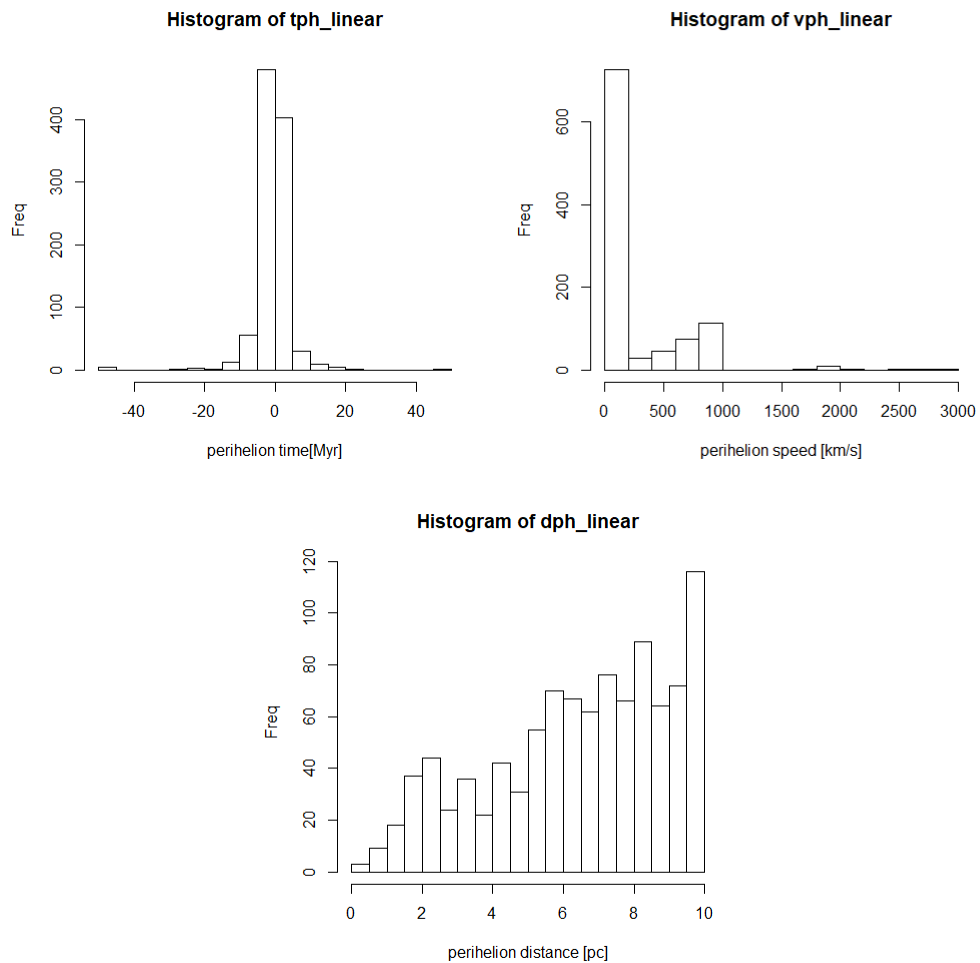


FIGURE 3.1: distribution of the encounter parameters of all stars with d_{ph}^{lin} less than 10pc. Most the encounters occur within ± 2 Myr. Clearly there are some outliers in the perihelion speed distributions which is likely caused by the high radial velocities. The number of encounters rises roughly linearly along a straight line.

Chapter 4

Finding encounters through simulations of stellar motions

4.1 Sampling the initial conditions of the candidate stars

In order to estimate the uncertainty in determining the encounter parameters, 1000 clones are drawn from the covariance matrix for each star. 1000 clones were chosen in order to provide a statistically representative sample for uncertainty estimation. These clones were drawn from a multivariate normal distribution. A multivariate normal distribution is a generalisation of the one dimensional normal distribution to higher dimensions. A multivariate normal distribution is often used to describe, at least approximately, any set of (possibly) correlated real-valued random variables each of which clusters around a mean value. The covariance matrix is an important concept to help understand the shape and size of the multivariate normal distribution. A covariance matrix is a matrix with elements in the i,j position representing the covariance between the i^{th} and j^{th} elements of a random vector. Closely related to a covariance matrix is the correlation matrix. For random variables X and Y , if the correlation co-efficient is ρ then the covariance of X and Y can be written as

$$\rho \times \sigma_X \sigma_Y = cov[X, Y] \quad (4.1)$$

where σ_X and σ_Y are the variances in X and Y .

The matrix can be written as following

$$C = \begin{bmatrix} \sigma_X^2 & cov[X, Y] \\ cov[X, Y] & \sigma_Y^2 \end{bmatrix} \quad (4.2)$$

Gaia TGAS provides uncertainty for five of the astrometric parameters and their correlation coefficient. I assume that radial velocity is not correlated with the other parameters and thus draw clones from a normal distribution. Clones were created for each star by using the 'mvtnorm' (Genz et al., 2018) package in R, which is an algorithm for interrogating a multivariate normal distribution. The covariance matrix to create the clones for any candidate is illustrated below

$$U = \begin{bmatrix} \sigma_\alpha^2 & cov[\alpha, \delta] & cov[\alpha, \pi] & cov[\alpha, \mu_\alpha] & cov[\alpha, \mu_\delta] & 0 \\ cov[\alpha, \delta] & \sigma_\delta^2 & cov[\delta, \pi] & cov[\delta, \mu_\alpha] & cov[\delta, \mu_\delta] & 0 \\ cov[\alpha, \pi] & cov[\delta, \pi] & \sigma_\pi^2 & cov[\pi, \mu_\alpha] & cov[\pi, \mu_\delta] & 0 \\ cov[\alpha, \mu_\alpha] & cov[\delta, \mu_\delta] & cov[\pi, \mu_\alpha] & \sigma_{\mu_\alpha}^2 & cov[\mu_\alpha, \mu_\delta] & 0 \\ cov[\alpha, \mu_\delta] & cov[\delta, \mu_\delta] & cov[\pi, \mu_\delta] & cov[\mu_\alpha, \mu_\delta] & \sigma_{\mu_\delta}^2 & 0 \\ 0 & 0 & 0 & 0 & 0 & \sigma_{rv}^2 \end{bmatrix} \quad (4.3)$$

Figure 4.1 shows the distribution of the initial conditions of a typical candidate star. These distributions are reasonably smooth. Larger clone clouds are possible and have been created with a population of 2 million clones per candidate star. Although the distributions are smoother, the increase in computational time in order to integrate these 2 million data set is excessive. Accounting for the systematic error in parallax which is ± 0.3 mas Gaia Collaboration et al. (2016), makes very little changes in the encounter parameter. For example the closest encounter in my catalogue HIP 89825(GL 710)'s encounter parameters did not make a significant change while accounting for the offset in the parallax. Gaia DR1s limitations were also discussed in chapter 2.1.

4.2 The galactic potential

In order to improve the accuracy of the encounter parameters of candidate stars, their motion was integrated through a three dimensional axisymmetric galactic potential. This axisymmetric galactic model in cylindrical co-ordinate (r, ϕ, z) is

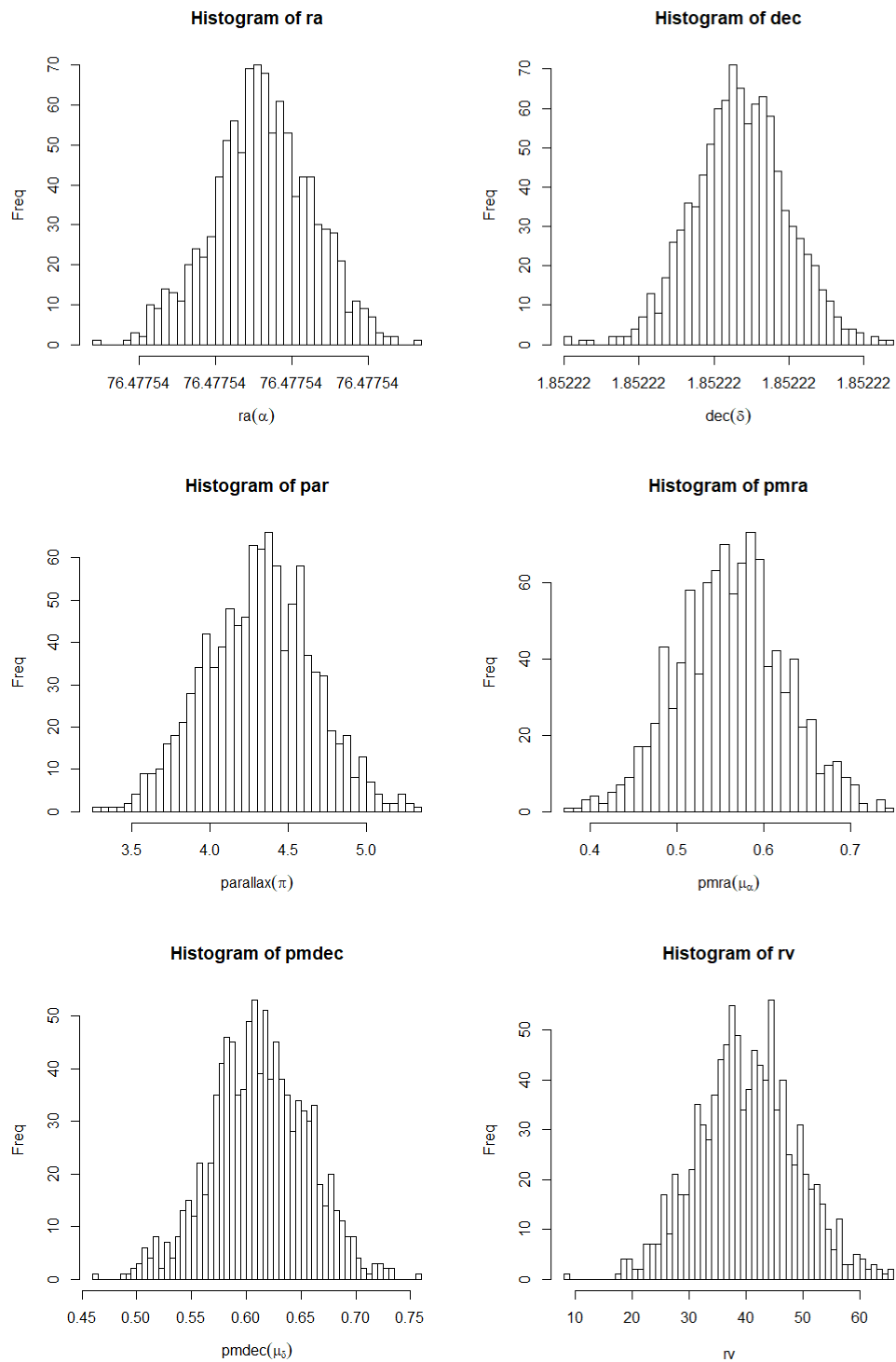


FIGURE 4.1: A typical distribution of astrometric parameters for a 1000 clones for one candidate star. In this case the star chosen is HIP 23714.

$$\phi = \phi_h + \phi_b + \phi_d \quad (4.4)$$

where h , b and d represents the halo, bulge and disk of the galaxy. The components are defined (in cylindrical co-ordinates) as

$$\phi_{b,h} = -\frac{GM_{b,h}}{\sqrt{R^2 + z^2 + b_{b,h}^2}} \quad (4.5)$$

$$\phi_d = -\frac{GM_d}{\sqrt{R^2 + (a_d + \sqrt{(z^2 + b_d^2)})^2}} \quad (4.6)$$

The bulge and halo are spherically symmetric distributions with their own distinct length scales b_b and b_h . The bulge and halo are modelled after Plummer's model (Plummer (1911)). The third component is the axisymmetric disk is based on that introduced by Miyamoto and Nagai (1975). The disk is a highly flattened spheroid with length scales a_d and b_d . R represents cylindrical distance from the galactic centre and $z=0$ is the mid plane of the disk. M is the mass of the component and b , a are the scale lengths and G is the gravitational constant. M_b , M_h and M_d are the masses of the bulge, halo and disk respectively. The values for these model parameters used in this thesis were adopted from García-Sánchez et al. (2001).

This is a simplification of the true potential of the galaxy. This same potential was adopted by García-Sánchez et al. (2001), Bailer-Jones (2015), Feng and Bailer-Jones (2014). Although other Galactic models are available, my results are relatively insensitive to the choice of Galactic models due to the fact that most encounters occur within 10 Myr, much shorter than the orbital period of the Sun (about 200 Myr) around the Galactic centre. However I will test this in chapter 6. The reason is that since the distance to most of the stars are smaller than the scale length of the components, the experience of the potentials felt by the Sun and star are not dramatically different.

The adopted values of the Sun's velocity components with respect to the Local Standard of Rest(LSR) are $(U_\odot, V_\odot, W_\odot) = (11.1 \pm 0.72, 12.24 \pm 0.47, 7.25 \pm 0.36) \text{ kms}^{-1}$. A precise value for the Sun's height above the vertical plane (z_\odot) is yet to be determined. Quite a lot of studies have been done in the past to determine The Sun's vertical height from the galactic midplane.

TABLE 4.1: Galactic model parameters adopted from García-Sánchez et al. (2001)

components	Parameters	Value
Bulge	M_b	$1.3955 \times 10^{10} M_\odot$
	b_b	0.35 kpc
Halo	M_h	$6.9766 \times 10^{11} M_\odot$
	b_h	24.0 kpc
Disk	M_d	$7.9080 \times 10^{10} M_\odot$
	a_d	3.55 kpc
	b_d	0.25 kpc

Here I adopt the Sun's vertical height above the plane from Majaess et al. (2009) which z_\odot is 26 pc. The distance from the Sun to the galactic centre is taken to be 8.27 kpc (Schönrich (2012)).

TABLE 4.2: Solar parameters adopted

components	Parameters	Value
Solar Parameters	z_\odot	26 pc
	R_\odot	8.27 kpc
	$(U_\odot, V_\odot, W_\odot)$	$(11.1 \pm 0.72, 12.24 \pm 0.47, 7.25 \pm 0.36) \text{ kms}^{-1}$

4.3 Co-ordinate transformation

In order to study the motion of the stars in the Galaxy, I convert the positions and velocities of stars from the equatorial to the Galactic co-ordinate system. Since the equatorial co-ordinates and galactic co-ordinates do not share the same zero point for longitude, it is a non trivial procedure.

A more general way to solve this co-ordinate transformation is by using Euler angles. This process follows the co-ordinate transformation from (http://personal.psu.edu/rbc3/A501/c1_spherical_astronomy.pdf).

I convert the equatorial coordinates into Cartesian coordinates, and then rotate the coordinate system about the z , x , and z' axes subsequently. Each of these rotations is a simple matrix multiplication which uses a 3D rotation matrix. The Euler angles are

- the angle required to match the ascending node (α_0)
- the inclination of the galactic pole from the celestial equator (δ_0)
- the angle required to have the galactic centre at 0 degree (l_0)

$$\begin{bmatrix} x \\ y \\ z \end{bmatrix} = \begin{bmatrix} \cos\theta \cos\phi \\ \sin\theta \cos\phi \\ \sin\phi \end{bmatrix} \quad (4.7)$$

$$\begin{bmatrix} x' \\ y' \\ z' \end{bmatrix} = \begin{bmatrix} \cos l_0 & \sin l_0 & 0 \\ -\sin l_0 & \cos l_0 & 0 \\ 0 & 0 & 1 \end{bmatrix} \begin{bmatrix} 1 & 0 & 0 \\ 0 & \cos\delta_0 & \sin\delta_0 \\ 0 & -\sin\delta_0 & \cos\delta_0 \end{bmatrix} \begin{bmatrix} \cos\alpha_0 & \sin\alpha_0 & 0 \\ -\sin\alpha_0 & \cos\alpha_0 & 0 \\ 0 & 0 & 1 \end{bmatrix} \begin{bmatrix} x \\ y \\ z \end{bmatrix} \quad (4.8)$$

Converting back to spherical co-ordinates it stands as

$$\cos b \cos(l - l_0) = \cos\delta \cos(\alpha - \alpha_0) \quad (4.9)$$

$$\cos b \sin(l - l_0) = \cos\delta \sin(\alpha - \alpha_0) + \sin\delta \sin\delta_0 \quad (4.10)$$

$$\sin b = \sin\delta \cos\delta_0 - \cos\delta \sin(\alpha - \alpha_0) \sin\delta_0 \quad (4.11)$$

$$\cos\delta \sin(\alpha - \alpha_0) = \cos b \sin(l - l_0) \cos\delta_0 - \sin b \sin\delta_0 \quad (4.12)$$

$$\sin\delta = \cos b \sin(l - l_0) \sin\delta_0 + \sin b \cos\delta_0 \quad (4.13)$$

Where $\alpha_0(1950) = 282.25^\circ$, $\delta_0(1950) = 62.6^\circ$, $l_0 = 33^\circ$ (http://personal.psu.edu/rbc3/A501/c1_spherical_astronomy.pdf).

Given the proper motion components and radial velocity and parallax of a star, the galactic space velocity components (U,V,W) can be found (Johnson and Soderblom, 1987). A right handed co-ordinate system was used to calculate U,V,W so that they are positive in the direction of the galactic centre, galactic rotation and north galactic pole respectively. The galactic space velocity components are then,

$$\begin{bmatrix} U \\ V \\ W \end{bmatrix} = B \begin{bmatrix} rv \\ k\mu_\alpha/\pi \\ k\mu_\delta/\pi \end{bmatrix} \quad (4.14)$$

where rv is in kms^{-1} , μ_α and μ_δ is in $masyr^{-1}$ and π is in mas . k is the equivalent of kms^{-1} to one astronomical unit in one year which is 4.74057 and $B = T \times A$ where T and A are transformation matrix defined below

T is the transformation matrix which is given below.

$$T = \begin{bmatrix} \cos\theta_0 & \sin\theta_0 & 0 \\ \sin\theta_0 & -\cos\theta_0 & 0 \\ 0 & 0 & 1 \end{bmatrix} \begin{bmatrix} -\sin\delta_{NGP} & 0 & \cos\delta_{NGP} \\ 0 & -1 & 0 \\ \cos\delta_{NGP} & 0 & \sin\delta_{NGP} \end{bmatrix} \begin{bmatrix} \cos\alpha_{NGP} & \sin\alpha_{NGP} & 0 \\ \sin\alpha_{NGP} & -\cos\alpha_{NGP} & 0 \\ 0 & 0 & 1 \end{bmatrix} \quad (4.15)$$

A defines a co-ordinate transformation matrix.

$$A = \begin{bmatrix} \cos\alpha\cos\delta & -\sin\alpha & -\cos\alpha\sin\delta \\ \sin\alpha\cos\delta & \cos\alpha & -\sin\alpha\sin\delta \\ \sin\delta & 0 & -\cos\delta \end{bmatrix} \quad (4.16)$$

The RA and DEC of the North Galactic Pole are $\alpha_{NGP} = 192.25^\circ$ and $\delta_{NGP} = 27.4^\circ$ (Johnson and Soderblom, 1987)

4.4 Numerical integration of the candidate stars

As mentioned in the previous sections of this chapter in order to acquire a more accurate perihelion estimation, the candidate star's orbit and Sun's orbit were numerically integrated through a galactic potential (section 4.2). I simulate the orbits of the stars from -10 Myr to +10 Myr with a time step of 0.01 Myr. The nominal orbits for the candidate stars were numerically integrated using the 'Adams' method which is implemented in an R package 'deSolve' (Soetaert et al., 2010). Since 0.01 Myr may not resolve the perihelion distance properly, using a linear motion approximation at the point where the separation between the Sun and the star is at the minimum, a refined perihelion distance can be calculated. The refined time and distance at the periapsis can be calculated by using the following equation

$$t_{ph} = -\frac{r_0 v_0}{v_0^2} \quad (4.17)$$

$$d_{ph} = r_0 + v_0 t_{ph} \quad (4.18)$$

$$v_{ph} = v_0 \quad (4.19)$$

where r_0 and v_0 are the position and velocity of the candidate star with respect to the Sun. This approach is similar to that of Bailer-Jones (2015).

These 1000 clones per candidate star gives a probability distribution over the parameter. From these I calculate the mean for the perihelion parameters (time,distance and velocity). The reason behind choosing mean over median is to have a statistic which is influenced by the whole distribution. Since the distribution of perihelia distances for the candidate stars is quite asymmetric, I calculate the 5% and 95% quantiles of the encounter parameters.

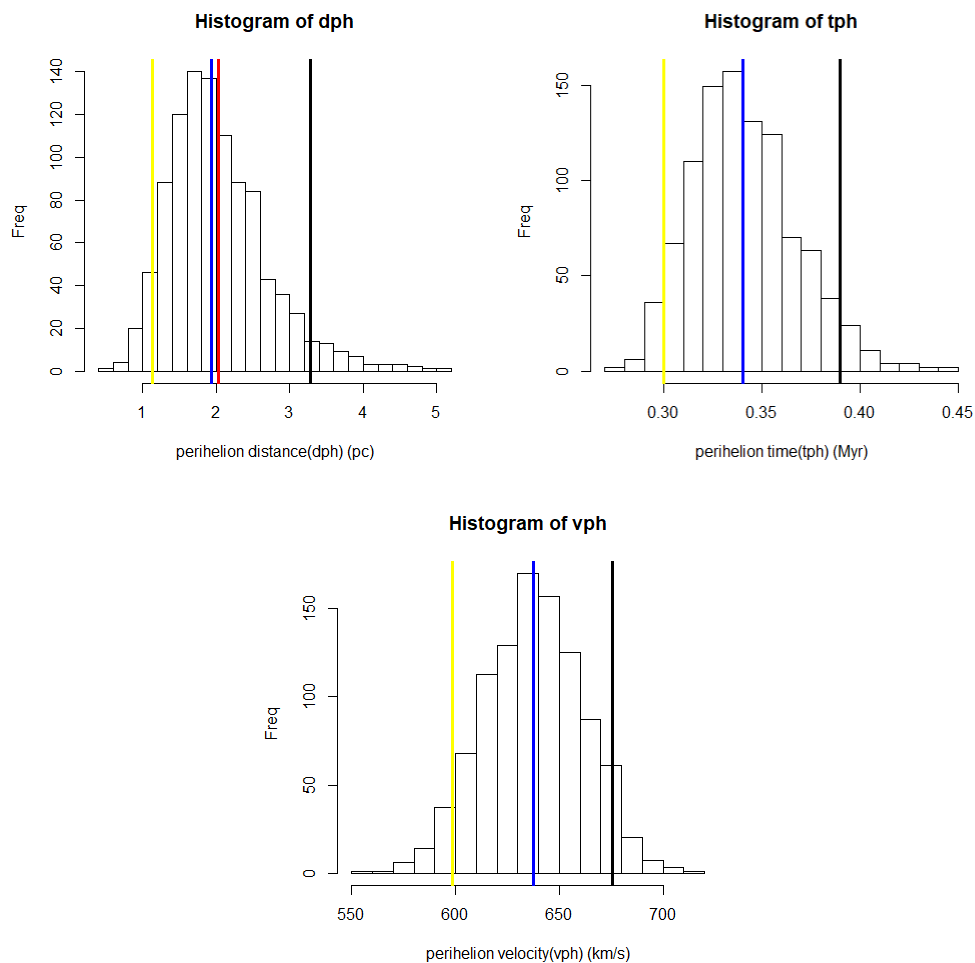


FIGURE 4.2: distribution of encounter parameters from 1000 clones of TYC 8532-891-1. The red,blue,yellow and black lines represents the mean, nominal, 5% and 95% quantiles of encounter parameters of TYC 8532-891-1 . Sometimes not all of these line appear in the histogram because the values coincide with each other.

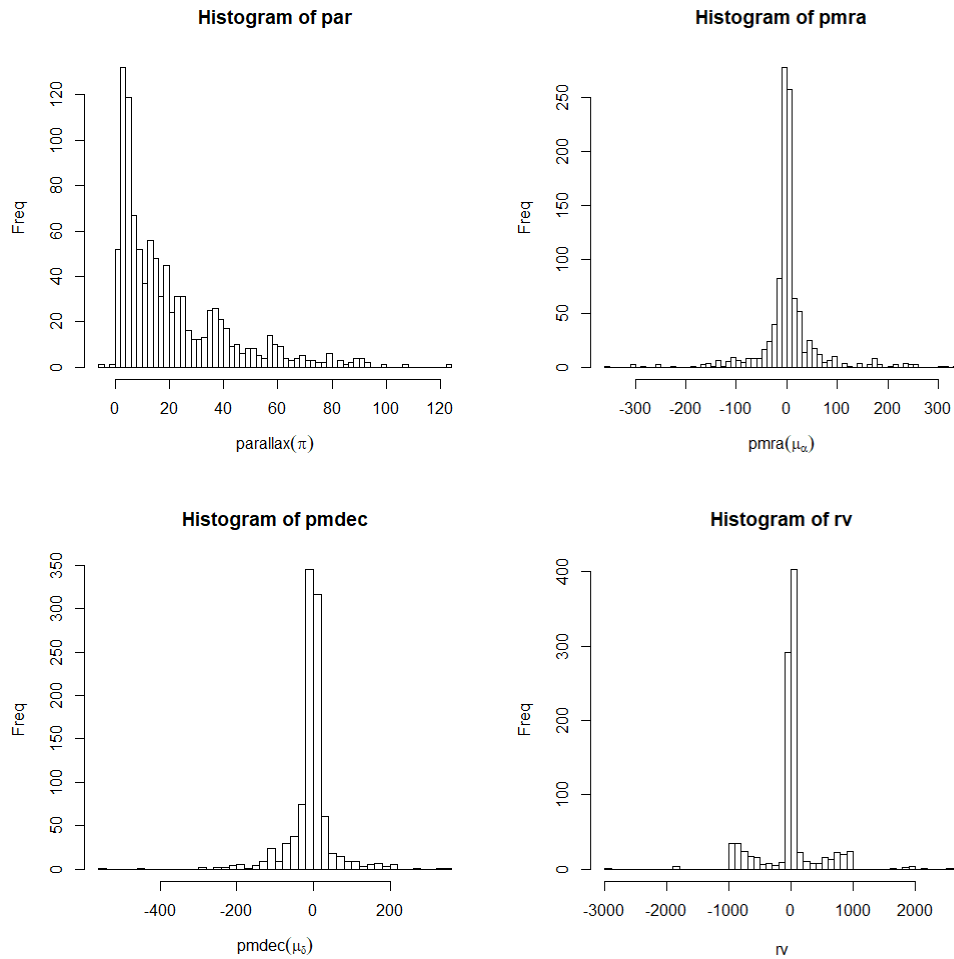


FIGURE 4.3: distribution of proper motions (μ_α , μ_δ) and radial velocity of the candidate stars. One striking feature in this plot are the elevated wings in the radial velocity histogram. These reflect the presence of some high velocities that may prove to be nonphysical when better spectroscopy is available.

4.5 Principal component analysis

A close observation of the three dimensional plot of the 1000 clones of a star will show that they are formed in a swarm of 1000 clones coming as close as the perihelion distance. These three dimensional plot also shows this distribution of the clones to be very flat and after applying necessary rotation these distributions can easily be shown in a two dimensional plot.

Principal Component Analysis is a statistical procedure that uses an orthogonal transformation which converts a set of observations of possibly correlated variables into a set of values that are linearly uncorrelated variables which are called principal components. Principal component analysis gives a sense of the global shape of the distribution in an overall sense. The principal

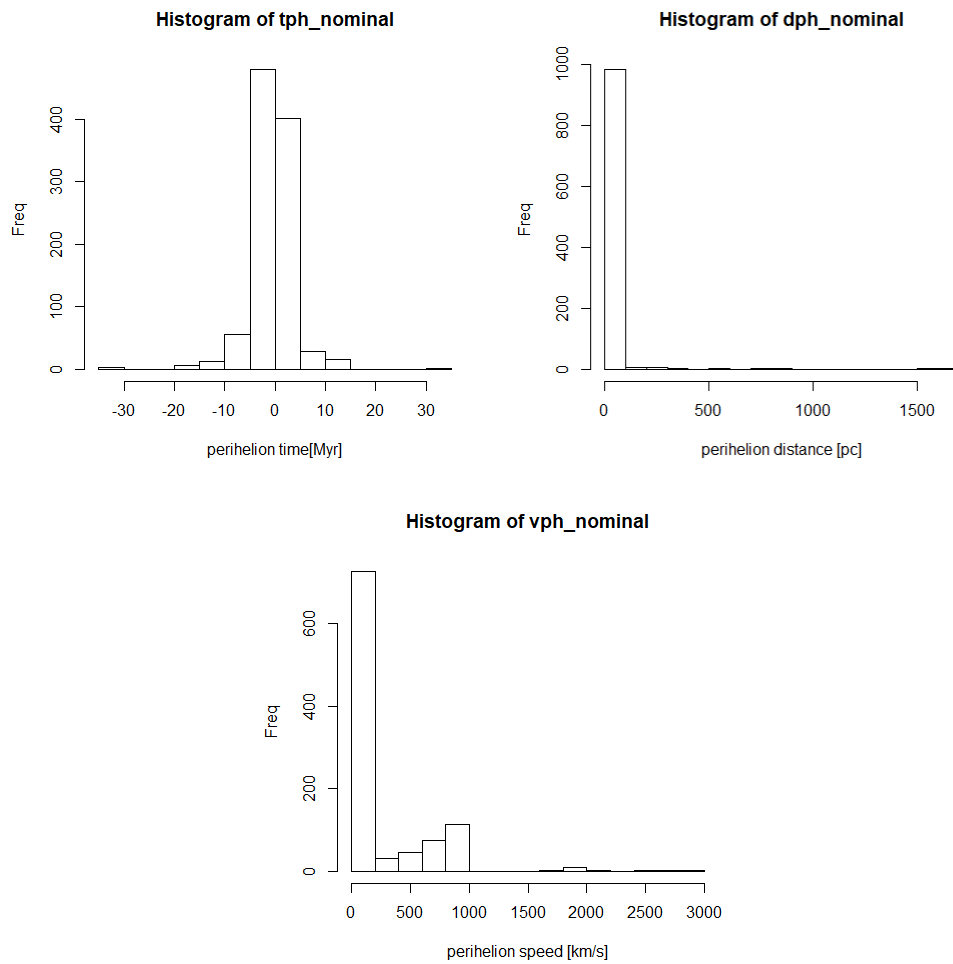


FIGURE 4.4: distribution of the nominal encounter parameters of the candidate stars. The outliers in the velocity shows the presence of the high radial velocity stars. A closer look at the distribution of the encounter distance will show that there are some nominal distances that are further away from the 10 pc limit. This may have been caused by large errors in the radial velocity.

axes are defined by the initial distribution and the size of the breadth on the distribution and the more the axes differ in size, the greater the anisotropy in the distribution.

The numerical simulation provides galactocentric co-ordinates for both Sun and the star. In order to go back to the heliocentric frame the Sun's co ordinates are to be subtracted from the star's co-ordinates. These co- ordinates can then be presented in a covariance matrix. This method is similar to the Dybczyński and Berski (2015) method of conducting a principal component

analysis. This covariance matrix is as follows

$$P = \begin{bmatrix} cov(x,x) & cov(x,y) & cov(x,z) \\ cov(y,x) & cov(y,y) & cov(y,z) \\ cov(y,x) & cov(z,y) & cov(z,z) \end{bmatrix} \quad (4.20)$$

A Jacobi transformation was used to determine the eigenvalues and corresponding eigenvectors. A 3x3 matrix is constructed where the in the first column eigenvector corresponding to the largest eigenvalue is placed and so forth. This matrix along with the vector of (x,y,z) of clone co-ordinates in heliocentric frame gives the new co ordinates(x',y',z')

$$\begin{bmatrix} x' \\ y' \\ z' \end{bmatrix} = \begin{bmatrix} v_1 & v_2 & v_3 \end{bmatrix}^T \begin{bmatrix} x \\ y \\ z \end{bmatrix} \quad (4.21)$$

I have used the `pca` function in MATLAB to perform the principal component analysis. The `coeff` syntax returns the principal component analysis which is also known as loadings for the $n \times p$ matrix X. Rows of matrix X corresponds to observations and columns to variables. $p \times p$ matrix represents the co-efficient matrix. Each column of the `coeff` contains a co-efficient for each principal component in a descending order of component variance. The `score` and `latent` syntaxes returns the component scores and the principal component variances. Rows of `score` correspond to observations and the columns to components. The principal component variances are the eigenvalues of covariance matrix of X.

A closer look at figure 4.5 shows that there is a comparable level of scattering in the planes x-y plane and the y-z. The distribution of the clones in the x-z plane is flat. Figure 4.6 shows the distributions of clones of a star with principal component analysis. The levels of scattering in the x'y',y'z,x'z' in the galactic heliocentric frame. From this figure it can be clearly seen that the cluster of clones is very flat.

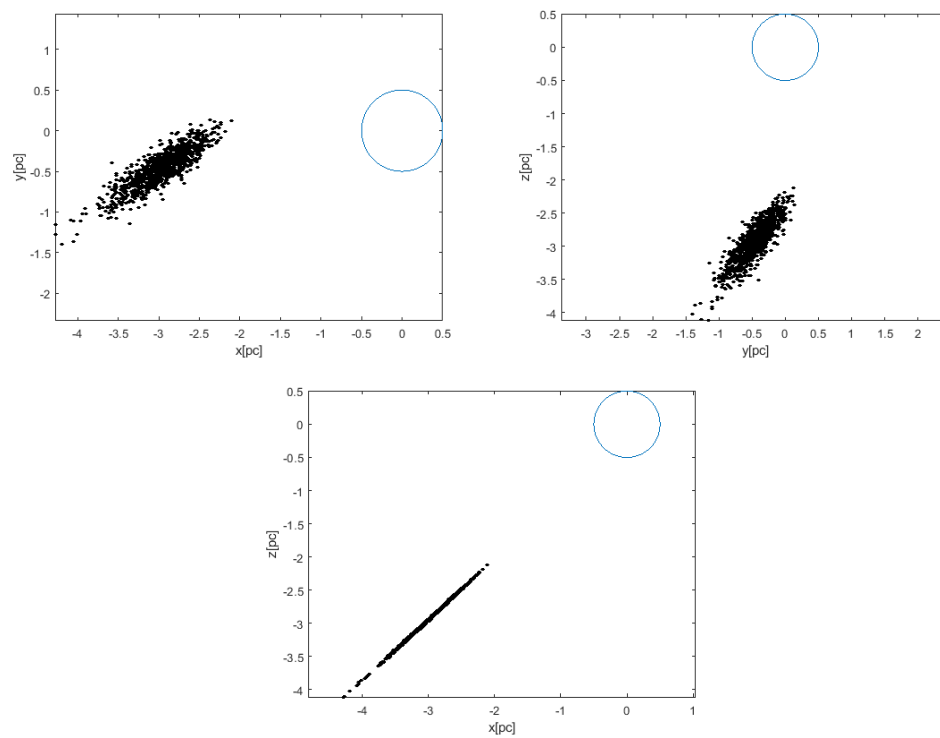


FIGURE 4.5: distribution of 1000 clones of star TYC 5009-137-1 in the original galactic heliocentric frame. The black dots represent the clones of the star and the blue circle represents the Oort cloud at 0.5 pc.

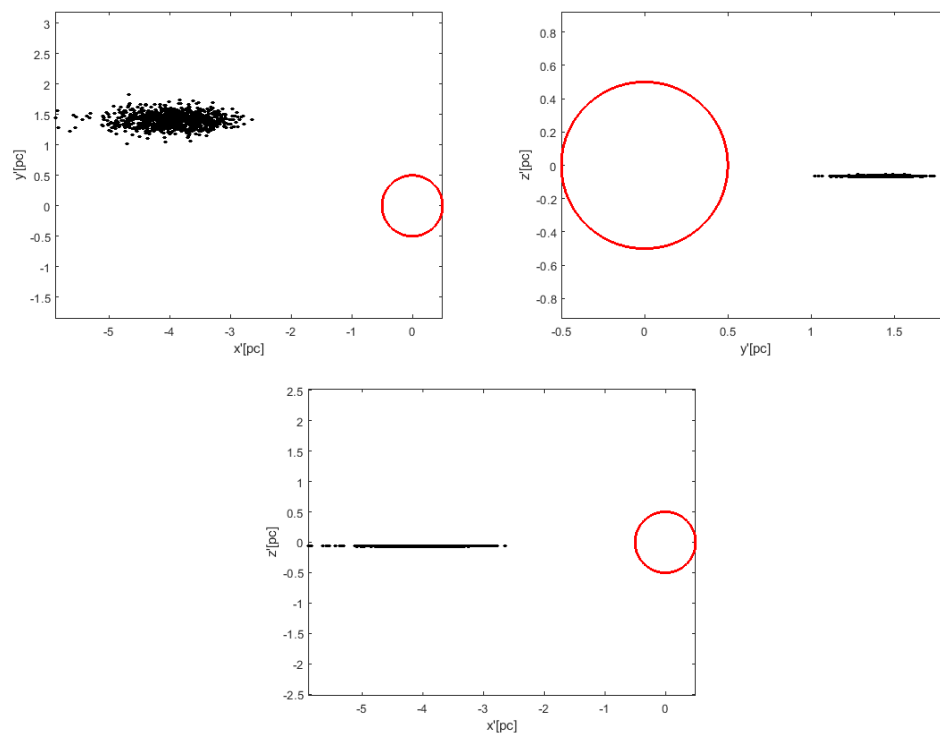


FIGURE 4.6: Distribution of the clones of TYC 5009-137-1 in the $x'y'z'$ heliocentric frame which has been obtained from the xyz frame after rotations determined using principal component analysis. The green dots represents the clones of TYC 5009-137-1. The black dot is the Sun and the Red circle represents the Oort cloud at 0.5pc.

Chapter 5

Results

5.1 A new catalogue and the analysis of the new catalogue

Some of the TGAS stars have appeared more than once across the catalogue. They were treated as single stars. Applying the linear motion approximation to 216833 stars, 1003 have been found to have a perihelion distance less than 10pc. After that only these 1003 stars were considered as potential encounter candidates. Their orbits (both the nominal and 10^3 clones) were integrated and the encounter parameters (d_{ph}, t_{ph}, v_{ph}) were calculated. This involved 1.003 million orbital integration each 1000 orbital integration taking around 2.5 minutes to complete. Table 5.1 below represents the different limits on the perihelion after orbit integration. Tables 5.2 and 5.3 represent the stars with a mean perihelion distance (d_{ph}^{mean}) less than 2pc. These tables also show the nominal values of the encounter parameter of these stars and their 5% and 95% quantiles. Negative t_{ph} value corresponds to an encounter that occurred in the past.

Figure 5.2 shows the mean perihelion distance vs mean perihelion time. It can be seen in figure 5.2 that most of the encounters occur within 2 Myr while a few of the encounters occur at 5-10

d_{max}	Number of stars
∞	1003
10	846
5	240
2	46
1	7
0.5	2

TABLE 5.1: the number of stars with different perihelion distances after orbital integration.

ID	cat	d_{ph}^{nom} pc	d_{ph}^{mean} pc	$d_{ph}^{5\%}$ pc	$d_{ph}^{95\%}$ pc	t_{ph}^{nom} Myr	t_{ph}^{mean} Myr	$t_{ph}^{5\%}$ Myr	$t_{ph}^{95\%}$ Myr
HIP 89825	p	0.063	0.063	0.037	0.089	1.35	1.35	1.31	1.41
HIP 89825	x	0.063	0.063	0.037	0.089	1.35	1.35	1.31	1.41
TYC 6403-151-1	r	0.415	0.459	0.284	0.74	0.06	0.07	0.04	0.11
TYC 6622-652-1	r	0.532	0.553	0.307	0.867	-0.1	-0.1	-0.11	-0.09
TYC 8822-592-1	r	0.603	0.606	0.521	0.712	-0.1	-0.1	-0.11	-0.09
TYC 9524-1668-1	r	0.842	0.863	0.581	1.205	0.19	0.19	0.17	0.21
TYC 7567-304-1	r	0.959	0.961	0.857	1.073	0.09	0.09	0.09	0.1
TYC 9339-404-1	r	1.023	1.033	0.802	1.292	0.15	0.15	0.14	0.16
TYC 4888-146-1	r	1.138	1.771	0.603	4.286	-0.13	-0.15	-0.26	-0.09
HIP 94512	p	1.15	1.159	0.963	1.377	3.38	3.39	3.15	3.66
TYC 7973-1145-1	r	1.189	1.202	1.076	1.357	0.23	0.23	0.21	0.24
TYC 5033-879-1	r	1.365	1.668	0.662	3.026	-0.71	-0.71	-0.84	-0.61
HIP 30344	x	1.385	1.389	1.285	1.496	-1.56	-1.56	-1.67	-1.45
TYC 5302-849-1	r	1.411	1.414	1.33	1.499	0.08	0.08	0.08	0.08
TYC 6468-434-1	r	1.428	1.436	1.248	1.652	0.15	0.15	0.14	0.17
TYC 8894-1893-1	r	1.435	1.438	1.277	1.618	0.1	0.1	0.09	0.11
TYC 8855-429-1	r	1.466	1.467	1.396	1.547	0.09	0.09	0.09	0.1
TYC 7597-372-1	r	1.499	1.584	0.771	2.618	0.26	0.26	0.23	0.3
HIP 26335	p	1.569	1.568	1.538	1.596	-0.5	-0.5	-0.51	-0.49
HIP 26335	x	1.565	1.564	1.544	1.585	-0.5	-0.5	-0.5	-0.49
HIP 40317	p	1.592	1.595	1.452	1.753	-2.22	-2.22	-2.3	-2.15
TYC 6471-517-1	r	1.604	1.603	1.528	1.679	-0.08	-0.08	-0.08	-0.07
TYC 8769-364-1	r	1.619	1.662	1.123	2.303	-0.33	-0.33	-0.38	-0.3
TYC 8856-611-1	r	1.623	1.693	1.177	2.291	-0.28	-0.29	-0.32	-0.25
HIP 25240	p	1.628	1.627	1.504	1.756	-0.95	-0.95	-0.99	-0.91
HIP 25240	x	1.629	1.63	1.504	1.768	-0.95	-0.95	-0.99	-0.91
TYC 9327-264-1	r	1.652	1.891	0.97	3.072	-1.89	-1.9	-2.02	-1.78
HIP 25240	g	1.668	1.675	1.532	1.83	-0.97	-0.97	-1.02	-0.93
TYC 8560-8-1	r	1.697	1.719	1.253	2.245	-0.63	-0.63	-0.65	-0.61
TYC 8496-973-1	r	1.702	1.767	1.343	2.375	-0.22	-0.23	-0.3	-0.18
TYC 9163-286-1	r	1.705	1.812	0.543	3.588	-0.57	-0.57	-0.66	-0.49
TYC 5046-284-1	r	1.705	1.715	1.509	1.929	0.21	0.21	0.19	0.22
HIP 30344	p	1.733	1.735	1.663	1.816	-1.95	-1.95	-2.03	-1.89
HIP 30344	g	1.757	1.759	1.697	1.827	-1.98	-1.98	-2.03	-1.93
TYC 7465-1009-1	r	1.773	1.875	1.321	2.696	-0.13	-0.13	-0.17	-0.1
HIP 30067	x	1.806	1.807	1.74	1.872	-0.65	-0.65	-0.66	-0.64
HIP 30067	g	1.809	1.811	1.749	1.878	-0.65	-0.65	-0.66	-0.64
HIP 30067	p	1.809	1.808	1.744	1.873	-0.65	-0.65	-0.66	-0.64
TYC7593-343-1	r	1.89	1.936	1.481	2.483	0.46	0.46	0.41	0.52
HIP 26624	p	1.909	1.911	1.727	2.114	-1.85	-1.85	-1.92	-1.78
HIP 26624	x	1.909	1.911	1.727	2.114	-1.85	-1.85	-1.92	-1.78
TYC 9528-1994-1	r	1.929	1.939	1.716	2.175	-0.1	-0.1	-0.11	-0.1
TYC 9446-745-1	r	1.945	1.958	1.698	2.263	0.06	0.06	0.06	0.07
TYC 8470-213-1	r	1.954	1.962	1.788	2.16	-0.17	-0.17	-0.18	-0.15
TYC 6080-573-1	r	1.982	1.99	1.733	2.285	0.06	0.06	0.06	0.07
HIP 20359	x	1.995	1.995	1.942	2.047	0.36	0.36	0.36	0.36

TABLE 5.2: Encounter parameters for all the stars with a mean perihelion distance less than 2 pc. The column named cat indicates the name of the input catalogue where the radial velocity were obtained from g= GCS catalogue, P= pulkuvo Catalogue, r= RAVE DR5 catalogue, x= XHIP catalogue. The encounter parameters are set as d_{ph}, t_{ph} respectively, nom represents the nominal values, mean represents the mean values, 5% and 95% represents the 5% and 95% quantiles of each encounter parameter.

ID	cat	v_{ph}^{nom} kms^{-1}	v_{ph}^{mean} kms^{-1}	$v_{ph}^{5\%}$ kms^{-1}	$v_{ph}^{95\%}$ kms^{-1}
HIP 89825	p	13.8	13.78	13.32	14.27
HIP 89825	x	13.8	13.78	13.32	14.27
TYC 6403-151-1	r	850.22	848.82	481.19	1231.06
TYC 6622-652-1	r	741.1	741.19	719.84	762.31
TYC 8822-592-1	r	1969.39	1969.39	1969.38	1969.4
TYC 9524-1668-1	r	887.45	887.45	887.44	887.46
TYC 7567-304-1	r	625.91	626.74	581.81	670.38
TYC 9339-404-1	r	929.62	930.64	881.24	976.21
TYC 4888-146-1	r	1896.76	1896.78	1896.74	1896.88
HIP 94512	p	30.4	30.42	29.94	30.93
TYC 7973-1145-1	r	537.22	536.84	517.41	555.44
TYC 5033-879-1	r	532.62	532.41	521.91	542.38
HIP 30344	x	18.34	18.34	17.07	19.65
TYC 5302-849-1	r	972.87	972.27	948.87	996.76
TYC 6468-434-1	r	827.22	826.28	773.97	877.68
TYC 8894-1893-1	r	889.94	892.03	813.12	968.47
TYC 8855-429-1	r	980.21	980.2	964.83	995.62
TYC 7597-372-1	r	960.9	958.9	848.61	1064.88
HIP 26335	p	22.21	22.22	21.88	22.55
HIP 26335	x	22.26	22.26	22.1	22.42
HIP 40317	p	34.55	34.55	34.05	35.03
TYC 6471-517-1	r	772.43	772.99	750.05	795.71
TYC 8769-364-1	r	643.6	643.27	593.07	693.69
TYC 8856-611-1	r	627.62	626.75	569.08	683.4
HIP 25240	p	55.03	55.05	54.52	55.54
HIP 25240	x	55	54.99	54.59	55.39
TYC 9327-264-1	r	52.67	52.67	51.14	54.22
HIP 25240	g	53.73	53.74	52.73	54.7
TYC 8560-8-1	r	86.47	86.48	85.53	87.46
TYC 8496-973-1	r	707.46	703.85	523.67	878.52
TYC 9163-286-1	r	345.08	344.99	307.91	383.16
TYC 5046-284-1	r	640.63	640.1	609.21	671.67
HIP 30344	p	14.65	14.63	14.1	15.12
HIP 30344	g	14.45	14.44	14.08	14.76
TYC 7465-1009-1	r	2123.44	2123.45	2123.42	2123.48
HIP 30067	x	40.66	40.66	40.51	40.81
HIP 30067	g	40.58	40.58	40.24	40.9
HIP 30067	p	40.58	40.59	40.42	40.75
TYC7593-343-1	r	338.97	339.07	304.72	374.96
HIP 26624	p	22.23	22.24	21.58	22.94
HIP 26624	x	22.23	22.24	21.58	22.94
TYC 9528-1994-1	r	949.37	949.49	934.00	964.32
TYC 9446-745-1	r	890.02	890.23	809.88	972.49
TYC 8470-213-1	r	240.7	240.41	219.92	261.69
TYC 6080-573-1	r	627.76	628.66	600.24	658.84
HIP 20359	x	79.23	79.24	78.9	79.57

TABLE 5.3: Encounter parameters for all the stars with a mean perihelion distance less than 2 pc. The column named cat indicates the name of the input catalogue where the radial velocity were obtained from g=GCS catalogue, P=Pulkuvo Catalogue, R= RAVE DR5 catalogue, X=XHIP catalogue. The encounter parameters are set as v_{ph} respectively, nom represents the nominal values, mean represents the mean values, 5% and 95% represents the 5% and 95% quantiles of each encounter parameter.

ID	cat	α deg	δ deg	π mas	μ_α $masyr^{-1}$	μ_δ $masyr^{-1}$	rv kms^{-1}
HIP 89825	p	274.96	-1.94	52.35	-0.47	-0.18	-13.80
HIP 89825	x	274.96	-1.94	52.35	-0.47	-0.18	-13.80
TYC 6403-151-1	r	354.36	-16.83	18.54	-14.11	-21.31	-850.18
TYC 6622-652-1	r	153.23	-25.00	13.14	-14.05	3.05	741.08
TYC 8822-592-1	r	336.23	-54.12	5.03	-5.46	3.25	1969.34
TYC 9524-1668-1	r	325.45	-82.96	5.84	3.63	4.03	-887.40
TYC 7567-304-1	r	48.61	-44.69	16.66	-20.62	28.48	-625.82
TYC 9339-404-1	r	358.16	-69.79	6.91	9.59	0.29	-929.55
TYC 4888-146-1	r	139.78	-4.57	3.83	0.29	-6.67	1896.71
HIP 94512	p	288.54	7.76	9.51	-0.56	0.11	-30.40
TYC 7973-1145-1	r	315.50	-43.12	7.99	-7.03	4.87	-537.16
TYC 5033-879-1	r	241.95	-1.35	2.60	-0.17	0.90	532.39
HIP 30344	x	95.74	-24.56	34.19	-3.49	5.24	18.30
TYC 5302-849-1	r	51.98	-14.44	12.69	-18.40	-42.88	-972.70
TYC 6468-434-1	r	70.77	-26.65	7.71	7.66	12.63	-827.14
TYC 8894-1893-1	r	94.34	-61.25	11.20	14.24	30.60	-889.81
TYC 8855-429-1	r	17.44	-65.46	10.65	-30.10	-16.66	-980.07
TYC 7597-372-1	r	86.72	-37.97	3.96	-4.10	2.48	-960.82
HIP 26335	p	84.13	11.33	87.66	-2.81	-56.37	22.00
HIP 26335	x	84.13	11.33	87.66	-2.81	-56.37	22.05
HIP 40317	p	123.49	-4.05	12.74	0.85	1.45	34.50
TYC 6471-517-1	r	71.03	-29.71	16.77	55.02	-48.69	772.14
TYC 8769-364-1	r	290.69	-57.47	4.59	0.65	-4.55	643.55
TYC 8856-611-1	r	24.13	-65.00	5.50	-1.54	6.26	627.48
HIP 25240	p	80.96	-0.87	18.75	-6.51	0.31	55.00
HIP 25240	x	80.96	-0.87	18.75	-6.51	0.31	54.97
TYC 9327-264-1	r	325.13	-69.42	9.83	1.22	-0.76	52.39
HIP 25240	g	80.96	-0.87	18.75	-6.51	0.31	53.70
TYC 8560-8-1	r	116.21	-57.18	17.84	-9.64	1.71	86.41
TYC 8496-973-1	r	49.84	-56.13	6.26	5.67	-8.23	707.34
TYC 9163-286-1	r	89.34	-67.65	4.99	-1.12	-2.84	344.93
TYC 5046-284-1	r	244.66	-7.08	7.33	-4.46	11.60	-640.57
HIP 30344	p	95.74	-24.56	34.19	-3.49	5.24	14.60
HIP 30344	g	95.74	-24.56	34.19	-3.49	5.24	14.40
TYC 7465-1009-1	r	311.00	-34.78	3.68	-10.73	1.19	2123.36
HIP 30067	x	94.92	16.01	36.93	-15.29	-14.57	40.58
HIP 30067	g	94.92	16.01	36.93	-15.29	-14.57	40.50
HIP 30067	p	94.92	16.01	36.93	-15.29	-14.57	40.50
TYC7593-343-1	r	74.74	-43.54	6.26	-5.32	-0.96	-338.83
HIP 26624	p	84.88	-3.56	23.79	-4.40	2.29	22.20
HIP 26624	x	84.88	-3.56	23.79	-4.40	2.29	22.20
TYC 9528-1994-1	r	316.94	-84.63	10.17	38.22	11.67	949.18
TYC 9446-745-1	r	243.62	-78.09	17.70	-85.47	-76.10	-889.49
TYC 8470-213-1	r	1.61	-59.56	24.42	56.58	-17.26	240.41
TYC 6080-573-1	r	165.88	-17.68	24.62	-136.68	-81.36	-627.01
HIP 20359	x	65.40	48.34	34.19	-36.40	13.96	-79.05

TABLE 5.4: Astrometric parameters for all the stars with a mean perihelion distance less than 2 pc. The column named cat indicates the name of the input catalogue where the radial velocity were obtained from g=GCS catalogue, P=Pulkuvo Catalogue, R= RAVE DR5 catalogue, X=XHIP catalogue. The encounter parameters are set as α δ π μ_α μ_δ rv respectively.

ID	cat	$\Delta\alpha$ mas	$\Delta\delta$ mas	$\Delta\pi$ mas	$\Delta\mu_\alpha$ $masyr^{-1}$	$\Delta\mu_\delta$ $masyr^{-1}$	Δrv kms^{-1}
HIP 89825	p	0.23	0.22	0.27	0.13	0.09	0.30
HIP 89825	x	0.23	0.22	0.27	0.13	0.09	0.30
TYC 6403-151-1	r	0.35	0.27	0.55	1.84	0.89	226.44
TYC 6622-652-1	r	0.44	0.15	0.69	2.79	0.72	12.89
TYC 8822-592-1	r	0.14	0.28	0.25	0.31	0.58	0.00
TYC 9524-1668-1	r	0.17	0.25	0.38	0.62	0.56	0.00
TYC 7567-304-1	r	0.13	0.21	0.23	0.61	1.11	24.85
TYC 9339-404-1	r	0.22	0.19	0.25	0.88	0.63	28.74
TYC 4888-146-1	r	0.66	0.58	1.00	3.13	2.16	0.00
HIP 94512	p	0.29	0.32	0.41	0.04	0.03	0.30
TYC 7973-1145-1	r	0.13	0.13	0.29	0.64	0.84	11.18
TYC 5033-879-1	r	0.25	0.10	0.25	0.70	0.39	6.22
HIP 30344	x	0.18	0.22	0.29	0.03	0.04	0.76
TYC 5302-849-1	r	0.25	0.19	0.22	0.97	0.72	13.97
TYC 6468-434-1	r	0.15	0.24	0.23	0.53	0.71	32.56
TYC 8894-1893-1	r	0.17	0.27	0.26	0.68	0.59	47.57
TYC 8855-429-1	r	0.19	0.10	0.24	0.52	0.73	9.51
TYC 7597-372-1	r	0.18	0.25	0.24	1.01	0.89	65.57
HIP 26335	p	0.20	0.25	0.29	0.08	0.06	0.20
HIP 26335	x	0.20	0.25	0.29	0.08	0.06	0.10
HIP 40317	p	0.22	0.19	0.24	0.12	0.09	0.30
TYC 6471-517-1	r	0.18	0.21	0.23	0.71	0.78	14.06
TYC 8769-364-1	r	0.21	0.17	0.26	0.66	0.91	30.20
TYC 8856-611-1	r	0.29	0.18	0.26	0.61	0.92	35.68
HIP 25240	p	0.28	0.29	0.47	0.04	0.03	0.30
HIP 25240	x	0.28	0.29	0.47	0.04	0.03	0.24
TYC 9327-264-1	r	0.20	0.27	0.34	0.48	1.03	0.95
HIP 25240	g	0.28	0.29	0.47	0.04	0.03	0.60
TYC 8560-8-1	r	0.17	0.32	0.33	1.43	1.03	0.60
TYC 8496-973-1	r	0.20	0.14	0.26	0.38	0.63	112.17
TYC 9163-286-1	r	0.10	0.21	0.30	0.78	1.23	22.72
TYC 5046-284-1	r	0.33	0.20	0.26	0.86	0.41	19.04
HIP 30344	p	0.18	0.22	0.29	0.03	0.04	0.30
HIP 30344	g	0.18	0.22	0.29	0.03	0.04	0.20
TYC 7465-1009-1	r	0.33	0.12	0.60	1.46	1.13	0.00
HIP 30067	x	0.17	0.32	0.40	0.04	0.03	0.09
HIP 30067	g	0.17	0.32	0.40	0.04	0.03	0.20
HIP 30067	p	0.17	0.32	0.40	0.04	0.03	0.10
TYC7593-343-1	r	0.19	0.26	0.25	0.59	0.76	20.43
HIP 26624	p	3.34	3.10	0.33	0.14	0.13	0.40
HIP 26624	x	3.34	3.10	0.33	0.14	0.13	0.40
TYC 9528-1994-1	r	0.25	0.23	0.28	0.69	1.17	8.79
TYC 9446-745-1	r	0.90	0.29	0.38	2.65	1.18	51.31
TYC 8470-213-1	r	0.20	0.17	0.23	0.47	0.46	12.57
TYC 6080-573-1	r	0.52	0.20	0.85	3.07	1.07	17.69
HIP 20359	x	0.21	0.19	0.28	0.10	0.07	0.21

TABLE 5.5: Error for the astrometric parameters for all the stars with a mean perihelion distance less than 2 pc. The column named cat indicates the name of the input catalogue where the radial velocity were obtained from g=GCS catalogue, P=Pulkuvo Catalogue, r= RAVE DR5 catalogue, x= XHIP catalogue. The encounter parameters are set as α δ π μ_α μ_δ rv respectively.

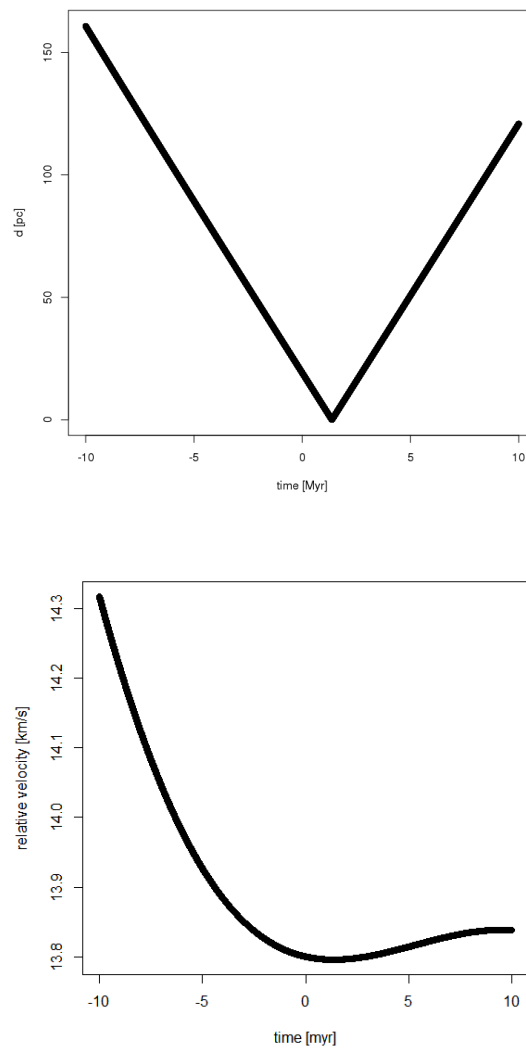


FIGURE 5.1: The nominal orbit of HIP 89825 relative to the Sun. Note carefully the compressed scale of the y axis of the lower plot.

Myr. Among these 846 candidates with a mean perihelion distance less than 10pc, 460 of them occur in the past while 386 of them are future encounters. Figure 5.3 shows all stars with a mean perihelion distance less than 2pc.

Figure 5.4 represents the distribution of the perihelion speeds on a logarithmic scale. It can be noticed from the plot that there are very large radial velocities present. For some stars the distribution of their encounter parameters are presented in figure 5.5.

From figure 5.5 it can be seen that the distributions are asymmetric. For the perihelion distances it is inevitable of course as it is strictly non negative. Over-plotted are the mean (red), nominal

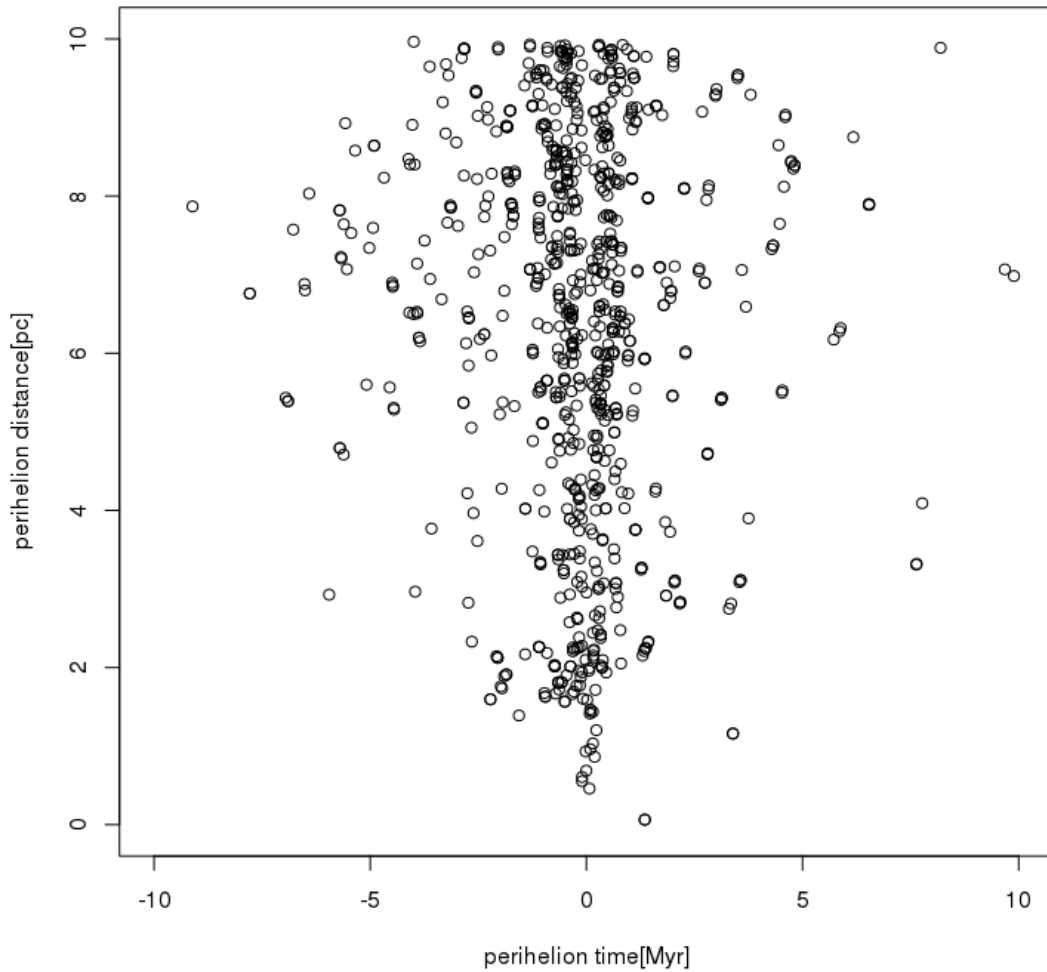


FIGURE 5.2: Mean perihelion distance, (d_{ph}^{mean}) vs mean perihelion time, (t_{ph}^{mean}) for all stars with d_{ph}^{mean} less than 10pc.

(blue) and linear (green) data for the encounter parameters. The different methods of calculating the encounter parameters (mean, nominal and linear approximation) correlate quite well with each other but there are some significant discrepancies in the estimation of the encounter parameters that cannot be ignored. Whilst using the linear approximation method, about 28% of stars deviate from the mean perihelion distance by 0.5pc or more; while using the nominal data, the deviation is 22% from the mean perihelion distance by 0.5pc or more. The discrepancy in the perihelion time is quite small. Using the linear approximation method, 14%, 5% and 3% stars differ from the mean perihelion distances by more than 0.1Myr, 0.5Myr and 1Myr respectively. Using nominal data from the numerical integration of the stars, 10% , 4% and 2% stars differ from the mean perihelion time by 0.1 Myr, 0.5 Myr and 1.0 Myr respectively. In the case of the

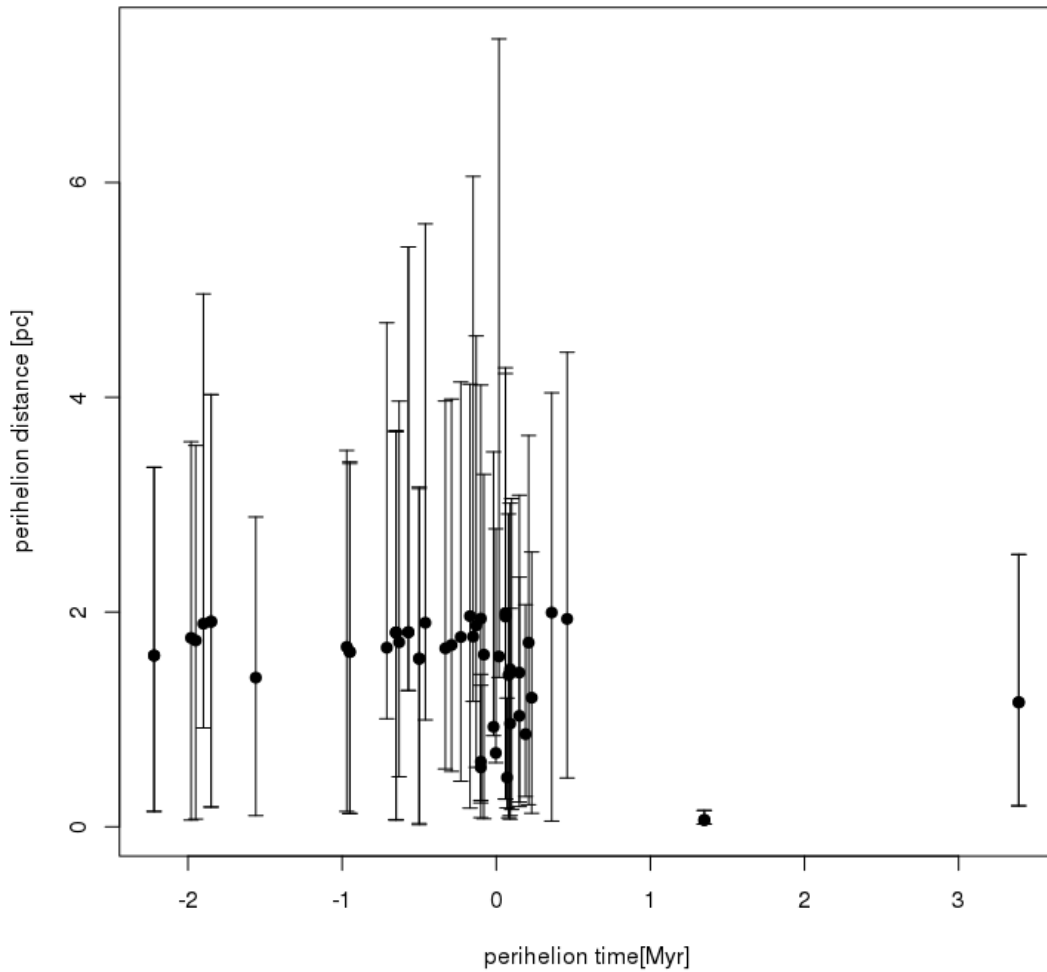


FIGURE 5.3: Mean perihelion distance vs mean perihelion time for all the stars with a d_{ph}^{mean} less than 2 pc. The error bar represents the 5% and 95% quantiles of the distributions for each of the stars

perihelion speed, 4% of stars (using both the linear approximation method and nominal method) deviate from the mean perihelion speed.

It can be noticed that the discrepancies are quite asymmetric in the encounter parameters (notably for perihelion distances). Figure 5.6 shows the discrepancy in the perihelion distances when nominal data is used as a function of the star's parallax. It can be seen that the nominal data have a tendency of underestimating the perihelion distance: 863 stars' perihelion distances have been underestimated while 134 stars' perihelion distances have been overestimated when nominal data have been used. The asymmetry is not as big when the linear approximation

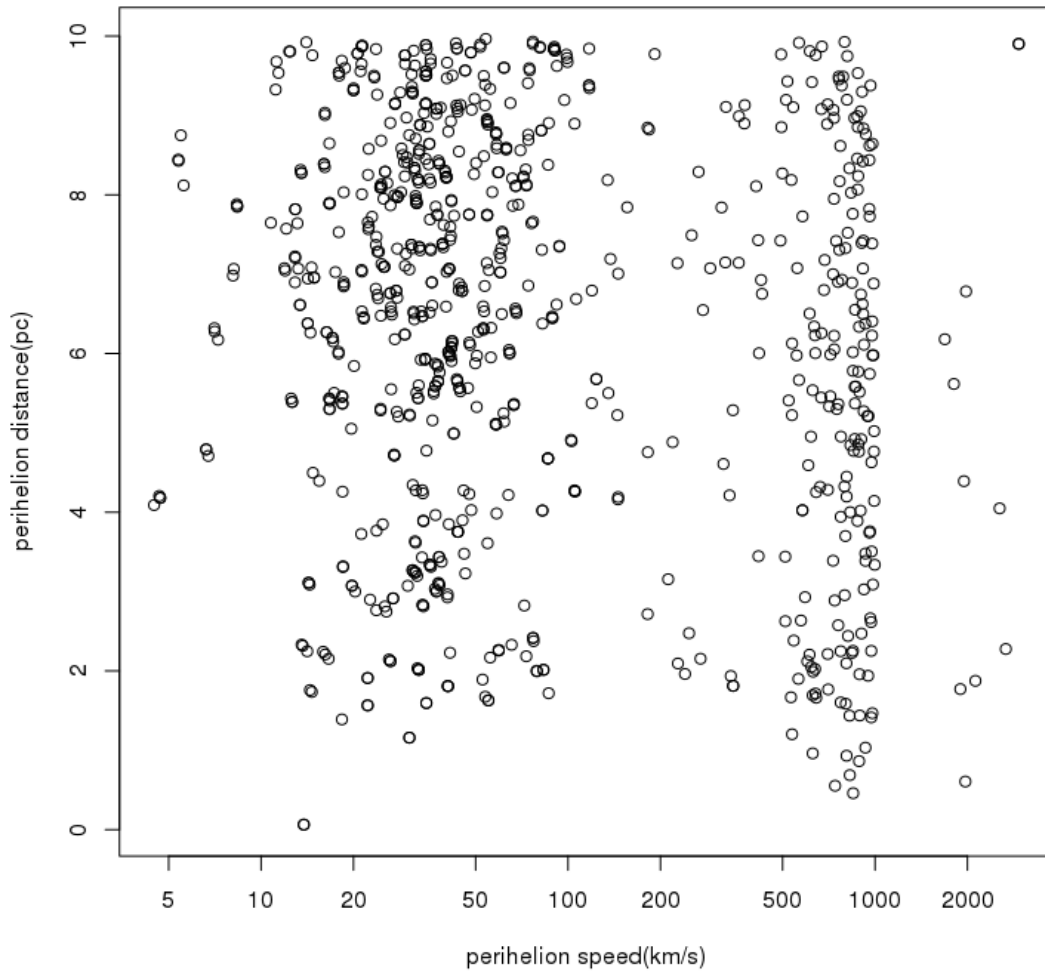


FIGURE 5.4: Mean perihelion distance vs mean perihelion speed on a logarithmic scale for all stars with a mean perihelion distance less than 10pc.

data was used to analyse how many of the stars' perihelion distances were underestimated or overestimated comparing to the mean perihelion distance. 666 stars distances were underestimated compared to 337 stars distances which were overestimated. Using both of these methods - nominal and linear approximation - will underestimate the distances of the encounter while overestimating the number of encounters found.

As the Sun orbits around the Galaxy, it will have encounters with other passing stars and gravitational perturbation from the galactic tide. These perturbations are strong enough to perturb the Oort cloud objects and send them towards the inner Solar System. The strength of these

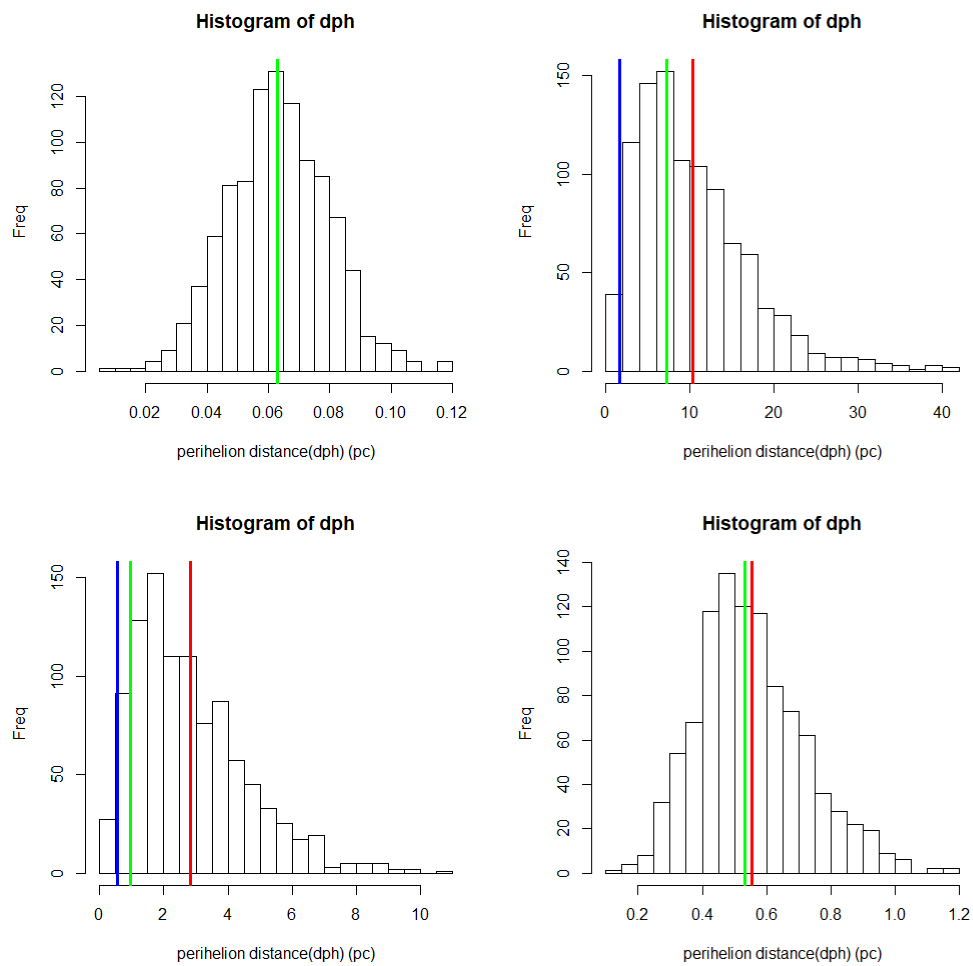


FIGURE 5.5: Distribution of perihelion distances from 1000 clones of four selected stars. The orders of the stars are: 1. HIP 89825, 2. TYC 6281-793-1, 3. TYC 8088-631-1, 4. TYC 6622-652-1. The red, green and blue lines represents the mean, linear and nominal distances of these stars. Sometimes not all of these lines appear in the histogram because the values coincide with each other.

perturbations are also dependent on the local stellar density and by how much the orbital motion of the Sun will modulate these influences and thus the rate of comet injection and impact to some degree. In the studies of perturbing the Oort cloud, a typical assumption is an isotropic distribution of the encounters. However in reality due to the Sun's peculiar motion with respect to the local standard of rest these stellar encounters are not isotropic. This anisotropy can be noticed by looking at the distribution of the direction of the encounter perihelia and the direction of the encounter velocity in the galactic latitude and longitude. The resulting histograms are shown in figures 5.10 and 5.11. From figure 5.10 it can be noticed that the encounter velocity concentrates in the antapex direction.

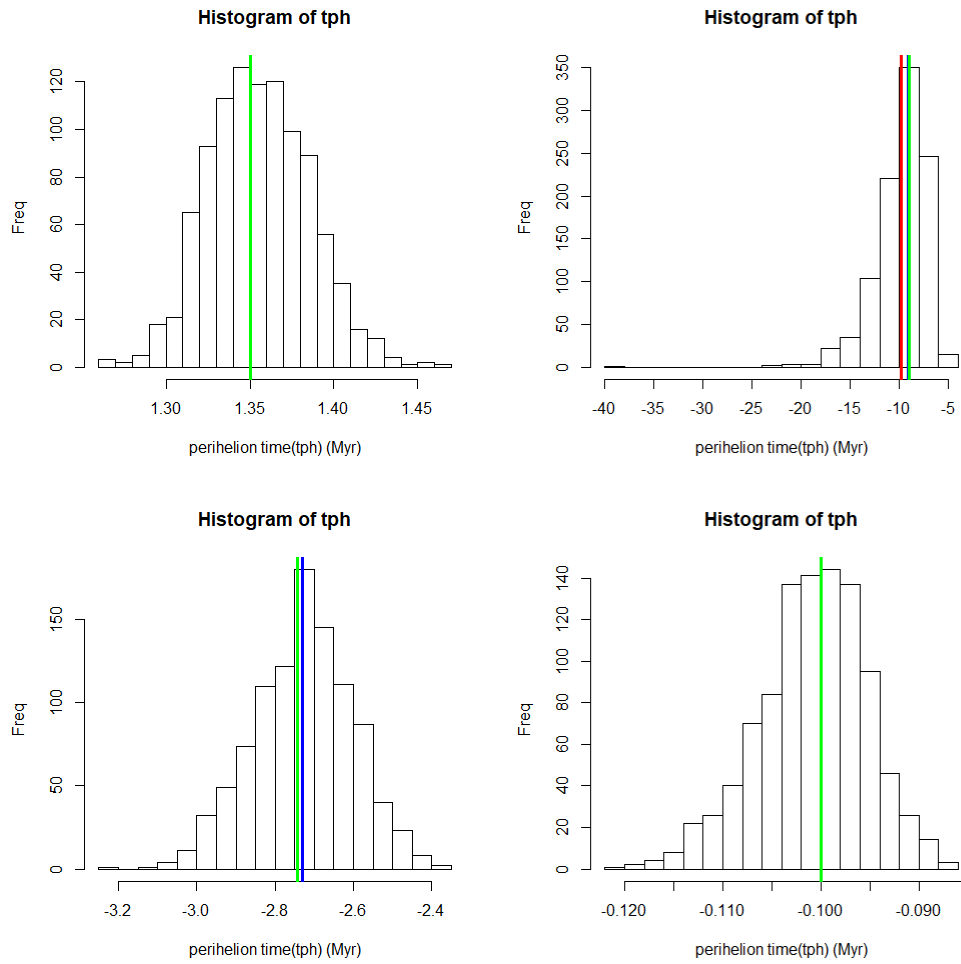


FIGURE 5.6: Distribution of perihelion times from 1000 clones of four selected stars. The orders of the stars are: 1. HIP 89825, 2. TYC 6281-793-1, 3. TYC 8088-631-1, 4. TYC 6622-652-1. The red, green and blue lines represents the mean, linear and nominal perihelion times of these stars. Sometimes not all of these lines appear in the histogram because the values coincide with each other.

The numbers of encounter perihelion directions within the 90 degrees of the Solar apex direction and the numbers within the 90 degrees of the Solar antapex direction are 513 and 490 respectively. In order to determine how significant the departure from randomness is for these encounters, the sky was divided into ten equal area sections and determine if the number of encounters in each section is not inconsistent with an uniform distribution across the celestial sphere. These sections are symmetric with respect to apex-antapex direction. These intervals are $(0^\circ, 36.9^\circ)$, $(36.9^\circ, 53.2^\circ)$, $(53.2^\circ, 66.4^\circ)$, $(66.4^\circ, 78.5^\circ)$, $(78.5^\circ, 90^\circ)$, $(90^\circ, 101.5^\circ)$, $(101.5^\circ, 113.6^\circ)$, $(113.6^\circ, 126.9^\circ)$, $(126.9^\circ, 143.13^\circ)$, $(143.13^\circ, 180^\circ)$. The number of encounter stars are $N = 1003$ and $s = 10$. The mean number of encounters in each section is the ratio of N/s which is ~ 100 . Assuming a Poisson distribution, the standard deviation is $\sigma = \sqrt{\lambda}$, where

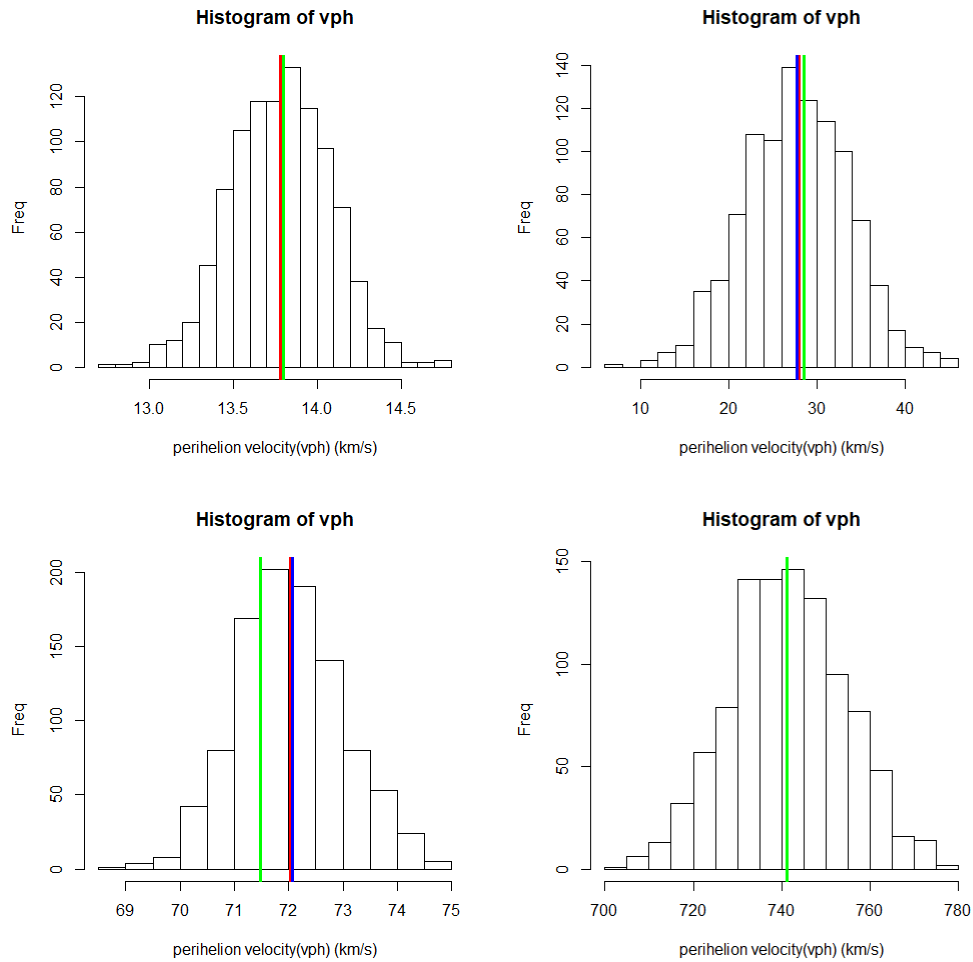


FIGURE 5.7: Distribution of velocity at the time of encounter from 1000 clones of four selected stars. The orders of the stars are: 1. HIP 89825, 2. TYC 6281-793-1, 3. TYC 8088-631-1, 4. TYC 6622-652-1. The red, green and blue lines represents the mean, linear and nominal velocity at the time of the encounter of these stars. Sometimes not all of these line appear in the histogram because the values coincide with each other.

λ is N/s . The standard deviation of the encounter number in each section is ~ 10 . The departure from randomness will not significant if the number of encounters in each section has a small difference with the mean number of encounters in table 5.5.

From table 5.5 it can be noticed that for the interval $(36.9^\circ, 53.2^\circ)$ the number of encounters is 1.8σ lower than the mean number of encounters and for the interval $(53.2^\circ, 66.4^\circ)$ the number of encounters is 1.9σ above the mean number of encounters. Despite these two intervals showing some proof of non-randomness, the difference from the mean is not significant enough to suggest a departure from a random distribution. Figure 5.12 shows the encounter perihelion on the plane of the sky as a function of galactic latitude and longitude.

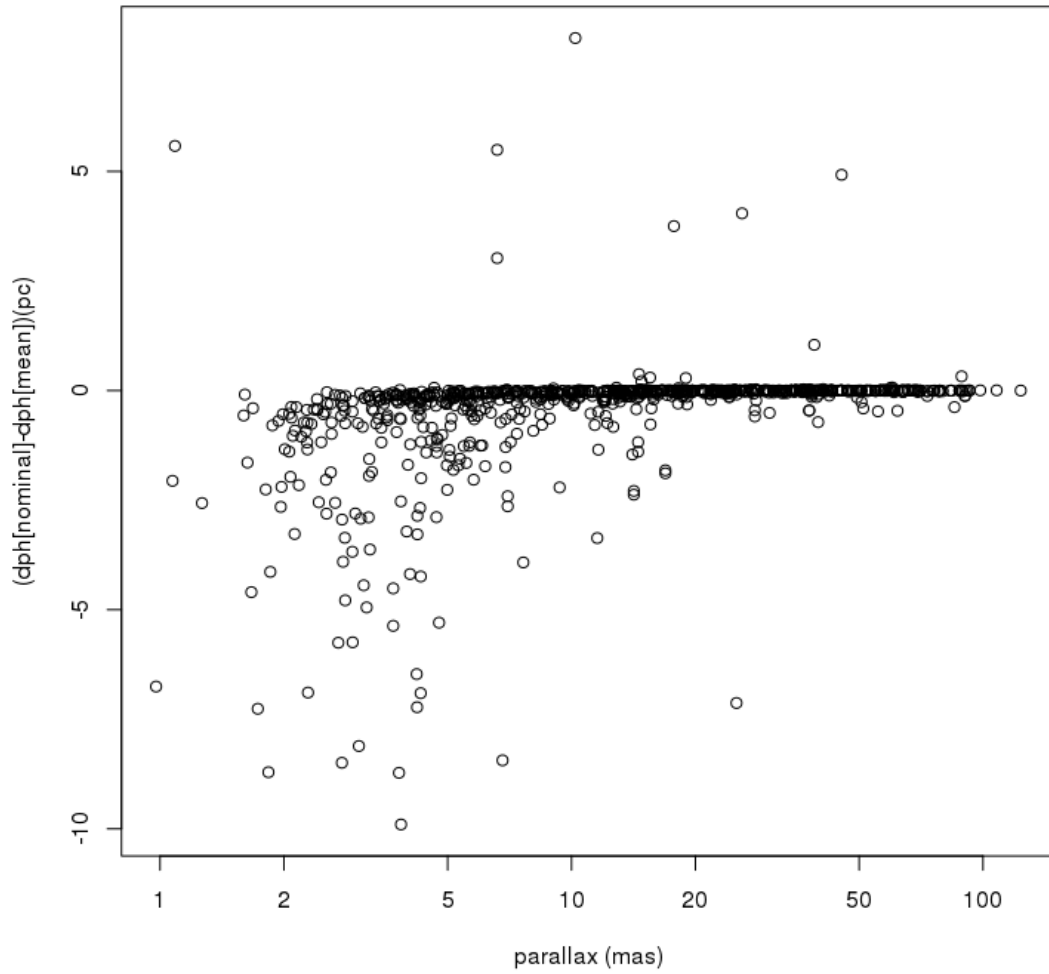


FIGURE 5.8: Difference between the nominal and mean perihelion distances as a function of the star's parallax on a log scale. In this case, for 54 stars difference data was omitted in the plot since they have a difference between their nominal and mean distances less than -10pc.

Angular intervals	No. of Encounters	(Value- λ)
(0°, 36.9°)	109	0.9 σ
(36.9°, 53.2°)	82	1.8 σ
(53.2°, 66.4°)	119	1.9 σ
(66.4°, 78.5°)	98	0.2 σ
(78.5°, 90°)	109	0.9 σ
(90°, 101.5°)	94	0.6 σ
(101.5°, 113.6°)	106	0.6 σ
(113.6°, 126.9°)	110	1.1 σ
(126.9°, 143.13°)	75	0.25 σ
(143.13°, 180°)	101	1.01 σ

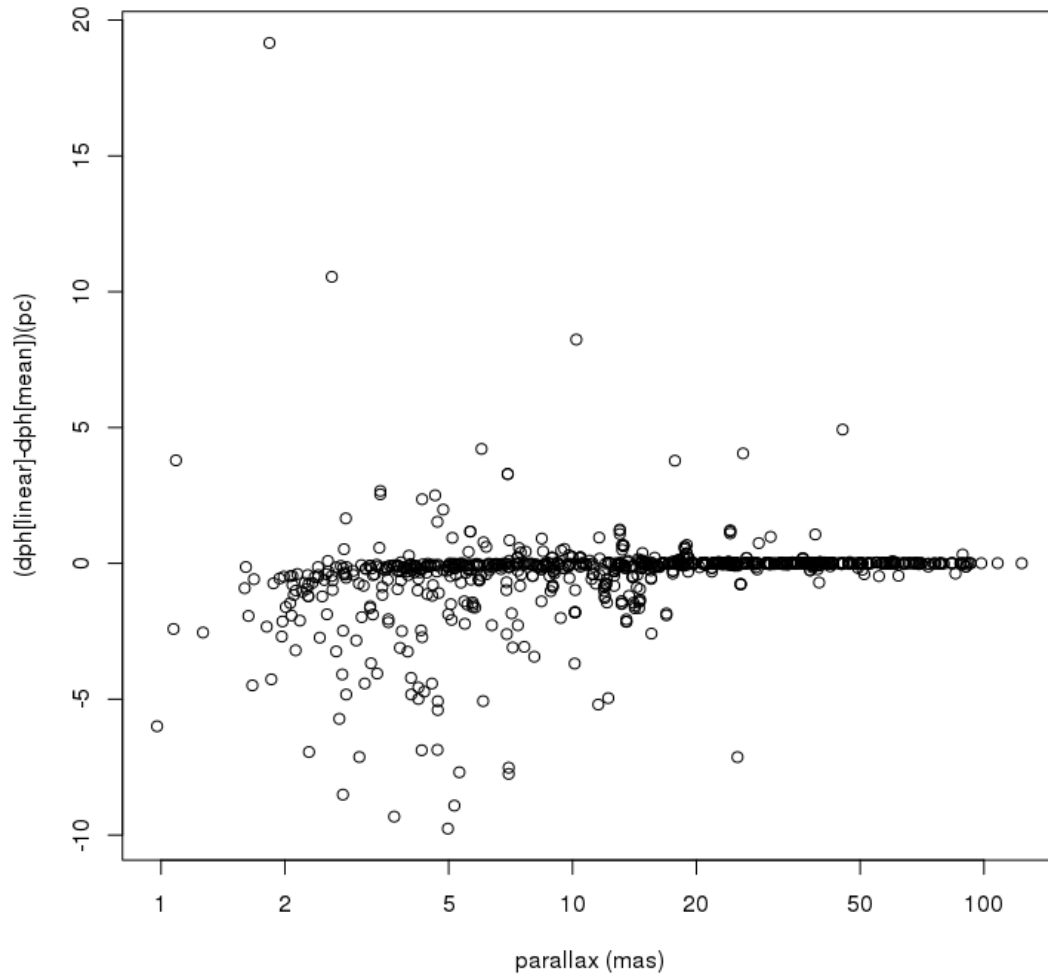


FIGURE 5.9: Difference between the linear and mean perihelion distances as a function of the star's parallax on a log scale. In this case, for 73 stars difference data was omitted in the plot since they have a difference between their linear and mean distances less than -10pc.

In order to understand the effect of the solar apex motion, an angle θ is defined as the angle between the encounter perihelia and the solar apex. Figure 5.13 shows the $\cos\theta$ distribution of all the encounters. The $\cos\theta$ distribution is useful in assessing the distribution of directions over the whole sphere. If there were no solar apex motion, the $\cos\theta$ distribution would be flat. If the distribution is flat, then the perihelion directions are uniformly distributed over the sphere. An anisotropy in the $\cos\theta$ distribution will suggest the effect of solar apex motion on the encounter perihelion direction.

Two obvious effects might lead to deviation from a uniform distribution: the local distribution of stars has irregularities, the local velocity distribution is ellipsoidal and not isotropic. For a small

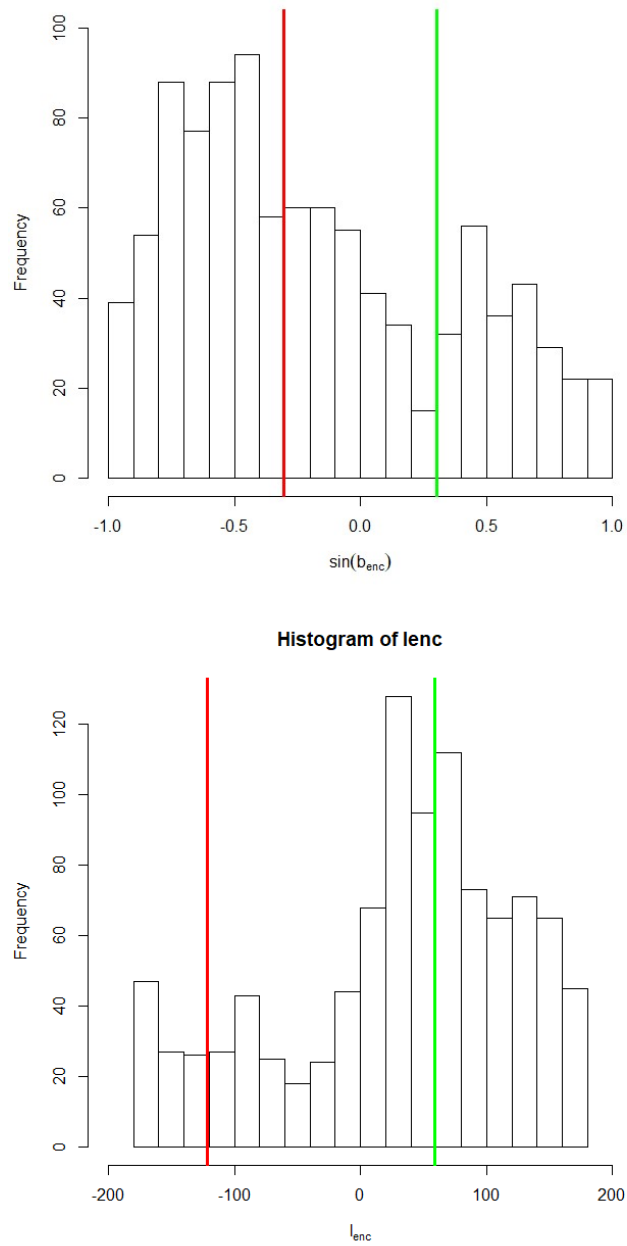


FIGURE 5.10: Distribution of the direction of the encounter velocities in galactic co ordinates as $\sin(b_{enc})$ and l_{enc} . The red and green line shows the solar antapex and apex directions respectively.

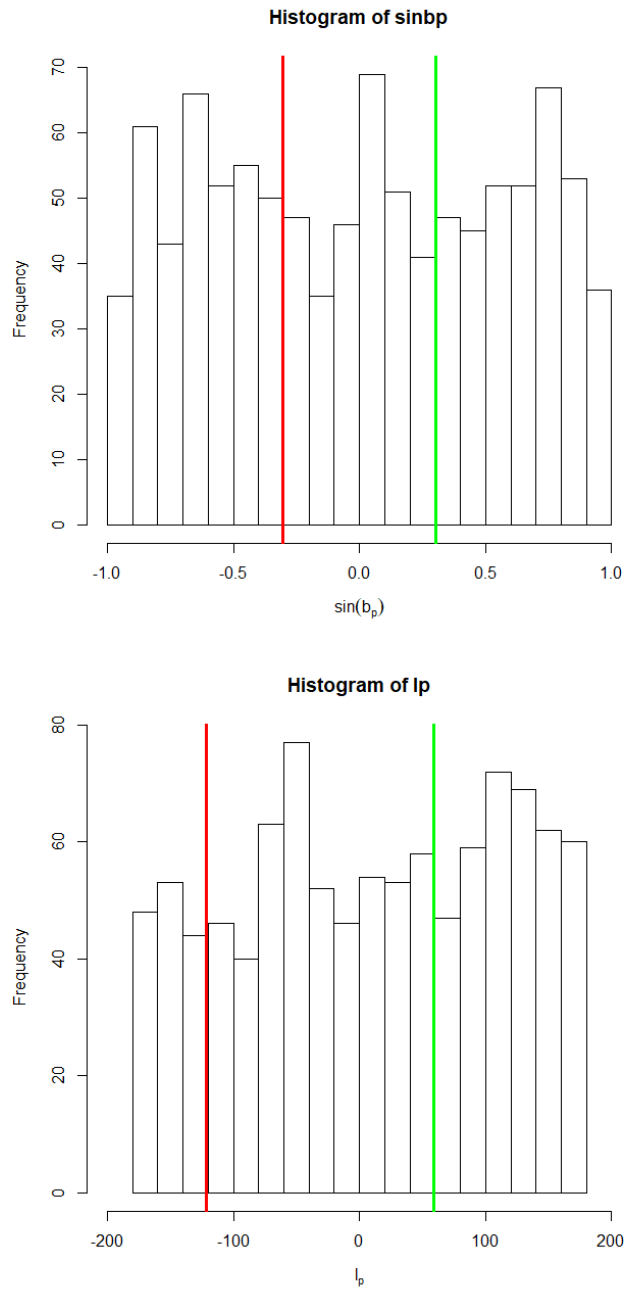


FIGURE 5.11: Distribution of the direction of the encounter perihelion in galactic coordinates as $\sin(b_p)$ and l_p . The red and green line shows the solar antapex and apex directions respectively.

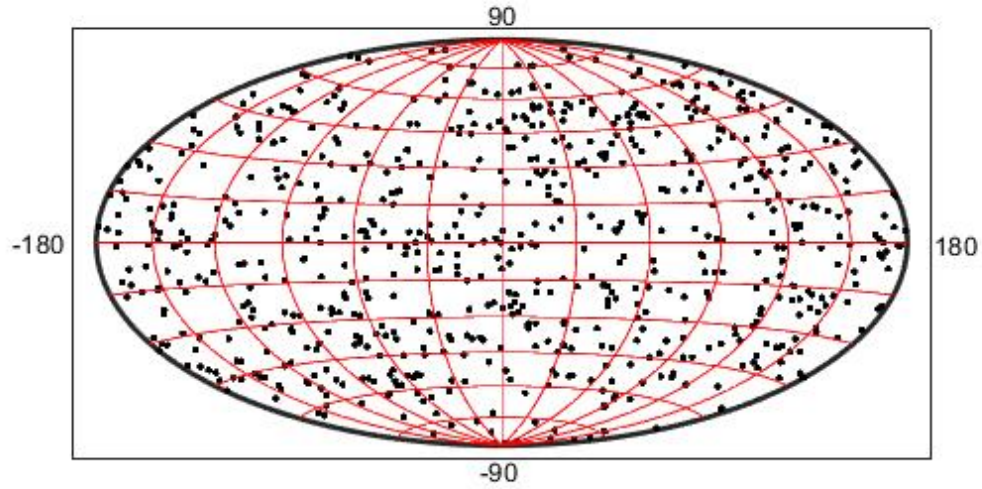


FIGURE 5.12: Distribution of encounters perihelia on the plane of the sky as a function of galactic latitude ($-90 \leq b \leq 90$) and longitude ($-180 \leq l \leq 180$). The stellar encounters are denoted by dots.

deflection, a star will have a perihelion direction that is nearly normal to the trajectory on which the star approaches the Sun. For large deflections this will not be the case. Consider a scenario where the Sun's motion is so dominant that the neighbouring stars are effectively at rest. In this case the encounter direction always points towards the antapex. As a result, if the deflections are weak, the perihelia direction are likely to be close to 90 degrees from the antapex direction. In the other limiting case, consider a scenario where the solar motion is negligible. In this case the encounter trajectories are isotropically distributed across the sky. As a result even if the encounters are all weak, the perihelion directions are also isotropically distributed. In order to have a better understanding of the influence of the solar apex motion on the encounter perihelion direction the encounters were further divided into two sections based on their perihelion speed: stars with speed less than 50kms^{-1} and stars with speed greater than 50kms^{-1} and two sections based on their radial velocity. Figure 5.14 and 5.15 shows the $\cos\theta$ distribution of the stars with speeds less than 50kms^{-1} and stars with speeds greater than 50kms^{-1} . From the figure 5.14 it can be seen that the encounter perihelion for low speed stars are concentrated near the plane

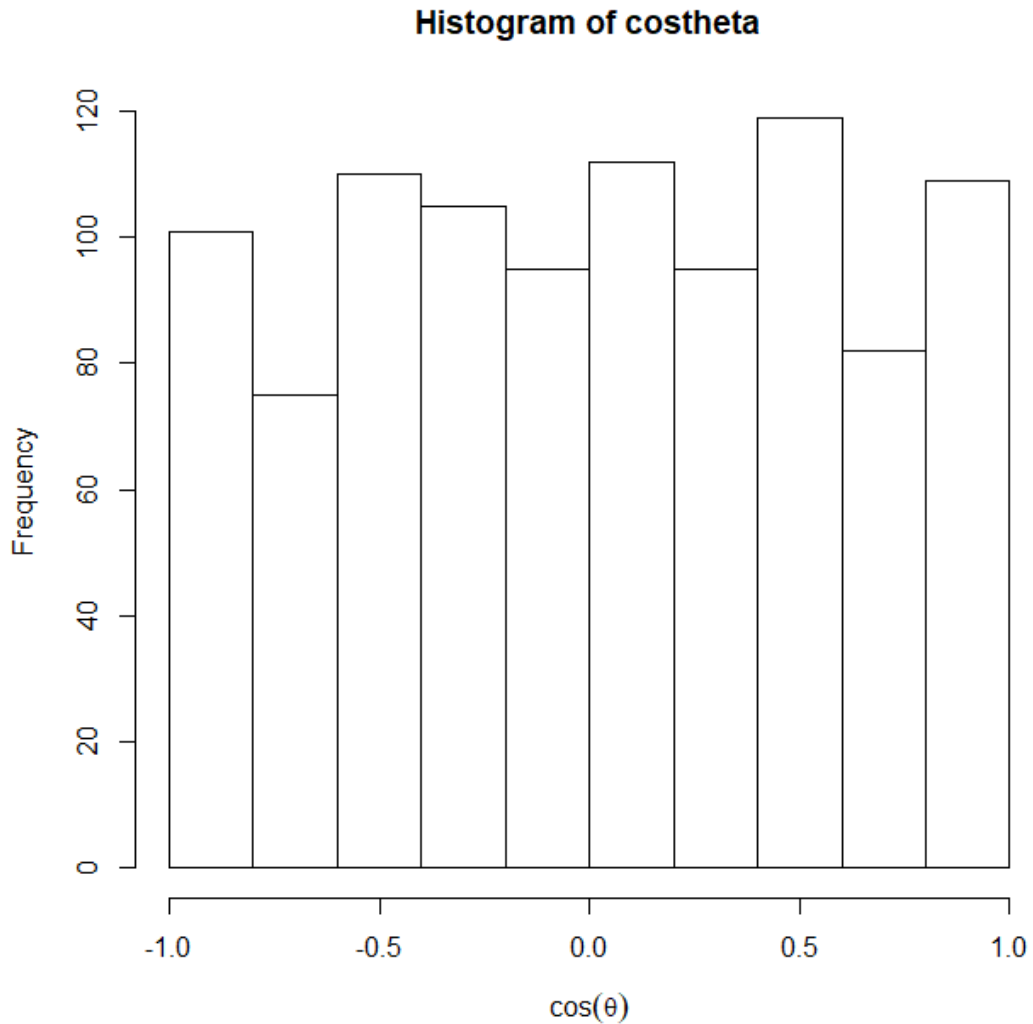


FIGURE 5.13: Distribution of cosine of the angle between the encounter perihelion and solar apex. This plot includes all the encounter stars irrespective to their perihelion speed.

perpendicular to the apex-antapex direction. For the high speed stars the distribution of $\cos\theta$ is more anisotropic. For all stars with a radial velocity less than 50 km/s the perihelion direction is concentrated near the plane perpendicular to the apex-antapex direction while for stars with radial velocity greater than 50 km/s the distribution is not inconsistent with flat. Sky plots of these velocity cuts are included from figure 5.19 to 5.22.

I have found 52 stars that will have an encounter with the Sun with a mean perihelion distance less than 2pc. 6 of them are common with close encounters found by Bobylev and Bajkova(2017). I have found 9 stars that will have an encounter with the Sun with a mean perihelion distance of less than 1pc. HIP 89825(GJ 710) still remains the closest encounter of the Sun as

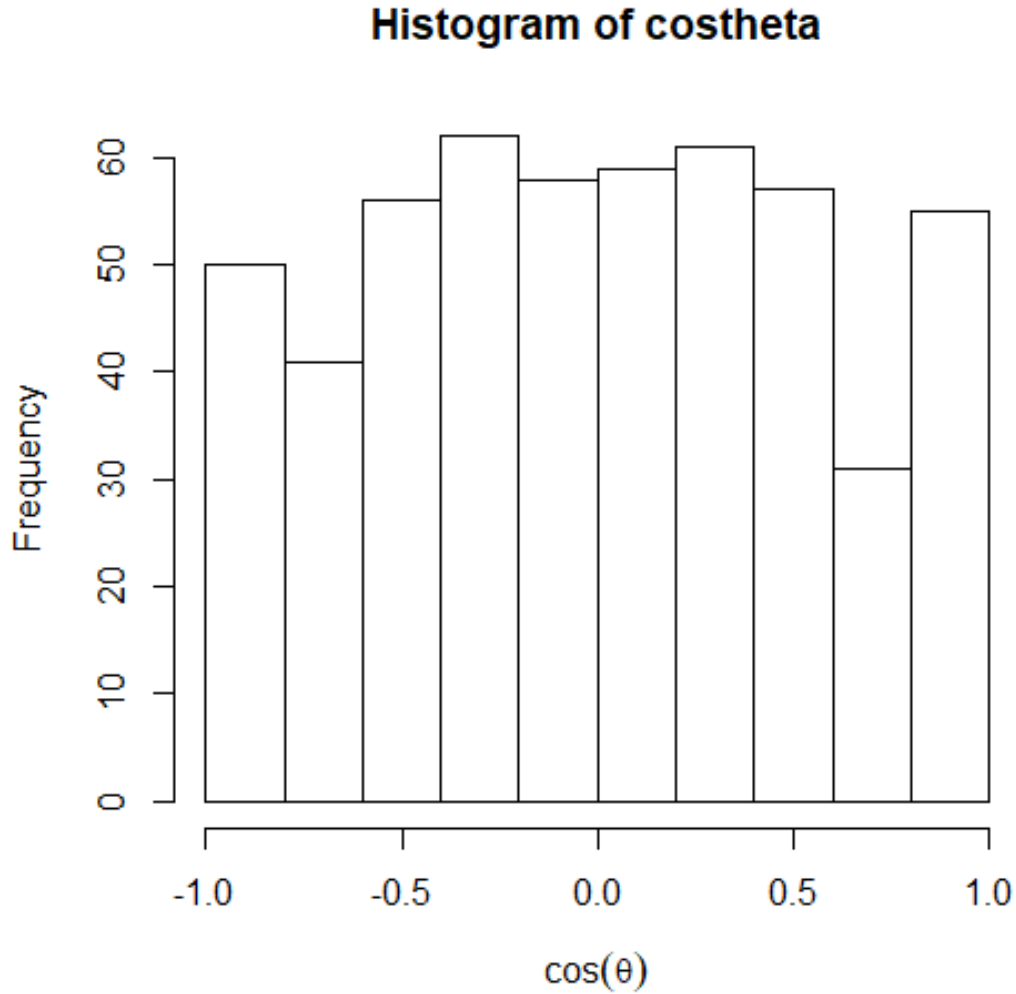


FIGURE 5.14: Distribution of cosine of the angle between the encounter perihelion and solar apex for stars with encounter speed less than 50km s^{-1}

found by Berski and Dybczyński (2016).

5.2 Individual encounters

The Oort cloud is believed to have extended to 0.5 pc. If a star is big and slow it will have a significant influence on the Oort cloud, even when it is a few pc away. Here I present some of the interesting stellar encounters from table 5.2 and 5.3. The letter after the Hipparcos or Tycho2 id means it is from an input catalogue mentioned in table 5.2 and 5.3. The spectral types and colours data have been gathered from Simbad.

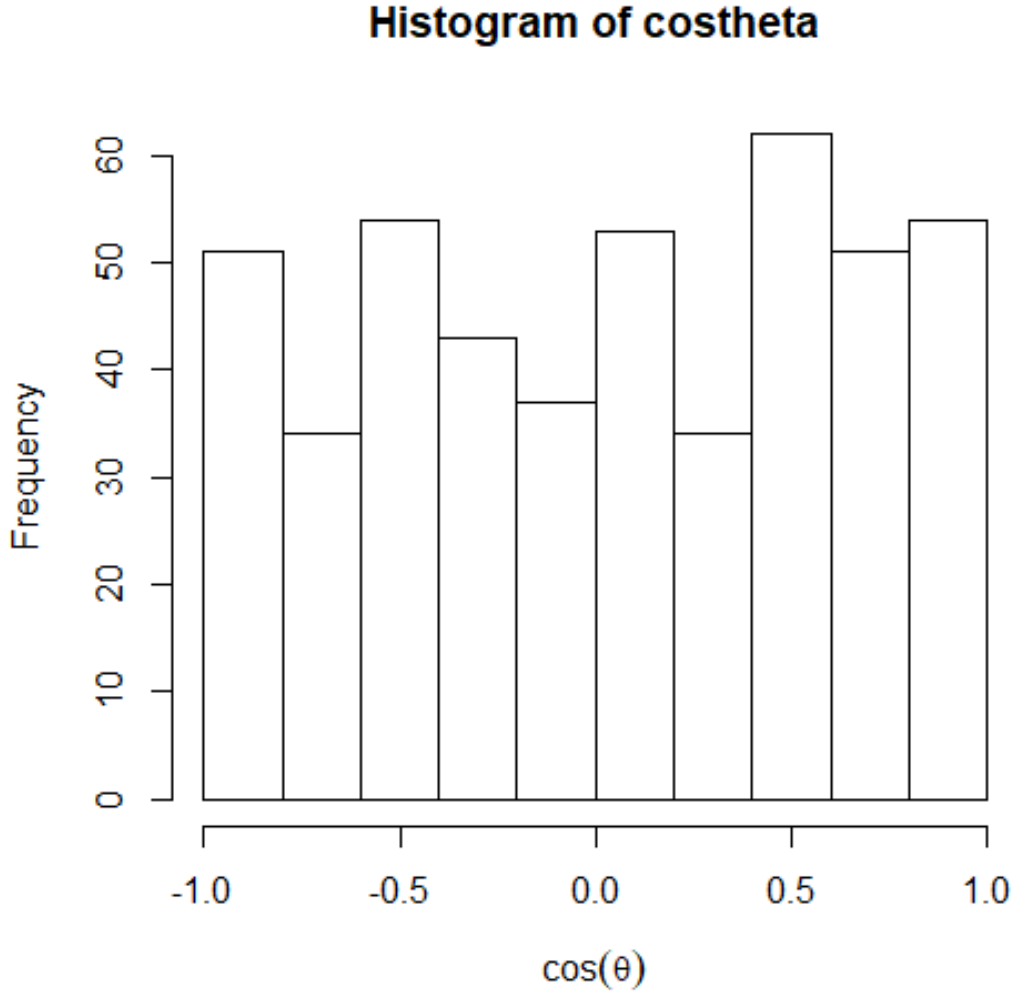


FIGURE 5.15: Distribution of cosine of the angle between the encounter perihelion and solar apex for stars with perihelion speed greater than 50 km s^{-1} . Note the reduced of the number of stars at $\cos\theta = 0$ compared to figure 5.14.

HIP 89825(GL 710)

HIP 89825 or Gliese 710 is a well known future visitor of the Solar System and has come up in previous studies of the close encounters. Because of the high precision of the TGAS astrometry this star's encounter parameters are well determined. The result presented in table 5.2 and 5.3 also agrees with the results of Berski and Dybczyński (2016) and Bobylev and Bajkova (2017). This star is a K7 dwarf with a mass of $0.6M_{\odot}$ and a radius of $0.67R_{\odot}$. The effective temperature for the star is 4190K (Franchini et al. (2014)). This star's nominal closest approach will be $d_{ph}^{nom} = 0.063 \text{ pc}$ in $t_{ph}^{nom} = 1.35 \text{ Myr}$ in the future. Analysing the results of 1000 clones presents a mean

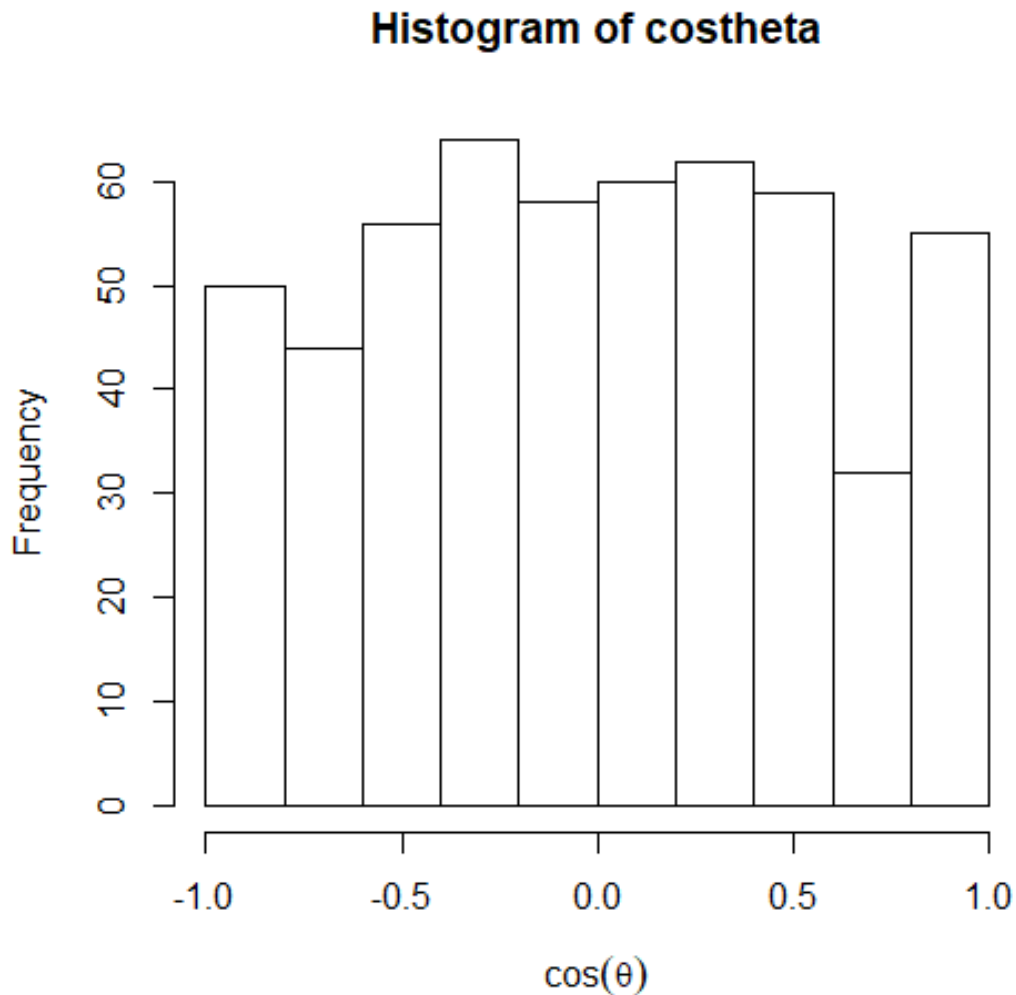


FIGURE 5.16: distribution of cosine of the angle between the encounter perihelion and solar apex for stars with radial velocity smaller than 50km s^{-1}

distance of 0.063 pc as the closest approach. Mean time of the closest approach from the cloud of clones is 1.35 Myr. The cloud clone HIP 89825 is very small and is represented in figure 5.19.

A recent study on HIP 89825's(GJ 710) influence on the Oort cloud was done by Berski and Dybczyński (2016). The study showed that the star may not have any effect on the major planetary bodies in the Solar System but will have a significant effect on the Oort cloud. According to the study after the passage of HIP 89825(GJ 710) up to 0.1% of the Oort cloud comet will be removed from the Oort cloud where 0.01% of the Oort cloud comet will be pushed to observable orbits. Taking into account the real expected number of comets in the Oort cloud which is 10^{11} ,

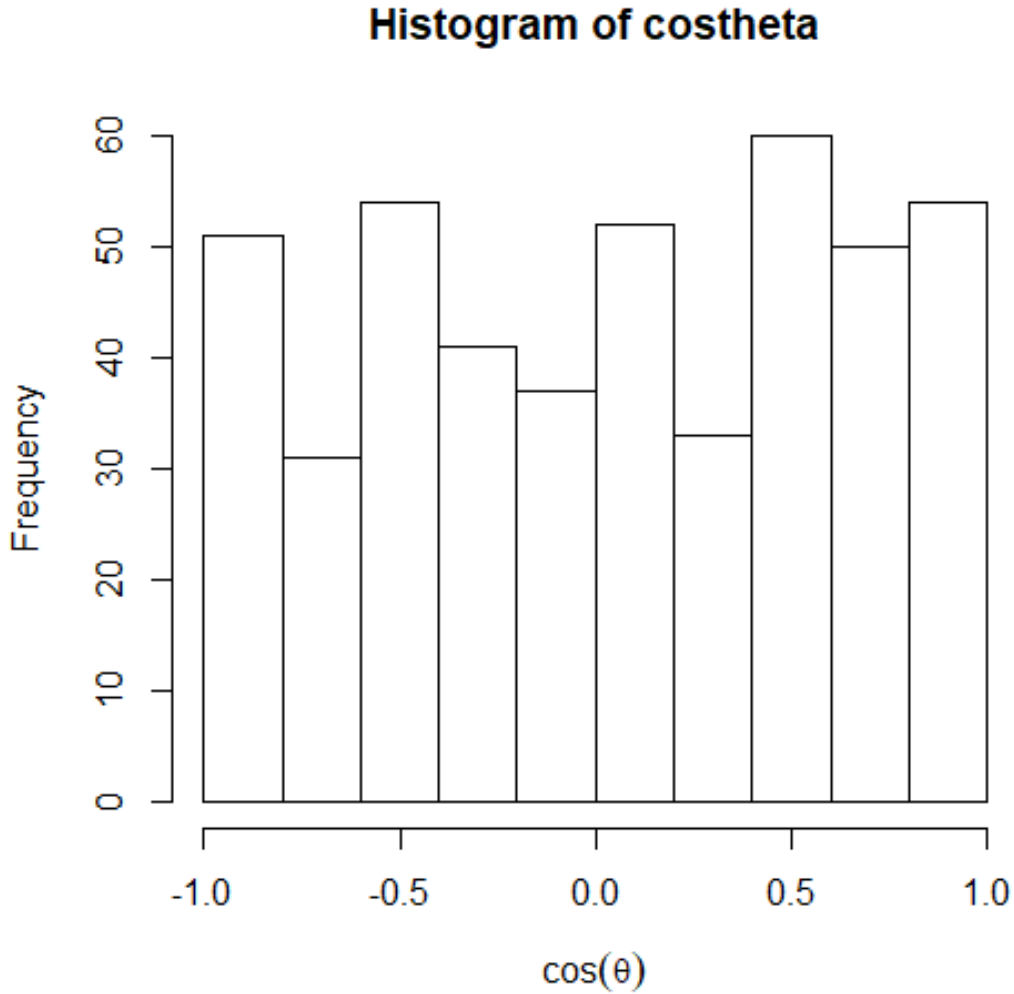


FIGURE 5.17: Distribution of cosine of the angle between the encounter perihelion and solar apex for stars with radial velocity greater than 50 km s^{-1}

this paper suggested that HIP 89825 will trigger an observable cometary shower that has a mean density of approximately 10 comets a year which will last for 3-4Myr.

TYC 6403-151-1.r

This star will be a close encounter of the Solar System. The effective temperature of the star is 3800K(Rave DR5) and possibly a M0 dwarf star. Analysing 1000 clones the estimated mean perihelion distance of the star is $d_{ph}^{mean} = 0.459$ pc. The mean time of the closest approach is $t_{ph}^{mean} = 0.07$ Myr. This star also appears in Bobilev and Bajkova(2017). This star is one of the few stars that has a large radial velocity(-850 ± 226) km s^{-1} . If this velocity measurement is correct this star will not be bound to the Galaxy as described by the Galactic potential in chapter

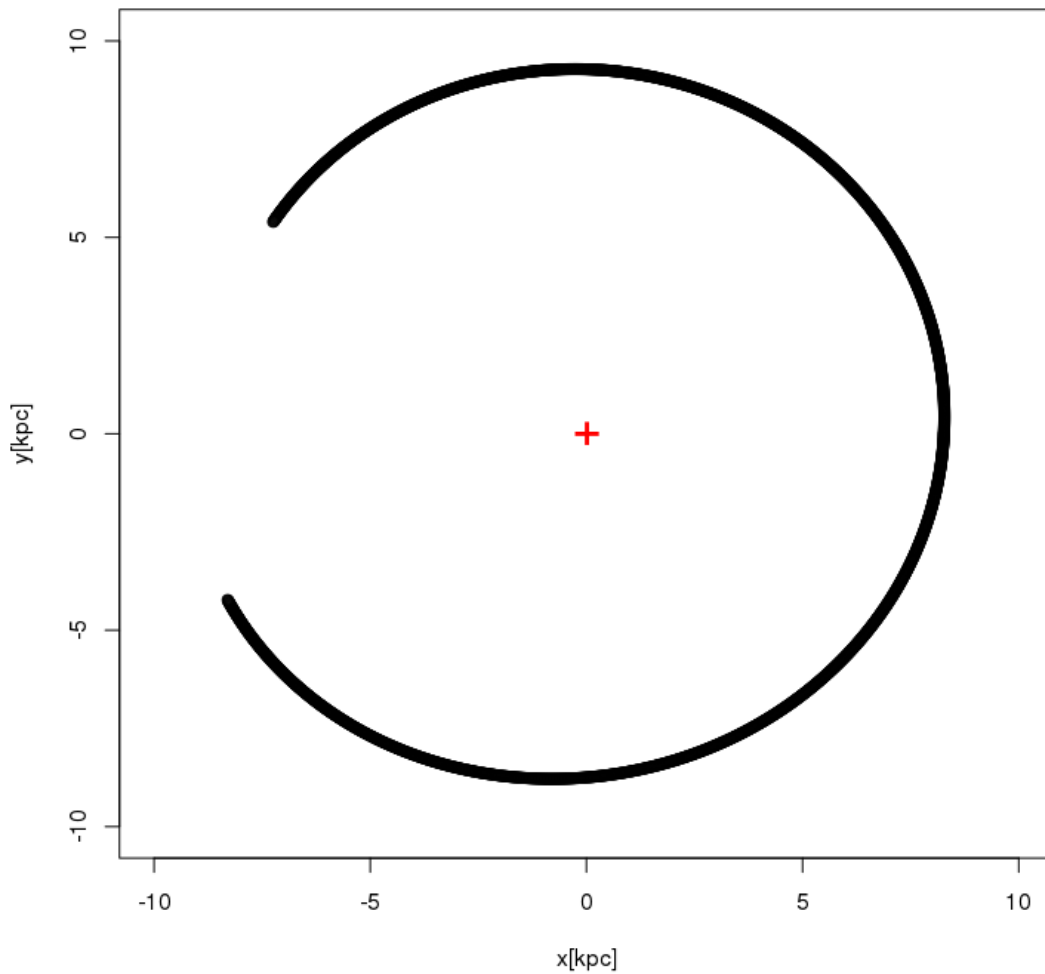


FIGURE 5.18: Sun's orbit around the galactic centre. The '+' denotes the galactic centre. This integration have been done for ± 100 Myr.

4.2.

HIP 94512

This star appears twice in the catalogue (Pulkovo and XHIP). This star is a future encounter in the Solar System. It is an A3 type star. The mean encounter distance of the star is 1.15 pc and the mean time for the closest approach is 3.38 Myr. The clone distribution of the star is well dispersed in figure 5.20.

TYC 8088-631-1

One of the past encounters of the Solar System. The nominal encounter distance for this star is 0.558 pc while the mean of the 1000 clones of the star is 2.824 pc. This is due to the proper

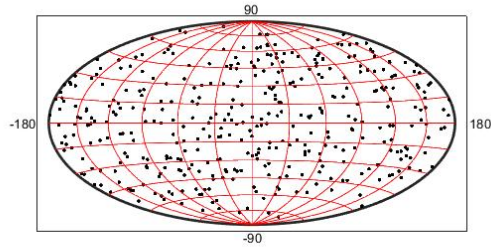


FIGURE 5.19: Distribution of encounters perihelia on the plane of the sky as a function of galactic latitude ($-90 \leq b \leq 90$) and longitude ($-180 \leq l \leq 180$) for encounter stars with a radial velocity greater than 50 km s^{-1} . The stellar encounters are denoted by dots.

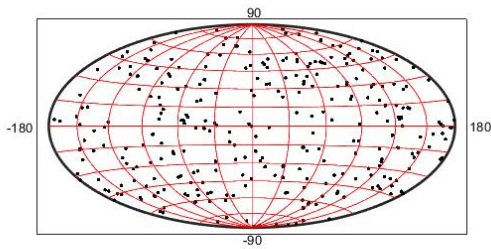


FIGURE 5.20: Distribution of encounters perihelia on the plane of the sky as a function of galactic latitude ($-90 \leq b \leq 90$) and longitude ($-180 \leq l \leq 180$) for encounter stars with a radial velocity less than 50 km s^{-1} . The stellar encounters are denoted by dots.

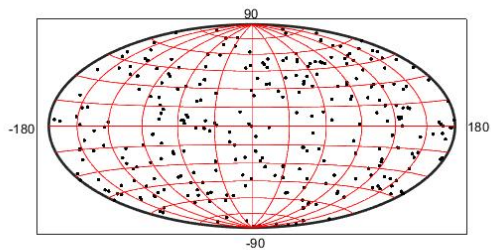


FIGURE 5.21: Distribution of encounters perihelia on the plane of the sky as a function of galactic latitude ($-90 \leq b \leq 90$) and longitude ($-180 \leq l \leq 180$) for encounter stars with a perihelion speed less than 50 km s^{-1} . The stellar encounters are denoted by dots.

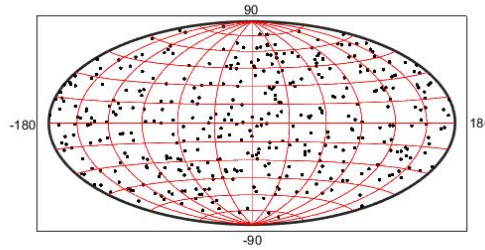


FIGURE 5.22: Distribution of encounters perihelia on the plane of the sky as a function of galactic latitude ($-90 \leq b \leq 90$) and longitude ($-180 \leq l \leq 180$) for encounter stars with a perihelion speed greater than 50 km s^{-1} . The stellar encounters are denoted by dots.

motion in the right ascension and proper motion in declination have errors being larger than the given value. This resulted in a widespread distribution of the clones. This encounter happened 2.73 Myr ago.

TYC 6622-652-1.r

This star is one of three stars which have a mean perihelion distance is less than 1 pc that occurred in the past. The effective temperature of this star as obtained from the RAVE DR5 catalogue is 3800K which also makes it a possible M0 dwarf star. Analysing 1000 clones of the star the estimated mean closest approach of the star is 0.553 pc . The mean time of the closest approach was 0.1 Myr in the past. This star also has a large radial velocity $(741 \pm 13) \text{ km s}^{-1}$. The needle like shape of the clones distribution is due to the high radial velocity of the star.

TYC 8822-592-1r

This is the second of the the stars that have a mean perihelion distance less than 1 pc that occurred in the past. The effective temperature of the star is $(5100 \pm 756)\text{K}$ and it is possibly a K1 star based on its effective temperature from RAVE DR5. Analysing 1000 clones the estimated mean closest perihelion distance of the star is 0.603 pc . The mean time at the perihelion distance is 0.1 Myr in the past. The radial velocity of this star has a very large value and according to RAVE DR5 catalogue it has no quoted error $(1969 \pm 0) \text{ km s}^{-1}$. The interpretation of this star should be taken with caution.

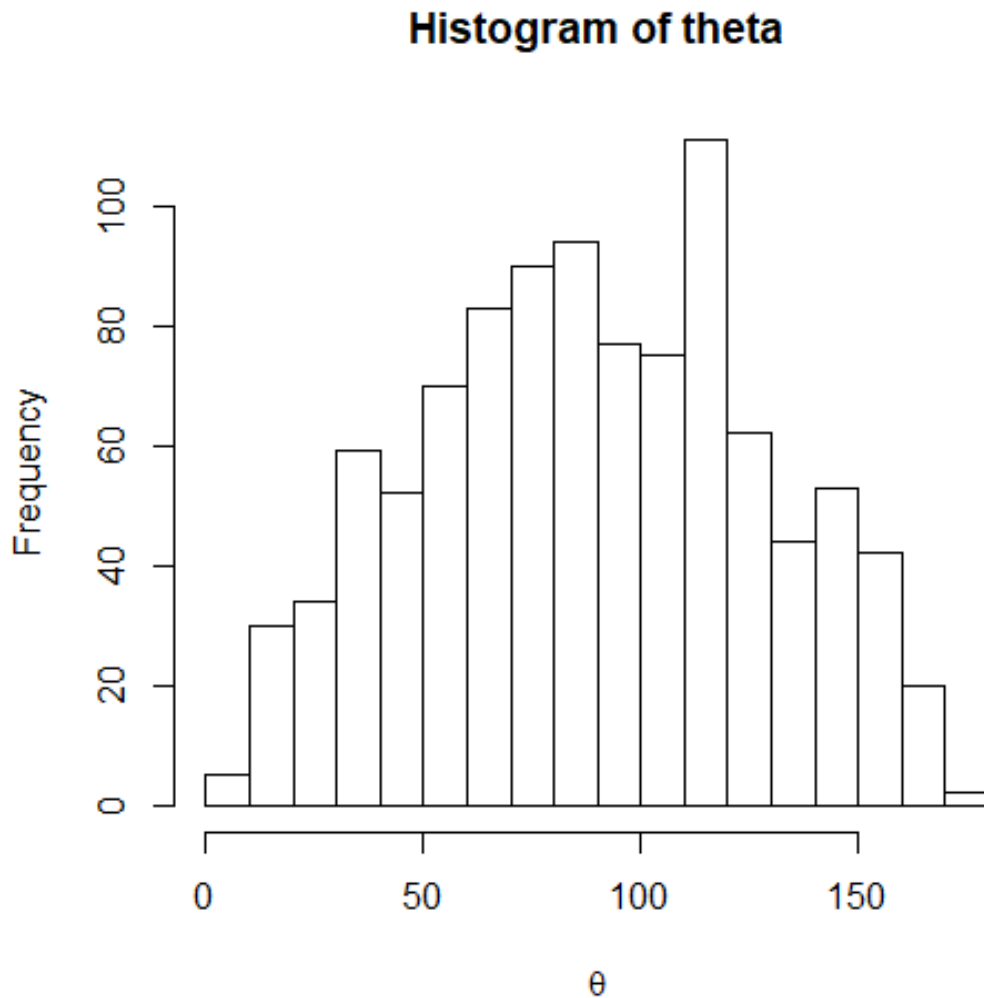


FIGURE 5.23: Distribution of the angle between the encounter perihelion and solar apex. This plot includes all the encounter stars irrespective to their perihelion speed. The shape of this distribution is similar to the figure 7 of García-Sánchez et al. (2001)

TYC 9524-1668-1

This star is another large radial velocity star from RAVE DR5 catalogue. This star is a F2V star and a future close encounter candidate. This star's mean perihelion distance is 0.863 pc and the mean time during the closest approach is 0.19 Myr.

TYC 7068-802-1

Another star with proper motions in the right ascension and proper motion in the declination errors larger than the given data. This errors have resulted in a widespread distribution of the

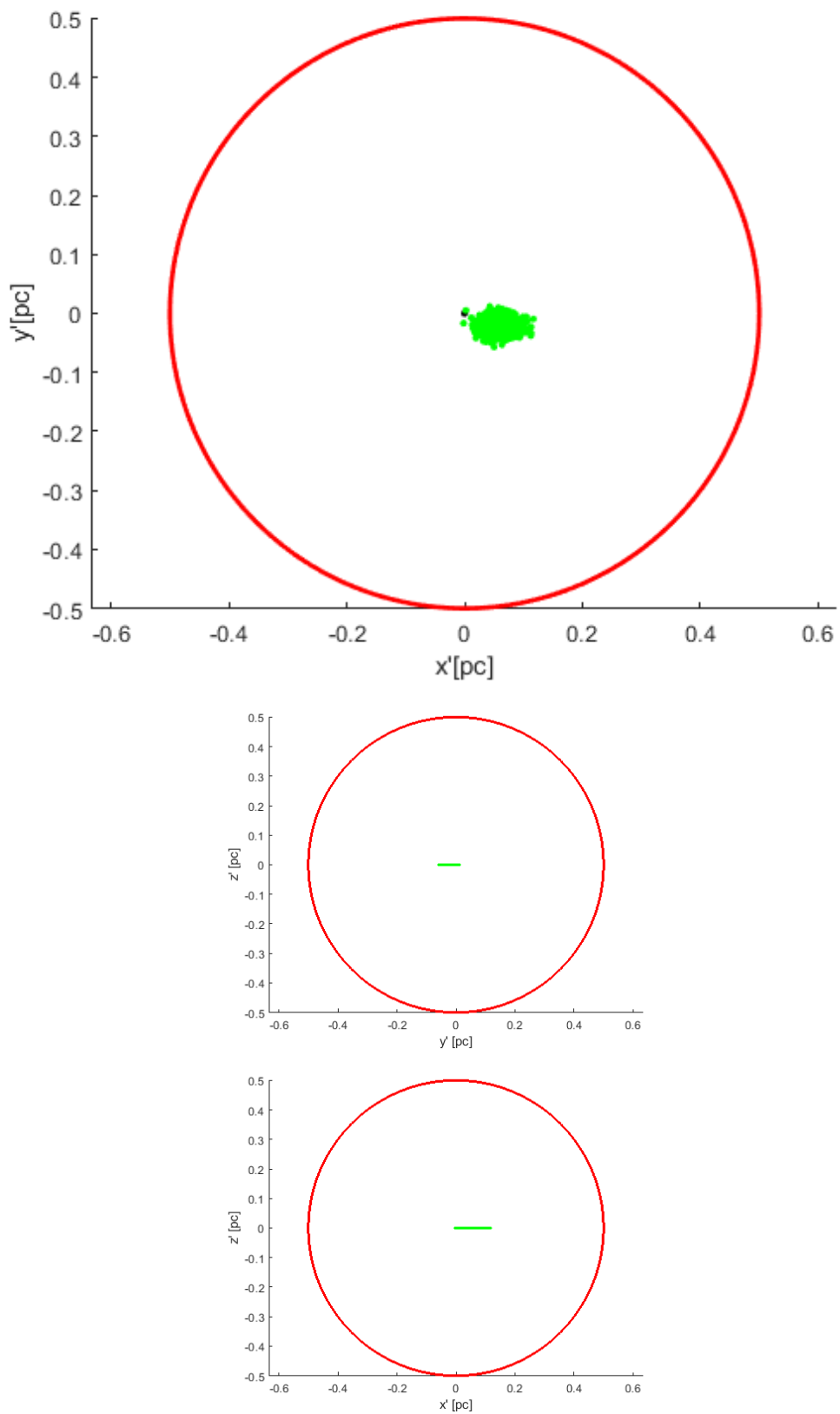


FIGURE 5.24: Distribution of the clones of HIP89825 in the $x'y'z'$ heliocentric frame which has been obtained from the xyz frame after rotations determined using principal component analysis. The green dots represents the clones of HIP89825. The black dot is the Sun and the Red circle represents the Oort cloud at 0.5pc.

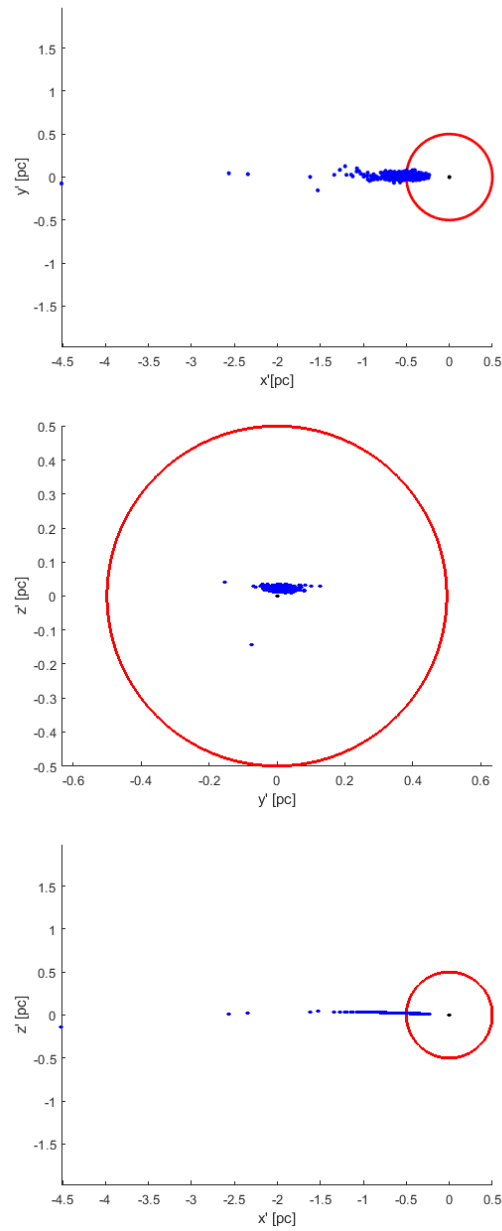


FIGURE 5.25: Distribution of the clones of TYC 6403-151-1 in the $x'y'z'$ heliocentric frame which has been obtained from the xyz frame after rotations determined using principal component analysis. The blue dots represents the clones of TYC 6403-151-1. The black dot is the Sun and the Red circle represents the Oort cloud at 0.5pc.

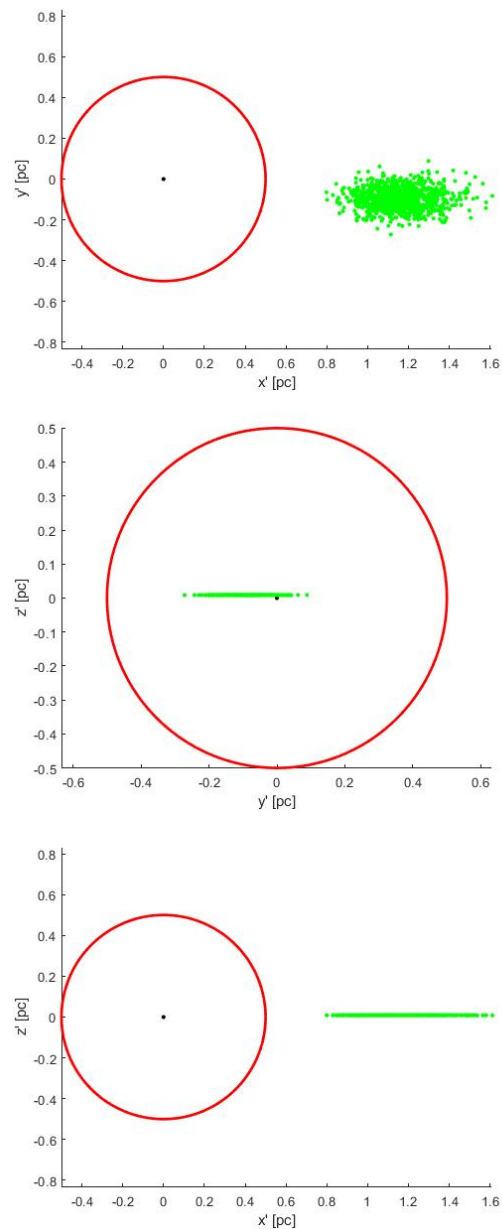


FIGURE 5.26: Distribution of the clones of HIP 94512 in the $x'y'z'$ heliocentric frame which has been obtained from the xyz frame after rotations determined using principal component analysis. The green dots represents the clones of HIP 94512. The black dot is the Sun and the Red circle represents the Oort cloud at 0.5pc.

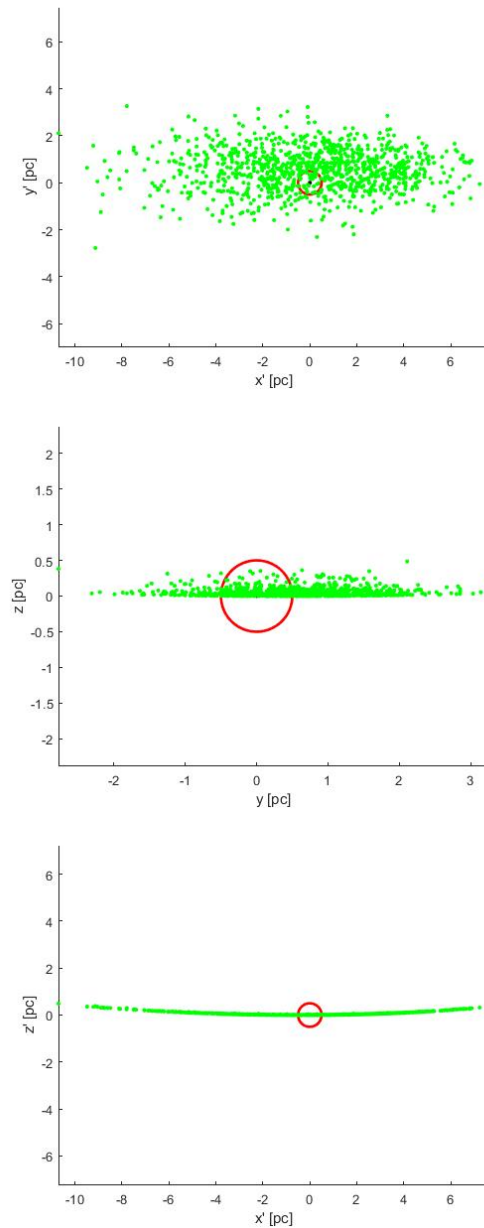


FIGURE 5.27: Distribution of the clones of TYC 8088-631-1 in the $x'y'z'$ heliocentric frame which has been obtained from the xyz frame after rotations determined using principal component analysis. The green dots represents the clones of TYC 8088-631-1. The black dot is the Sun and the Red circle represents the Oort cloud at 0.5pc.

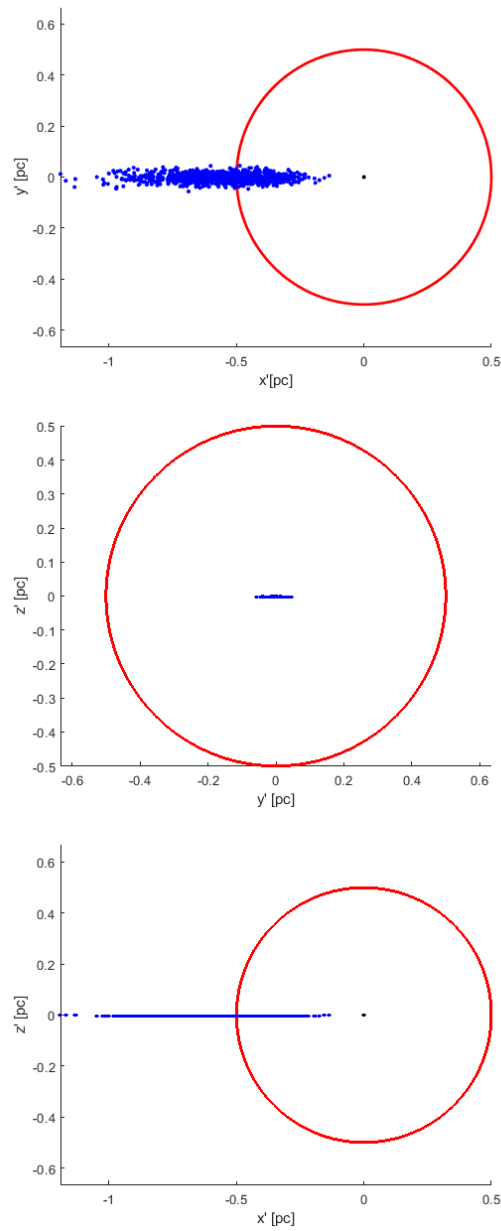


FIGURE 5.28: Distribution of the clones of TYC 6622-652-1 in the $x'y'z'$ heliocentric frame which has been obtained from the xyz frame after rotations determined using principal component analysis. The blue dots represents the clones of HIP89825. The black dot is the Sun and the Red circle represents the Oort cloud at 0.5pc.

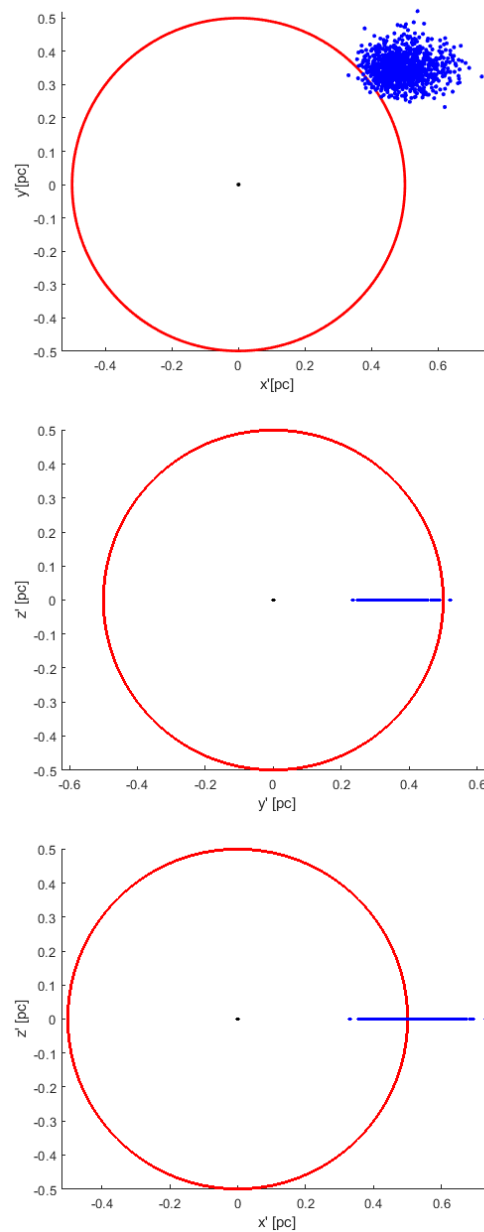


FIGURE 5.29: Distribution of the clones of TYC 8822-592-1 in the $x'y'z'$ heliocentric frame which has been obtained from the xyz frame after rotations determined using principal component analysis. The blue dots represents the clones of TYC 8822-592-1. The black dot is the Sun and the Red circle represents the Oort cloud at 0.5pc.

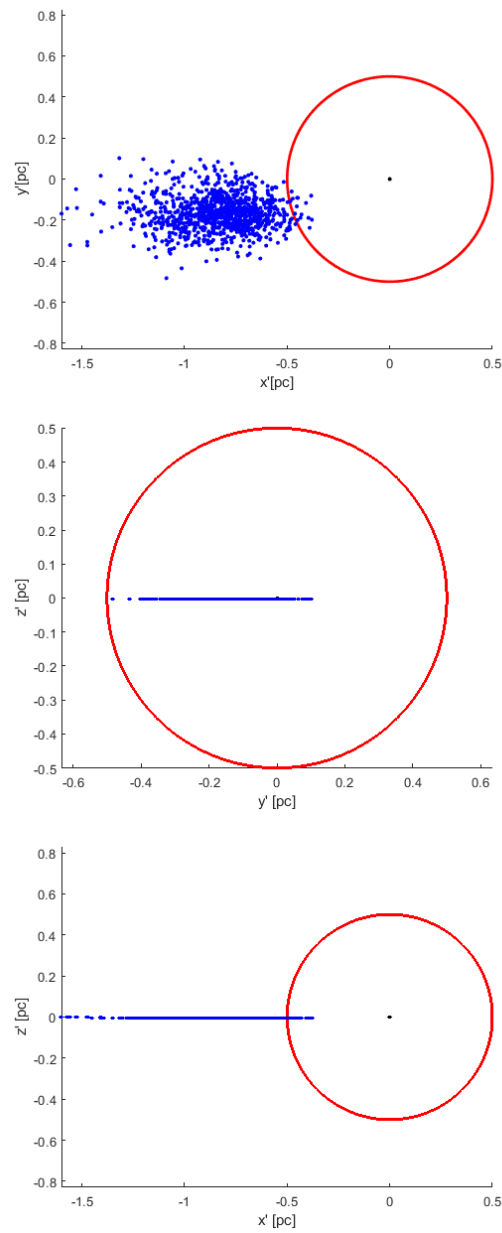


FIGURE 5.30: Distribution of the clones of TYC 9524-1668-1 in the $x'y'z'$ heliocentric frame which has been obtained from the xyz frame after rotations determined using principal component analysis. The blue dots represents the clones of TYC 9524-1668-1. The black dot is the Sun and the red circle represents the Oort cloud at 0.5pc.

clones. It is a past encounter with a mean perihelion distance 2.329 pc while the nominal solution gives an perihelion distance of 1.146 pc. This encounter happened 2.65 Myr ago.

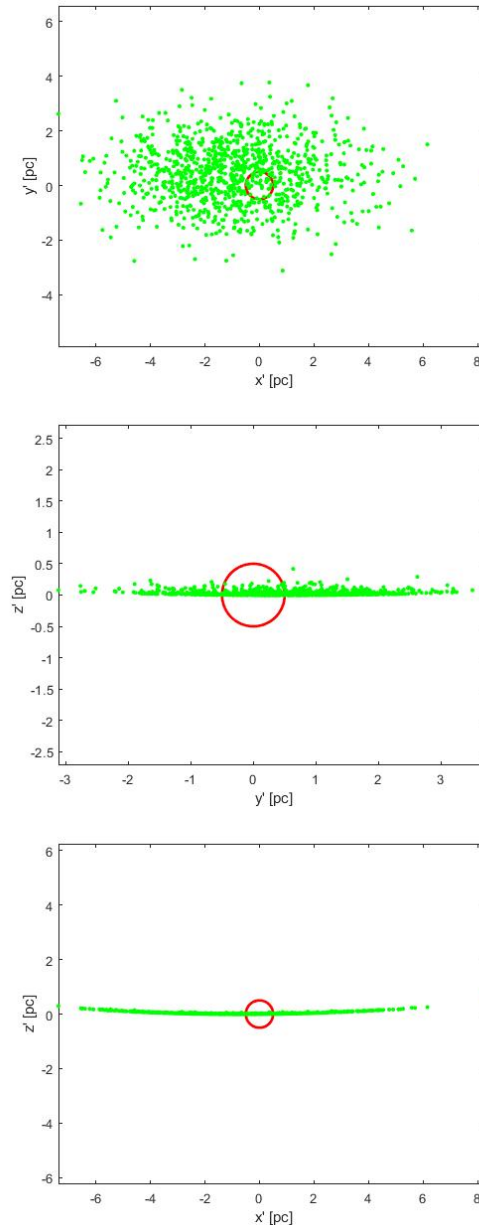


FIGURE 5.31: Distribution of the clones of TYC 7068-802-1 in the $x'y'z'$ heliocentric frame which has been obtained from the xyz frame after rotations determined using principal component analysis. The green dots represents the clones of TYC 7068-802-1. The black dot is the Sun and the Red circle represents the Oort cloud at 0.5pc.

TYC 7567-304-1

This is another star with a large radial velocity gathered from RAVE DR5 catalogue. This is a possible K3V star and also a future close encounter candidate. This star's mean perihelion distance is 0.961 pc and the mean perihelion time during the closest approach is 0.09 Myr.

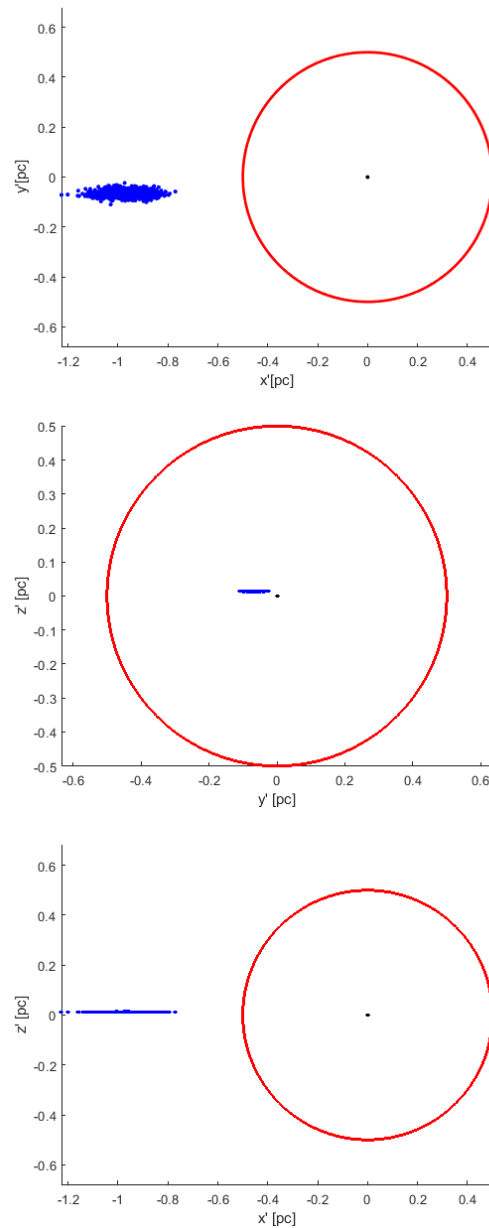


FIGURE 5.32: Distribution of the clones of TYC 7567-304-1 in the $x'y'z'$ heliocentric frame which has been obtained from the xyz frame after rotations determined using principal component analysis. The blue dots represents the clones of TYC 7567-304-1. The black dot is the Sun and the Red circle represents the Oort cloud at 0.5pc.

Chapter 6

Discussions

6.1 Completeness of the catalogue

This survey in no way makes a claim to be a complete list of close encounters of Solar System up to a certain limit in distance. A number of incompleteness issues have arisen during the course of making this particular catalogue. Not every single star in the TGAS catalogue have been subjected to numerical integration since the TGAS catalogue only contained five astrometric parameters and did not provide radial velocity of the stars. Four other catalogues were used to gather radial velocity for the stars in the TGAS catalogue. Only for 11% of the stars in the TGAS catalogue, all the six astrometric parameters then completed. Not all of those stars with all six astrometric parameters were subjected to numerical integration due to limited time and a one year thesis project along with the limitations in computing time. A linear motion approximation was used instead to select the number of encounters with a perihelion encounter distance of less than 10pc. There can be some stars beyond the 10pc limit which have, within their 1000 clones a possibility of having a mean distance less than 10pc. It can be said that the larger the upper limit i set for approach distance of the encounters, more problematic is the completeness of the catalogue.

6.2 Data Issues

Aside from the methods and the adopted models, it is also necessary to look at the reliability of the data. The RAVE DR5 catalogue has quite a significant number of stars with large radial

velocity values compared to the other three catalogues from which radial velocity was gathered. This however does not automatically imply that these radial velocities are wrong. All the stars' radial velocities gathered from RAVE DR5 from stars with a mean perihelion distance less than 2pc have really large radial velocities and they have quite low SNRs(Signal to noise ratio). One of the reasons can be poor extraction of radial velocity from low SNRs. Although the error for some of these radial velocity is large it is still not consistent with typical radial velocity measurements of stars. Some of the RAVE DR5 radial velocities have no quoted error corresponding to the value. They maybe some outliers in the radial velocity spectra. Gaia DR1 also has its own limitations.

Gaia DR1 is incomplete at the bright end and also has an ill defined faint magnitude. Many bright stars at $G \leq 7$ are missing. There is a systematic offset of ± 0.3 mas present in the parallax (Gaia Collaboration et al., 2016).Accounting for this systematic makes very little changes in the encounter parameter. For example the closest encounter in my catalogue HIP 89825(GL 710)'s encounter parameters didn't make a significant change while accounting for the offset in the parallax. Gaia DR1s limitations were also discussed in chapter 2.1.

The larger the radial velocity the shorter the encounter distance. I can only find encounters from the stars that I have numerically integrated. More encounters probably exist beyond this subset of TGAS stars but that depends on acquiring their radial velocity.

6.3 Difference in encounter parameters estimation

A significant difference can be noticed between the encounter data of the stars gathered from linear, nominal and the encounter data obtained by analysing the numerically integrating the clones. As mentioned in chapter 5 it can be seen that the nominal and linear approximation data tends to underestimate the encounter distances. One of the reasons behind that tendency to underestimate is due to the non linear transformation between parallax and distance (Lutz and Kelker (1973)). For example, assume a star has a mean parallax of 10 mas and a fraction of the probability lies within 1-10 mas and also a fraction of the probability also lies within 10-20 mas. Once converted into distances that fraction lies within 1000-100 pc and 100-50 pc. So, the mean of the distance distribution will be larger than the nominal distance. Then it can be said that the mean perihelion distance will always be larger than the nominal perihelion distance.

The linear motion approximation also shows the same tendency of underestimating the perihelion distance. It is because like the nominal distance it also suffers from the same bias. Another reason is the fact that the linear motion approximation method neglects gravity. Parallax bias and the neglect of gravity results in poor estimates of the encounter parameters.

Due to the significant amount of difference found in chapter 5 it will not be logical to determine close stellar encounters solely based on linear motion approximation or nominal data.

6.4 Dependence on the Galactic Potential Model

The encounter parameters obtained from the numerical integration of the Sun and the encountering stars orbit definitely depends on the adopted galactic potential. In this study a simple three component axisymmetric time independent galactic model was chosen without the spiral arms or galactic bar. Compared to the length scales (please refer to table 4.1), the difference in the potential experienced by the Sun and the encountering star remains small given that the separation between them remains small too.

The potential adopted in this work is similar to the potential used in Bailer-Jones (2015) and García-Sánchez et al. (2001). García-Sánchez et al. (2001) studied the sensitivity of their results by making changes in the galactic potential. A variation in the z_{\odot} (Sun's vertical height from the galactic mid-plane) ranging from 0-20 pc and a variation in the r_{\odot} (the distance of the Sun from the galactic centre) ranging from 7.5-8.5 kpc. These changes had a minimal effect on the 156 encountering stars with a perihelion distance less than 5pc. Only 8 out of those 156 encountering stars had a change in their perihelion distances by more than 0.05pc. That study also included a spiral arm in their galactic potential and found only 8 stars had a change in their perihelion distances by 0.1pc.

In this study I have altered the values of the distance of the Sun's distance from the galactic centre for all the stars with a mean perihelion distance less than 2pc. The changes were minimal.

In common with past studies on close stellar approaches, the gravitational attraction between the Sun and the encountering star was neglected. The stars move on a hyperbolic orbit with respect

to one another. The perihelion distance would be then

$$d_{ph}^{hyp} = \sqrt{a^2 + d^2} - a \quad (6.1)$$

Where a is defined as

$$a = \frac{GM}{v^2} \quad (6.2)$$

where M is the mass of the Sun and the encountering star, G is the gravitational constant, v is the speed of the star relative to the Sun. Bailer-Jones (2015) did similar kind of work to show by how much his perihelion distances would have been reduced if the Sun-star interaction were taken into account. Even for his most deviant case the perihelion distance is only reduced by 0.5%. Here I have done the same work of the difference in perihelion distance if the Sun-star interaction were taken into account. Taking into the closest approaching star from table 5.2 HIP 89825 the speed of the star during the encounter with the Sun is 13.8 km/s, the total mass of both the Sun and the star is $1.6M_{\odot}$ (HIP 89825 has a mass of $0.6 M_{\odot}$, Franchini et al. (2014)) the perihelion distance is 0.063 pc. Taking into account the Sun-star interaction the new perihelion distance is reduced by 0.1%.

The galactic potential used in this work is time independent and smooth. The smoothness in the potential indicates ignoring Sun's or encountering stars' interaction with other stars or molecular clouds along their orbits. In reality these interaction will lead to a deflected orbit of the Sun or the encountering star. For all the encountering stars (that were numerically integrated) the mean perihelion time ranges from -31 Myr to +30 Myr. The Sun moves approximately 523 pc over the next 30 Myr with respect to the LSR. Assume a star has an interaction with the Sun that results in a deflection in the Sun's path by 0.5 degrees or more considering this interactions happens in a hyperbolic orbit. the deflection orbit δ is

$$\delta = \frac{2a}{d} \quad (6.3)$$

where a is from equation 5.2 and d is the impact parameter. The closest approaching star from table 5.2 HIP 89825. From table 5.2 and 5.3 the encounter parameters were taken for this star. The star has a mean perihelion distance of 0.063 pc and a mean perihelion speed is 13.8 km/s. The deflection angle is then 0.066 degrees.

Bailer-Jones (2015) did the same work in order to deflect the Sun's orbit by 0.5 degrees. The study assumed a star with one solar mass at a speed of 34 km/s (the median of encounter stars' perihelion speed in that study) with a impact parameter of 0.0017 pc. The study also found the probability of no encounter after 330 pc is 0.997.

I now make the same assumption in my study where the Sun's orbit is deflected by 0.6 degrees if an encountering star has an one solar mass at a speed of 32 km/s (the median of my mean perihelion speed of encountering stars) with a impact parameter of the same 0.0017 pc. If I assume the same number of stellar density as Bailer-Jones (2015) of $\rho = 1 pc^{-3}$ then the average number of encounters after moving a certain distance of x is

$$\lambda = \pi d^2 x \rho \quad (6.4)$$

where λ is rate parameter the Poisson distribution of the probability of n number of encounters. if I chose x to be 523 pc therefore the $e^{-\lambda}$ is 0.995. The encounters in this study occurs in a much shorter path length than this, so neglecting the gravitational effect is justified in this study.

6.5 Comparing Results with another Close Encounter Study

During the writing of the thesis, Bailer-Jones (2018) published his close encounters with the Solar System based on Gaia DR1. Despite the methodology in terms of identifying encounters have been similar in nature, there are certain discrepancies remain between my catalogue and the catalogue of Bailer-Jones's. The main difference is in the selection of the encounters. Since Gaia TGAS did not have radial velocity of its stars, these radial velocities were obtained from various other catalogues. In this study I have used four catalogues to obtain relative velocity for these stars. These four catalogues are mentioned in Chapter 2 of this study. This gives me a total number of 216833 stars before I applied linear motion approximation. Bailer-Jones performed a cross match with 12 other catalogues. The author also removed all the stars with a radial velocity larger than 750 kms-1. This gives him a total number of 397788 stars. Another difference is the author calculated the median of the encounter parameters and in my study I found the mean of the encounter parameters. One interesting difference between this two studies is the missing HIP 22111 in my study. In his paper TYC 4744-1394-1 (HIP 22111) is the second closest encounter with a median perihelion distance of 0.87 pc. This star is missing from my catalogue of close

encounters. Somehow during the cross matching of the catalogues this star went missing from the list.

Chapter 7

Conclusion

The aim of the project is to find all stars which have passed or will pass the Sun within 2pc over the past/future 10 Myr using Gaia DR1. This represents a useful addition to knowledge in the area. I have found 1003 potential encounter candidates that satisfy this criterion out of more than 2 million nearby stars from the TGAS catalogue of Gaia DR1. From the covariance matrix given by the TGAS catalogue, I have generated 1000 clones for each of the candidate stars using a multivariate normal distribution algorithm. I then integrated these 1003 stars through an axisymmetric time independent galactic model to find the nominal encounter parameters and the mean of these encounter parameters. Since the distribution of these encounter parameters are asymmetric, I calculated the 5% and 95% quantiles for each of the candidates. From these 1003 stars, I found 846 candidates to have a mean perihelion distance less than 10pc, 52 stars with a perihelion speed less than 2 pc and 9 stars with a perihelion distance less than 1 pc. Some of these encounters have rather really large radial velocity. These stars were included in table 5.2 and 5.3 because of their closest proximity to the Sun. The new catalogue of possible encounters are presented in table 7.1 and 7.2. This catalogue represents a major result of this thesis. The clone clouds give a nice visualisation of how errors in astrometric parameters are reflected in uncertainties in encounter parameters. In particular the shape and size of these clouds gives a quantitative method of assessing the precision of the data. Some representative cloud figures from a larger collections are presented in chapter 5.

Several problems were faced in pursuit of searching for these encounters. One of the biggest problems was the lack of reliable radial velocity measurements. Only 216833 stars had the full six astrometric parameters required in order to trace an orbit and hence search for a close

ID	cat	d_{ph}^{nom} pc	d_{ph}^{mean} pc	$d_{ph}^{5\%}$ pc	$d_{ph}^{95\%}$ pc	t_{ph}^{nom} Myr	t_{ph}^{mean} Myr	$t_{ph}^{5\%}$ Myr	$t_{ph}^{95\%}$ Myr
HIP 89825	p	0.063	0.063	0.037	0.089	1.35	1.35	1.31	1.41
HIP 89825	x	0.063	0.063	0.037	0.089	1.35	1.35	1.31	1.41
HIP 94512	p	1.15	1.159	0.963	1.377	3.38	3.39	3.15	3.66
TYC 7973-1145-1	r	1.189	1.202	1.076	1.357	0.23	0.23	0.21	0.24
HIP 30344	x	1.385	1.389	1.285	1.496	-1.56	-1.56	-1.67	-1.45
TYC 6468-434-1	r	1.428	1.436	1.248	1.652	0.15	0.15	0.14	0.17
HIP 26335	p	1.569	1.568	1.538	1.596	-0.5	-0.5	-0.51	-0.49
HIP 26335	x	1.565	1.564	1.544	1.585	-0.5	-0.5	-0.5	-0.49
HIP 40317	p	1.592	1.595	1.452	1.753	-2.22	-2.22	-2.3	-2.15
HIP 25240	p	1.628	1.627	1.504	1.756	-0.95	-0.95	-0.99	-0.91
HIP 25240	x	1.629	1.63	1.504	1.768	-0.95	-0.95	-0.99	-0.91
TYC 9327-264-1	r	1.652	1.891	0.97	3.072	-1.89	-1.9	-2.02	-1.78
HIP 25240	g	1.668	1.675	1.532	1.83	-0.97	-0.97	-1.02	-0.93
TYC 8560-8-1	r	1.697	1.719	1.253	2.245	-0.63	-0.63	-0.65	-0.61
TYC 9163-286-1	r	1.705	1.812	0.543	3.588	-0.57	-0.57	-0.66	-0.49
HIP 30344	p	1.733	1.735	1.663	1.816	-1.95	-1.95	-2.03	-1.89
HIP 30344	g	1.757	1.759	1.697	1.827	-1.98	-1.98	-2.03	-1.93
HIP 30067	x	1.806	1.807	1.74	1.872	-0.65	-0.65	-0.66	-0.64
HIP 30067	g	1.809	1.811	1.749	1.878	-0.65	-0.65	-0.66	-0.64
HIP 30067	p	1.809	1.808	1.744	1.873	-0.65	-0.65	-0.66	-0.64
TYC7593-343-1	r	1.89	1.936	1.481	2.483	0.46	0.46	0.41	0.52
HIP 26624	p	1.909	1.911	1.727	2.114	-1.85	-1.85	-1.92	-1.78
HIP 26624	x	1.909	1.911	1.727	2.114	-1.85	-1.85	-1.92	-1.78
TYC 8470-213-1	r	1.954	1.962	1.788	2.16	-0.17	-0.17	-0.18	-0.15
HIP 20359	x	1.995	1.995	1.942	2.047	0.36	0.36	0.36	0.36

TABLE 7.1: Encounter parameters for all the stars with a mean perihelion distance less than 2 pc. Stars with perihelion speed greater than 600km s^{-1} were omitted. The column named cat indicates the name of the input catalogue where the radial velocity were obtained from g=GCS catalogue, P=Pulkovo Catalogue, r= RAVE DR5 catalogue, x= XHIP catalogue. The encounter parameters are set as d_{ph}, t_{ph} respectively, nom represents the nominal values, mean represents the mean values, 5% and 95% represents the 5% and 95% quantiles of each encounter parameter.

encounter. This number only counts for approximately 11% of all the stars found in the TGAS catalogue. The RAVE DR5 also contained rather large radial velocities for certain TGAS stars. Due to these large radial velocities some of these stars have an encounter distance less than 2 pc. Gaia DR1 was also missing the bright stars in the solar neighbourhood (e.g: Alpha Centauri, Proxima Centauri, Van Mannen's star).

The next Gaia data release (Gaia DR2) will provide radial velocities for stars brighter than 12 mag and more precise proper motions and parallaxes. These radial velocities will be precise to a few km/s (Gaia collaboration et al. 2016b). These improvements and the addition of the radial velocities for a few million stars will result in the improvement of the completeness of the

ID	cat	v_{ph}^{nom} kms^{-1}	v_{ph}^{mean} kms^{-1}	$v_{ph}^{5\%}$ kms^{-1}	$v_{ph}^{95\%}$ kms^{-1}
HIP 89825	p	13.8	13.78	13.32	14.27
HIP 89825	x	13.8	13.78	13.32	14.27
HIP 94512	p	30.4	30.42	29.94	30.93
TYC 7973-1145-1	r	537.22	536.84	517.41	555.44
TYC 5033-879-1	r	532.62	532.41	521.91	542.38
HIP 30344	x	18.34	18.34	17.07	19.65
HIP 26335	p	22.21	22.22	21.88	22.55
HIP 26335	x	22.26	22.26	22.1	22.42
HIP 40317	p	34.55	34.55	34.05	35.03
HIP 25240	p	55.03	55.05	54.52	55.54
HIP 25240	x	55	54.99	54.59	55.39
TYC 9327-264-1	r	52.67	52.67	51.14	54.22
HIP 25240	g	53.73	53.74	52.73	54.7
TYC 8560-8-1	r	86.47	86.48	85.53	87.46
TYC 9163-286-1	r	345.08	344.99	307.91	383.16
HIP 30344	p	14.65	14.63	14.1	15.12
HIP 30344	g	14.45	14.44	14.08	14.76
HIP 30067	x	40.66	40.66	40.51	40.81
HIP 30067	g	40.58	40.58	40.24	40.9
HIP 30067	p	40.58	40.59	40.42	40.75
TYC7593-343-1	r	338.97	339.07	304.72	374.96
HIP 26624	p	22.23	22.24	21.58	22.94
HIP 26624	x	22.23	22.24	21.58	22.94
TYC 8470-213-1	r	240.7	240.41	219.92	261.69
HIP 20359	x	79.23	79.24	78.9	79.57

TABLE 7.2: Encounter parameters for all the stars with a mean perihelion distance less than 2 pc. Stars with perihelion speed greater than $600kms^{-1}$ were omitted. The column named cat indicates the name of the input catalogue where the radial velocity were obtained from g=GCS catalogue, p=Pulkuvo Catalogue, r= RAVE DR5 catalogue, x= XHIP catalogue. The encounter parameters are set as v_{ph} respectively, nom represents the nominal values, mean represents the mean values, 5% and 95% represents the 5% and 95% quantiles of each encounter parameter.

catalogue and undoubtedly creating possible new candidate stars.

7.1 Future Work

An interesting thing to look into is the influence of Solar apex motion towards the encounter perihelia directions. In this thesis I have only studied it for the 1003 stars for 10 Myr. It is of interest then to study the full subset of TGAS stars with the full six astrometric parameters for a longer period of time in order to understand the influence of the Solar motion towards the encounter perihelia.

In the introduction I presented a discussion of the current state of knowledge about effects on the

Oort cloud from encounters. I would very much like to extend my own work in this direction. Some interesting developments include, considering the long term erosion of the Oort cloud and the possibility of cometary loss and transfer between stellar systems. Such transfers are very sensitive to the encounter geometry and can only be improved through better analysis of close encounters as has been presented here.

With future Gaia data releases another thing would be to look at is to how much Oort cloud objects these close encounters get to inject into the inner Solar System. This will be useful in terms to understanding the role of LPCs in terms of mass extinction level events in the terrestrial biosphere.

Another future plan is to perform numerical studies are needed to investigate whether the anisotropic perturbations from stellar encounters and the Galactic tide on the Oort cloud would lead to an anisotropic Oort cloud.

Bibliography

- Anderson, E. and Francis, C., 2012. XHIP: An extended hipparcos compilation. *Astronomy Letters*, 38:331.
- Bailer-Jones, C.A.L., 2015. Close encounters of the stellar kind. *A&A*, 575:A35.
- Bailer-Jones, C.A.L., 2018. The completeness-corrected rate of stellar encounters with the Sun from the first Gaia data release. *A&A*, 609:A8.
- Bailey, M.E., Clube, S.V.M., and Napier, W.M., 1990. *The origin of comets*.
- Berski, F. and Dybczyński, P.A., 2016. Gliese 710 will pass the Sun even closer. Close approach parameters recalculated based on the first Gaia data release. *A&A*, 595:L10.
- Bobylev, V.V. and Bajkova, A.T., 2017. Searching for stars closely encountering with the solar system based on data from the Gaia DR1 and RAVE5 catalogues. *Astronomy Letters*, 43:559.
- Casagrande, L., Schönrich, R., Asplund, M., et al., 2011. New constraints on the chemical evolution of the solar neighbourhood and Galactic disc(s). Improved astrophysical parameters for the Geneva-Copenhagen Survey. *A&A*, 530:A138.
- Dauphole, B. and Colin, J., 1995. Globular clusters as a new constraint for the potential of our Galaxy. *A&A*, 300:117.
- Dones, L., Levison, H., Duncan, M., et al., 2000. Formation of the Oort Cloud Revisited. In *AAS/Division for Planetary Sciences Meeting Abstracts #32*, volume 32 of *Bulletin of the American Astronomical Society*, page 1060.
- Duncan, M., Quinn, T., and Tremaine, S., 1987. The formation and extent of the solar system comet cloud. *AJ*, 94:1330.
- Dybczyński, P.A., 2002. Simulating observable comets. I. The effects of a single stellar passage *A&A*, 396:283.

- Dybczyński, P.A., 2005. Simulating observable comets. II. Simultaneous stellar and galactic action. *A&A*, 441:783.
- Dybczyński, P.A., 2006. Simulating observable comets. III. Real stellar perturbers of the Oort cloud and their output. *A&A*, 449:1233.
- Dybczyński, P.A. and Berski, F., 2015. On the accuracy of close stellar approaches determination. *MNRAS*, 449:2459.
- Feng, F. and Bailer-Jones, C.A.L., 2014. Exploring the role of the Sun's motion in terrestrial comet impacts. *MNRAS*, 442:3653.
- Franchini, M., Morossi, C., di Marcantonio, P., et al., 2014. The FEROS-Lick/SDSS observational data base of spectral indices of FGK stars for stellar population studies. *MNRAS*, 442:220.
- Gaia Collaboration, Brown, A.G.A., Vallenari, A., et al., 2016. Gaia Data Release 1. Summary of the astrometric, photometric, and survey properties. *A&A*, 595:A2.
- García-Sánchez, J., Weissman, P.R., Preston, R.A., et al., 2001. Stellar encounters with the solar system. *A&A*, 379:634.
- Genz, A., Bretz, F., Miwa, T., et al., 2018. *mvtnorm: Multivariate Normal and t Distributions*. R package version 1.0-8.
- Gontcharov, G.A., 2006. Pulkovo Compilation of Radial Velocities for 35 495 Hipparcos stars in a common system. *Astronomy Letters*, 32:759.
- Heisler, J., 1990. Monte Carlo simulations of the Oort comet cloud. , 88:104.
- Heisler, J. and Tremaine, S., 1986. The influence of the galactic tidal field on the Oort comet cloud. , 65:13.
- Heisler, J., Tremaine, S., and Alcock, C., 1987. The frequency and intensity of comet showers from the Oort cloud. , 70:269.
- Hills, J.G., 1981. Comet showers and the steady-state infall of comets from the Oort cloud. *AJ*, 86:1730.
- Høg, E., Fabricius, C., Makarov, V.V., et al., 2000. The Tycho-2 catalogue of the 2.5 million brightest stars. *A&A*, 355:L27.

- Johnson, D.R.H. and Soderblom, D.R., 1987. Calculating galactic space velocities and their uncertainties, with an application to the Ursa Major group. *AJ*, 93:864.
- Kordopatis, G., Gilmore, G., Steinmetz, M., et al., 2013. The Radial Velocity Experiment (RAVE): Fourth Data Release. *AJ*, 146:134.
- Kunder, A., Kordopatis, G., Steinmetz, M., et al., 2017. The Radial Velocity Experiment (RAVE): Fifth Data Release. *AJ*, 153:75.
- Lutz, T.E. and Kelker, D.H., 1973. On the Use of Trigonometric Parallaxes for the Calibration of Luminosity Systems: Theory. *PASP*, 85:573.
- Majaess, D.J., Turner, D.G., and Lane, D.J., 2009. Characteristics of the Galaxy according to Cepheids. *MNRAS*, 398:263.
- Michalik, D., Lindegren, L., and Hobbs, D., 2015. The Tycho-Gaia astrometric solution . How to get 2.5 million parallaxes with less than one year of Gaia data. *A&A*, 574:A115.
- Miyamoto, M. and Nagai, R., 1975. Three-dimensional models for the distribution of mass in galaxies. , 27:533.
- Oort, J.H., 1950. The structure of the cloud of comets surrounding the Solar System and a hypothesis concerning its origin. , 11:91.
- Perryman, M.A.C., Lindegren, L., Kovalevsky, J., et al., 1997. The HIPPARCOS Catalogue. *A&A*, 323:L49.
- Plummer, H.C., 1911. On the problem of distribution in globular star clusters. *MNRAS*, 71:460.
- Rickman, H., Fouchard, M., Froeschlé, C., et al., 2008. Injection of Oort Cloud comets: the fundamental role of stellar perturbations. *Celestial Mechanics and Dynamical Astronomy*, 102:111.
- Schönrich, R., 2012. Galactic rotation and solar motion from stellar kinematics. *MNRAS*, 427:274.
- Soetaert, K., Petzoldt, T., and Setzer, R.W., 2010. Solving differential equations in r: Package *deSolve*. *Journal of Statistical Software*, 33(9):1.
- van Leeuwen, F., editor, 2007a. *Hipparcos, the New Reduction of the Raw Data*, volume 350 of *Astrophysics and Space Science Library*.

van Leeuwen, F., 2007b. Validation of the new Hipparcos reduction. *A&A*, 474:653.

Weissman, P.R., 1996. The Oort Cloud. In T. Rettig and J.M. Hahn, editors, *Completing the Inventory of the Solar System*, volume 107 of *Astronomical Society of the Pacific Conference Series*, pages 265–288.